# Dye Modification of Donor/Acceptor Interfaces in Polymer Solar Cells( Dissertation_全文 )

AUTHOR(S):

Honda, Satoshi

# Dye Modification of Donor/Acceptor Interfaces in Polymer Solar Cells

**Satoshi HONDA**

**2011**

# Contents

# *Part II*

# *Part III*

# Chapter 1

# General Introduction

## 1.1. Historical Background and Motivation

Polymer materials have excellent features such as flexibility, light-weight, processability, and ease of chemical modification, and hence, these materials are indispensable for modern people. Since the discovery of the conductive properties of doped polyacetylene in 1977,[1] for which its three main contributors Shirakawa, Heeger, and MacDiarmid were awarded the Nobel Prize in Chemistry in 2000, conjugated polymers have attracted a great deal of attention in various fields such as solar cells,[2–12] light-emitting diodes,[13] photodetectors,[14] field-effect transistors,[15] lasers,[16,17] sensors,[18,19] and optical probes[20] because of their new optoelectronic properties in addition to the basic properties as polymers mentioned above. Solar cells, which transform inexhaustible solar energy into electric energy, are one of the most promising long-term solutions for clean and renewable energy. There are solar cells based on inorganic semiconductors currently on the market that harvest solar energy efficiently.[21,22] These inorganic materials are stable and reliable in air and even at high temperatures. These solar cells are now being installed in solar factories and on roof-tops of buildings. On the other hand, organic solar cells based on polymer thin films have been actively studied as next-generation solar cells not only by industries but also by academic researchers because those devices possess many complicated but interesting phenomena such as photophysical dynamics and morphological formations of thin films, which are important in fundamental photophysical, polymer, and materials chemistry.

### *1.1.1. Polymer Solar Cells*

Polymer solar cells have attracted the attention of many physical and chemical scientists,[2–12] since the evidence for photoinduced electron transfer from the photoexcited state of a conjugated polymer (a poly(*p*-phenylenevinylene) derivative (PPV, Figure 1-1a)) onto buckminsterfullerene ($C_{60}$, Figure 1-1d) was reported in 1992.[23,24] These reports showed that the time scale for photoinduced charge transfer was sub-picosecond, more than 1000 times faster than the radiative and nonradiative decay of excited states. According to such efficient electron transfer, the photoactive layer of efficient polymer solar cells always consists of two compounds, a so-called electron donor and an electron acceptor material, in order to separate the photogenerated electron–hole pairs with a high yield.

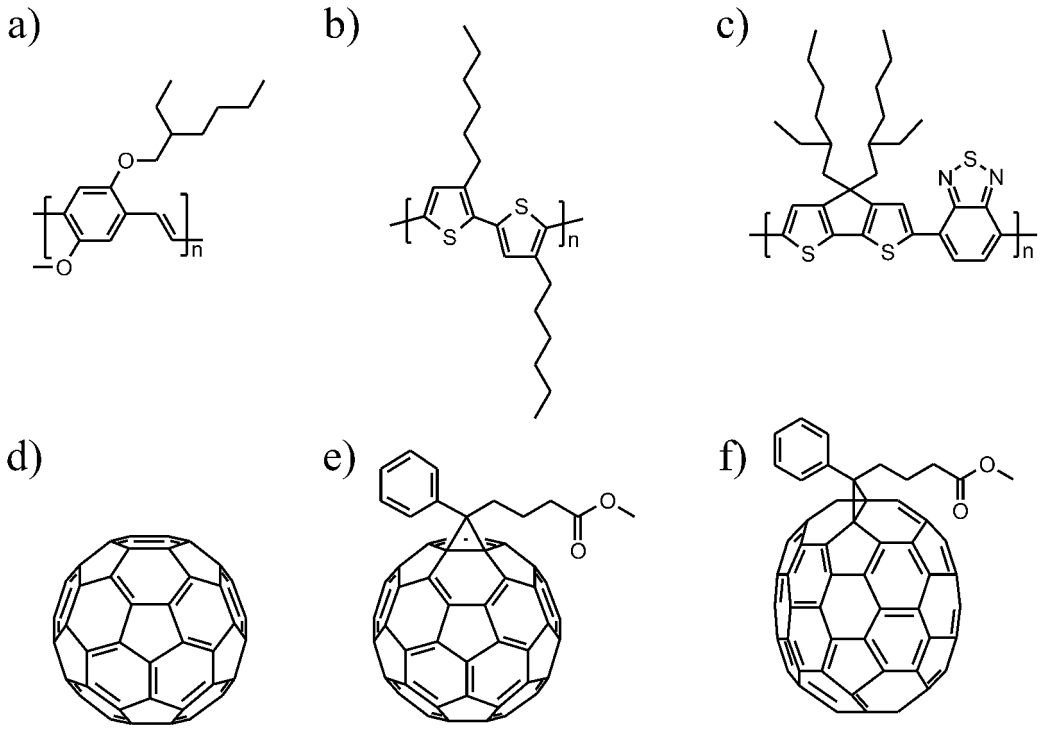


**Figure 1-1.** Chemical structures of conjugated polymers (a: MEH-PPV, b: RR-P3HT, and c: PCPDTBT, which is one of the low-bandgap polymers) and fullerenes (d: $C_{60}$, e: PCBM, and f: $PC_{71}BM$) used in polymer/fullerene solar cells as electron donor and acceptor materials, respectively.

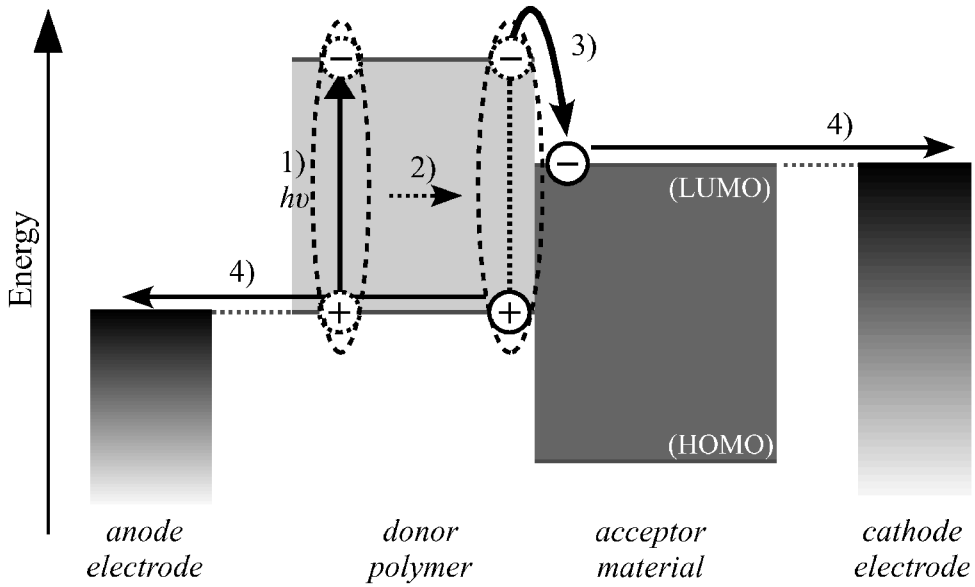


**Figure 1-2.** Schematic illustration of the photon-to-current conversion processes in polymer solar cells composed of four sequential steps: 1) light absorption and exciton generation, 2) exciton migration to the donor/acceptor interface, 3) charge separation at the interface, and 4) charge transport to electrodes.

The fundamental processes of photon-to-current conversion in the photoactive layer of polymer solar cells are illustrated in Figure 1-2. The processes consist of four sequential steps: 1) absorption of photons leads to the formation of excited states, which are bound electron–hole pairs called as excitons, 2) excitons diffuse to the donor/acceptor interface, 3) the charge separation occurs at that interface, and 4) the charge carriers are transported to the anode (for holes by the donor) and the cathode electrode (for electrons by the acceptor), to supply a direct current to an external circuit. Thus, the lower LUMO level of the acceptor than that of the donor and the higher HOMO level of the donor than that of the acceptor are required for an efficient photocurrent generation and extraction. There are two important differences between inorganic and organic solar cells. First, light absorption coefficients of organic materials are two orders of magnitude higher (typically ~ $10^5$ $cm^{-1}$,[2,25–27]) than those of inorganics, which is typically ~$10^3$ $cm^{-1}$ at around visible light wavelengths.[28,29] A conjugated polymer film with a thickness of ~300 nm is thick enough to absorb the most incident light.[27]

This enables greatly thinner and lighter photoactive layers for polymer solar cells than those for inorganic solar cells. Second, when an exciton is generated in an inorganic semiconductor, it can immediately dissociate into a free carrier.[30] In contrast, an exciton in conjugated polymers is tightly bound with binding energy of around 0.3–0.5 eV[31] and its dissociation must be promoted by acceptor materials. This limits the chance of charge generation only at the donor/acceptor interface. Moreover, the diffusion length of excitons generated in conjugated polymers is limited to be ~10 nm.[32–34] Thus, it is necessary for large photocurrent generation to enlarge the interfacial area of donor/acceptor. Such limitation strongly emphasizes the importance of donor/acceptor interfaces for polymer solar cells. One of the most promising device architectures to enlarge the interfacial area in photoactive layers of polymer solar cells is the phase separated structure of the donor:acceptor blend as introduced below.

The polymer solar cell, which exhibited clear photoinduced current–voltage characteristics, was reported in 1993 using PPV as a electron donor polymer and $C_{60}$ as an electron acceptor molecule with a planer heterojunction (PHJ) structure (Figure 1-3a). That report followed the photovoltaic property by using PHJ structure with a phthalocyanine derivative as a donor molecule and a perylene derivative as an acceptor molecule.[35] However, the photocurrent and

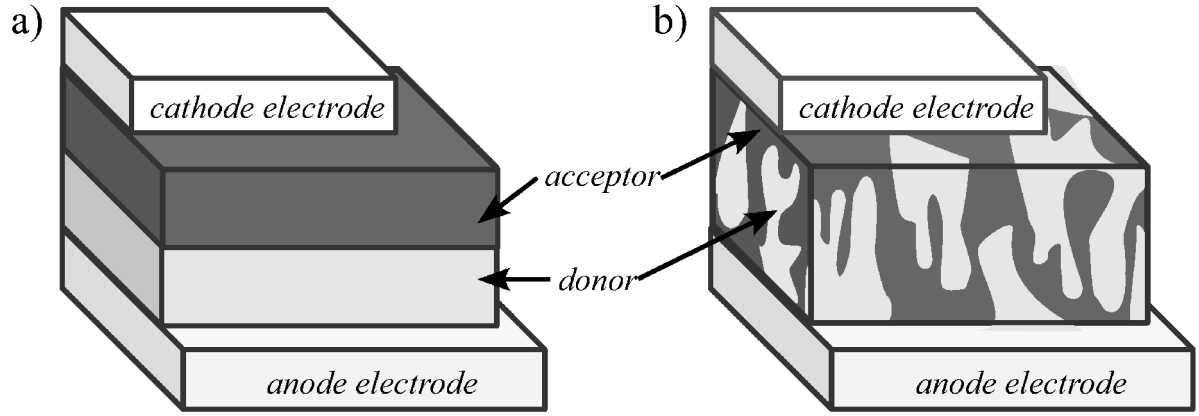


**Figure 1-3.** Schematic illustration of PHJ and BHJ structures as photoactive layers in polymer/fullerene solar cells.

hence the power conversion efficiency (PCE) in such PPV/$C_{60}$ PHJ solar cells was limited.[36] As described above, the limiting factor in this concept is the small amount of photogenerated charge carriers because of the small interface between donor and acceptor layers in PHJ structures. In 1995, however, remarkable progress in polymer solar cells was shown by Yu *et al.*[37] with the "bulk heterojunction" (BHJ) concept, which Hiramoto *et al.* reported on phthalocyanine:perylene diimide co-deposited solar cells in 1991.[38] The BHJ layer is the best architecture for polymer solar cells so far. The layer of BHJ consists of bicontinuous and interpenetrating donor and acceptor materials in a bulk volume (Figure 1-3b). Although the methodology is very simple (just coated from the blend solution), a nanoscale network of donor and acceptor phases by separation with a dimension of approximately 10 nm or even less was revealed by selective dissolving of $C_{60}$ from PPV:$C_{60}$ blend films and then measuring transmission electron microscopy (TEM) images.[39] Such a nanoscale network of donor and acceptor phases can overcome the limitation observed in PHJ solar cells.

Besides fullerene, electron-accepting conjugated polymers and metal oxides have been studied as acceptor materials for polymer solar cells. "All-polymer solar cells" using an electron donor polymer and an electron acceptor polymer were developed by Halls *et al.* in 1995.[40] In polymer/polymer solar cells, both active materials exhibit a high absorption coefficient in visible regions of light and can cover complementary parts of the solar spectrum. Furthermore, it is easy to tune both components individually to optimize optical properties, charge transfer and charge collection processes. Until now, many acceptor polymers have been studied for such polymer/polymer solar cells, having prospects of high performance.[41–45] On the other hand, polymer/inorganic semiconductor solar cells referred to as "hybrid" solar cells became of interest in the late 1990s. Inorganic semiconductors based on metal oxides, such as $TiO_2$ and ZnO, have a large number of advantages as electron acceptors, including relatively high electron mobility, high electron affinity, good physical and

chemical stability, and ease in fabricating various structures ranging from a dense layer to dispersed nanocrystals and to rigid connected nanostructures. However, the PCE in such a device was low, typically less than 1%,[46–49] compared to polymer/fullerene devices in those days. This might have been caused by the difficulty in the achievement of high-quality polymer/metal oxide interfaces, because metal oxides are hydrophilic whereas commonly used conjugated polymers are hydrophobic by their alkyl side-chain. To improve the wetting of the metal oxide by the polymer, the surface of metal oxides have been modified using organic dye molecules.[50–54] However, most studies[51,52] have thus far focused on the photosensitizing effect of the dyes because they serve as an efficient photosensitizer in dye-sensitized solar cells[55] resulting in PCEs of over 11%.[56,57] The effect of interfacial dye modification has not been studied in detail.

Since 2000s, most of the research activity has been focused on the investigation of photoactive layers made of a polythiophene derivative (regioregular poly(3-hexylthiophene) (RR-P3HT, Figure 1-1b)) and a fullerene derivative (1-(3-methoxycarbonyl)propyl-1-phenyl[6,6]methanofullerene (PCBM, Figure 1-1e)). The wide interest in RR-P3HT was triggered by the first report showing the drastic effect of thermal annealing of RR-P3HT:fullerene blend films on the improvement of the photocurrent density and hence the PCE.[58,59] This enhancement is probably due to the well-ordered self organization of RR-P3HT chains.[60] Such organization is advantageous in polymer solar cells as follows: the formation of bicontinuous phase-separated network of RR-P3HT and fullerene,[61] significant increase in the hole mobility,[62–64] and strong red-shift in the absorption.[64] The PCEs up to ~5% have been demonstrated through the optimization of annealing conditions.[61,65,66] It was also revealed that the performance of RR-P3HT:PCBM devices was affected by molecular weight,[67] polydispersity,[68] regioregularity,[66] proper solvent,[69,70] solvent-vapor treatment,[65,71] and adding a small amount of additives with relatively high boiling points.[72,73] All these results indicated

that it is very complex to control the morphology of polymer:fullerene BHJ photoactive layers. Recently, several groups have revealed the phase-separated structures of blended films by TEM,[61,74] scanning probe microscopy (SPM),[75,76] and electron tomography.[77,78] The RR-P3HT:PCBM BHJ solar cells exhibit high external quantum efficiencies (EQEs, also called as incident photon-to-current conversion efficiencies (IPCEs)) of ~80% and fill factors of ~0.7.[61,65,66] However, RR-P3HT can absorb only a quarter of the total photons in the solar light because of its relatively wide bandgap 2.0 eV, which corresponds to the absorption bands below 620 nm as shown in Figure 1-4.[79,80]

For further improvement of the photocurrent in polymer solar cells, it is necessary to absorb photons in near-infrared (NIR) regions because solar spectrum exhibits a maximum photon flux around 700 nm (Figure 1-4). Consequently, a variety of low-bandgap polymers (LBPs) have been developed to absorb a broad range from visible to NIR regions of solar light most recently.[79–82] In 2007, poly-[2,6-(4,4-bis-(2-ethylhexyl)-4*H*-cyclopenta[2,1-*b*;3,4-*b*']-dithiophene)-*alt*-4,7-(2,1,3-benzothiadiazole) (PCPDTBT), which is one of the LBP

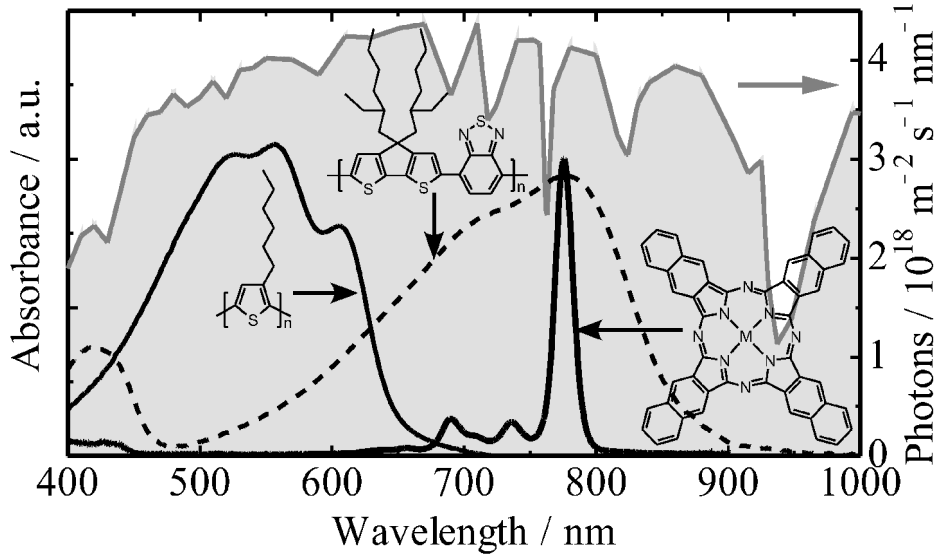


**Figure 1-4.** Absorption spectra and chemical structures of RR-P3HT (solid line), PCPDTBT (broken line), and a naphthalocyanine derivative (thick solid line) are shown together with the AM 1.5G standard solar spectrum.

(Figure 1-1c) having maximum absorption peak around 800 nm (Figure 1-4), based solar cells blended with $PC_{71}BM$ (Figure 1-1f) exhibited higher photocurrent (short-circuit current density ($J_{SC}$) of ~16 mA $cm^{-2}$)[81] than RR-P3HT:PCBM cells ($J_{SC}$ of ~10 mA $cm^{-2}$).[65] In 2009, Chen *et al.* reported a high PCE of 7.7% by using different LBP blended with $PC_{71}BM$.[82] Most recently, Nov., 29, 2010, Konarka's group reported the highest PCE of 8.3% on their homepage.[83]

On the other hand, dye sensitization by dye molecules absorbing NIR light is another way to improve the light-harvesting efficiency, but there have been few reports of success. Recently, the dye-sensitization effect has been demonstrated for polymer:fullerene BHJ solar cells.[84] In general, dye molecules are simply blended as the third component to absorb the solar light at longer wavelengths that the original donor and acceptor materials cannot harvest, for example, naphthalocyanines as shown in Figure 1-4. This is a simple and versatile method, and therefore various dye molecules are available. In most cases, however, dye introduction rarely improved the device performance if not degrading it. This is considered to be due to the formation of dye aggregations in blend films, which would reduce the absorption efficiency or the charge mobility of the active layer.[85–87] Moreover, for efficient sensitization, not only the suppression of dye aggregations but also the location of dye molecules in blend films should be important. The dye molecules doped into donor:acceptor blend films are required to generate charge carriers of donor cations and acceptor anions from dye excitons. In other words, dye molecules must be located at the interface between donor and acceptor as illustrated in Figure 1-5 in order to enhance the photocurrent density. This is a highly complicated but challenging and worthwhile investigation. This thesis focuses on the dye-sensitized ternary blend solar cells in detail.

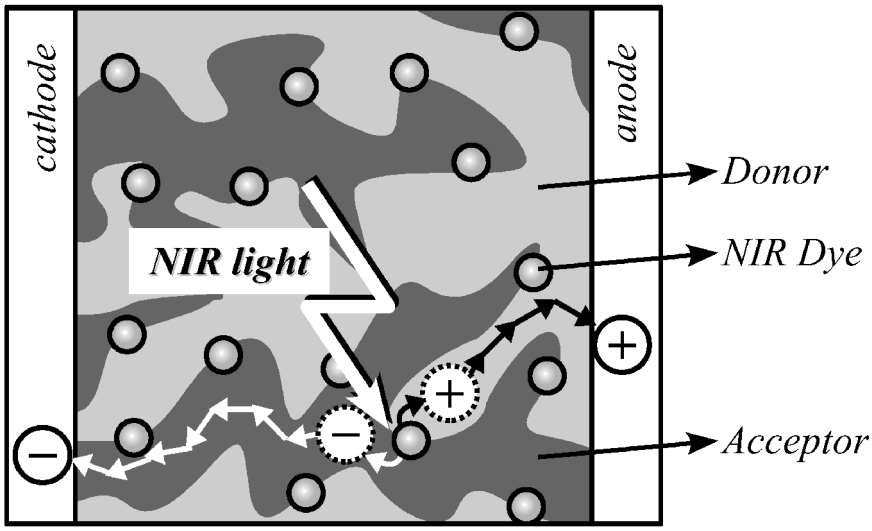


**Figure 1-5.** Schematic illustration of dye-sensitized ternary blend solar cells consisting of a donor, an acceptor, and a light-harvesting dye.

### *1.1.2. Dye Sensitization*

Here a brief history and essence of the dye sensitization, which is adopted to polymer solar cells in this thesis, are provided. Sensitization of solid materials implies usually an extension of photosensitivity towards longer wavelengths, where the original material is not sensitive to incident light. It is an interesting convergence of photography and photoelectrochemistry, both of which rely on photoinduced charge separation at a liquid/solid interface. This phenomenon was first discovered by Vogel, as early as 1873.[88] He investigated the sensitization of silver halide emulsions (with band gaps of 2.7–3.2 eV and therefore insensitive to much of the visible spectrum) with organic dyes, finding the photoresponse significantly extended into the red and even infrared, making possible the "panchromatic" broad-spectrum black and white film and then color photography. The first sensitization of a photoelectrode followed shortly thereafter, using a similar chemistry.[89] Their operating mechanism is by injection of electrons from photoexcited dye molecules into the conduction band of the n-type semiconductor substrates.[90] In subsequent years, Tsubomura *et al.* introduced a polycrystalline ZnO electrode having a high surface area to adsorb a large

amount of dyes.[91] Simultaneously, the idea developed that the dye could function most efficiently if chemically modified on the surface of the semiconductor.[91,92]

In 1991, O'Regan and Grätzel reported significantly high efficient dye-sensitized solar cells (DSSC) with a PCE of 7.1%.[93] The standard dye at the time was *tris*(2,2'-bipyridyl-4,4'-carboxylate)ruthenium (II) (Figure 1-6a), the function of the carboxylate being the attachment by chemisorption of the chromophore to the metal oxide surface. This was the highest PCE reported for organic solar cells, including polymer solar cells, in those days because of their efficient charge generation and collection processes. In dye-sensitized n-type semiconductor materials, such as $TiO_2$, a current is generated by electron injection from a photoexcited dye molecule into the conduction band of the semiconductor as shown in Figure 1-6b. Here, the semiconductor can efficiently accept electrons from dye excitons on the 100 fs or faster time scale.[94–97] This is due to the semiconductor chemically modified by the single dye layer. Such a dye layer does not require exciton migration to the interface. The fast electron injection

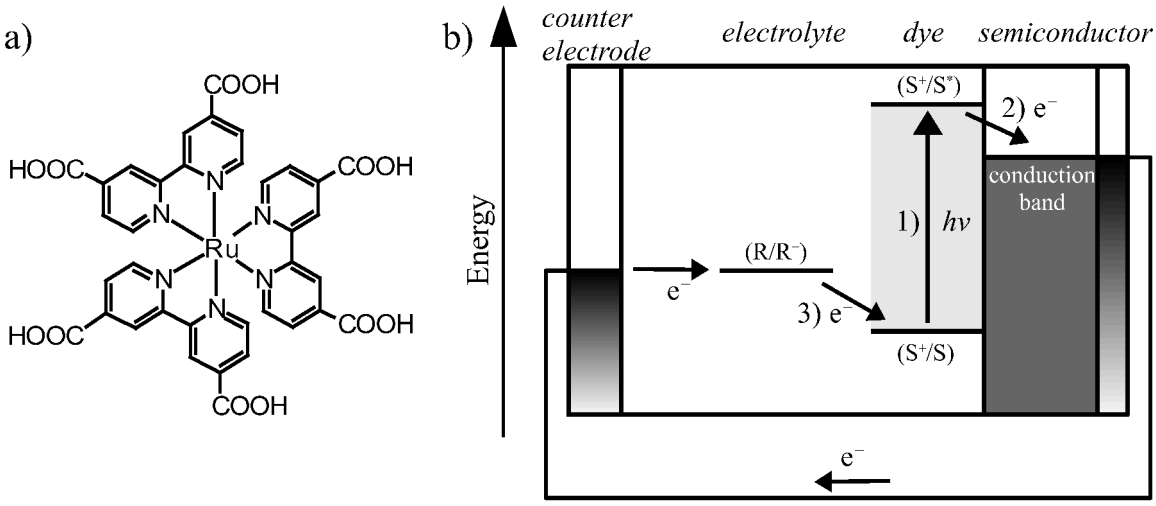


**Figure 1-6.** a) A structure of ruthenium (Ru) complex dye used in DSSC in 1990s. b) Schematic illustration of the photon-to-current conversion processes in DSSC: 1) light absorption by dyes attached on metal oxide semiconductors, 2) ultrafast electron injection from the excited state of dyes to conduction band of metal oxide, and 3) deoxidization of dye cations by electrolyte of redox couple ($R/R^-$). S, $S^*$, and $S^+$ represent sensitizer; photo-excited sensitizer; and oxidized sensitizer, respectively.

without exciton migration is the first key point for efficient dye sensitization. In addition, the high surface area of the semiconductor enables the efficient photon-harvesting by the single dye layer. To complete the circuit, the dye must be regenerated by electron transfer from a redox species in solution which is then reduced at the counter electrode (Figure 1-6b). Another key point is that the dye molecules are located just at the interface of the electron donor electrolyte and the electron acceptor metal oxide by the chemical modification. Moreover, it is also an essential key point for the highly efficient charge extraction to select the potential of the redox couple which mediates charge transfer between the electrode. In other words, the HOMO level of dyes must be lower than the potential of redox couple and the LUMO level of dyes must be higher than the conduction band of semiconductors. For further improvement of photosensitivity in DSSC, multi-colored dye sensitization with different dye molecules has been reported.[98] In most cases, however, unfavorable interactions between different dye molecules often cause degradation in the device performance. A few successful attempts have demonstrated that this problem can be avoided by constructing a dye-bilayer structure stained with two different dyes[99,100] or by selecting a suitable co-adsorbing material[101,102] to inhibit dye aggregation.

There are three key points to enhance the photosensitivity of polymer solar cells by dye molecules in DSSC: (i) the fast charge separation from the dye excitons, (ii) the selective localization of the dye at the polymer/fullerene interface, and (iii) the energy level alignment of the HOMO and LUMO energy levels of the dye (Figure 1-7a). The lower bandgap of the dye than that of the conjugated polymer is of course essential requirement for dye sensitization at longer wavelengths. The dyes of porphyrin, phthalocyanine, and naphthalocyanine derivatives shown in Figure 1-7b are well-known in various fields such as sensitizers,[103] light-emitting diodes,[104] optics,[105] and organic solar cells.[35,106,107] In particular, phthalocyanine and naphthalocyanine derivatives have a strong absorption band around 670

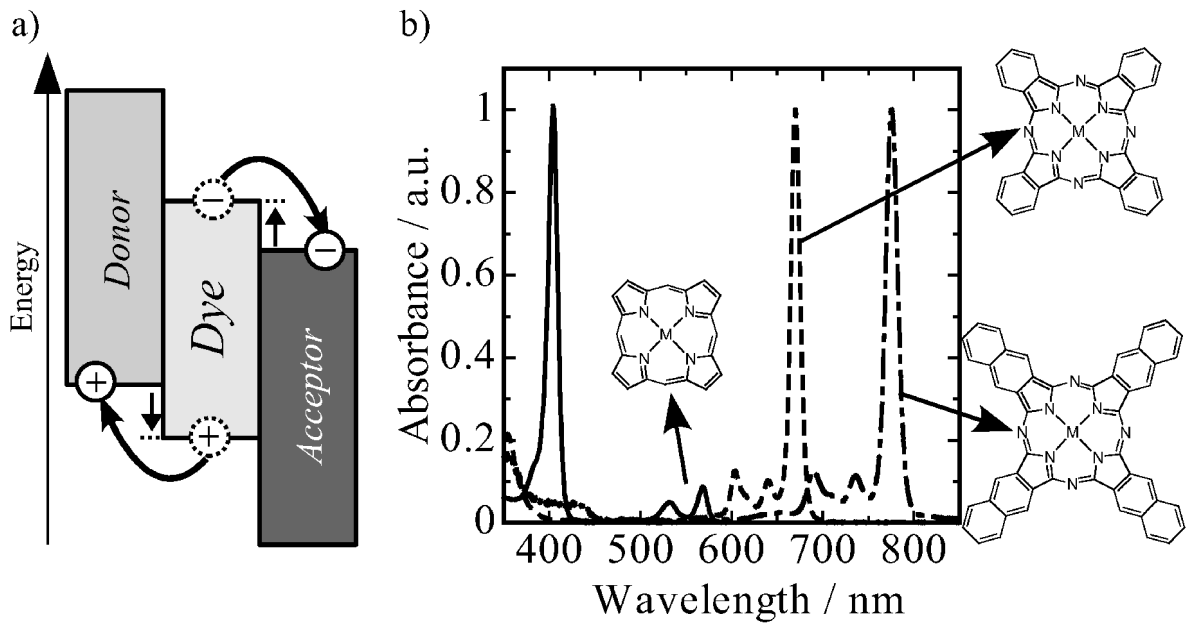


**Figure 1-7.** a) Schematic energy diagrams of a donor, an acceptor, and a dye as ternary blended materials in dye-sensitized polymer solar cells. For efficient dye sensitization, the dye must be located at the interface of donor/acceptor and LUMO level of the dye must be higher than that of the acceptor and HOMO level of the dye must be lower than that of the donor. b) Chemical structures and absorption spectra of porphyrin (solid line), phthalocyanine (broken line), and naphthalocyanine (dashed line) dyes dissolved in solution.

and 780 nm (Figure 1-7b), respectively,[104] and their HOMO and LUMO levels can be changed by changing the center metal atom and substituents connecting to (na)phthalocyanine rings.[104,108–112] Therefore, these dyes can be suitable as the third component doped into polymer solar cells to collect the NIR light.

### *1.1.3. Energy Transfer*

The energy transfer is an important photophysical process when two or more different chromophores such as conjugated polymers and dye molecules are close to each other by blending them in the same solution or film. The transfer of energy from initially excited donor to energy-accepting chromophores in the ground state is often referred to as "energy transfer" (Figure 1-8a). It can be considered that the energy transfer has a critical influence on the photophysical processes in dye-sensitized polymer solar cells. The general

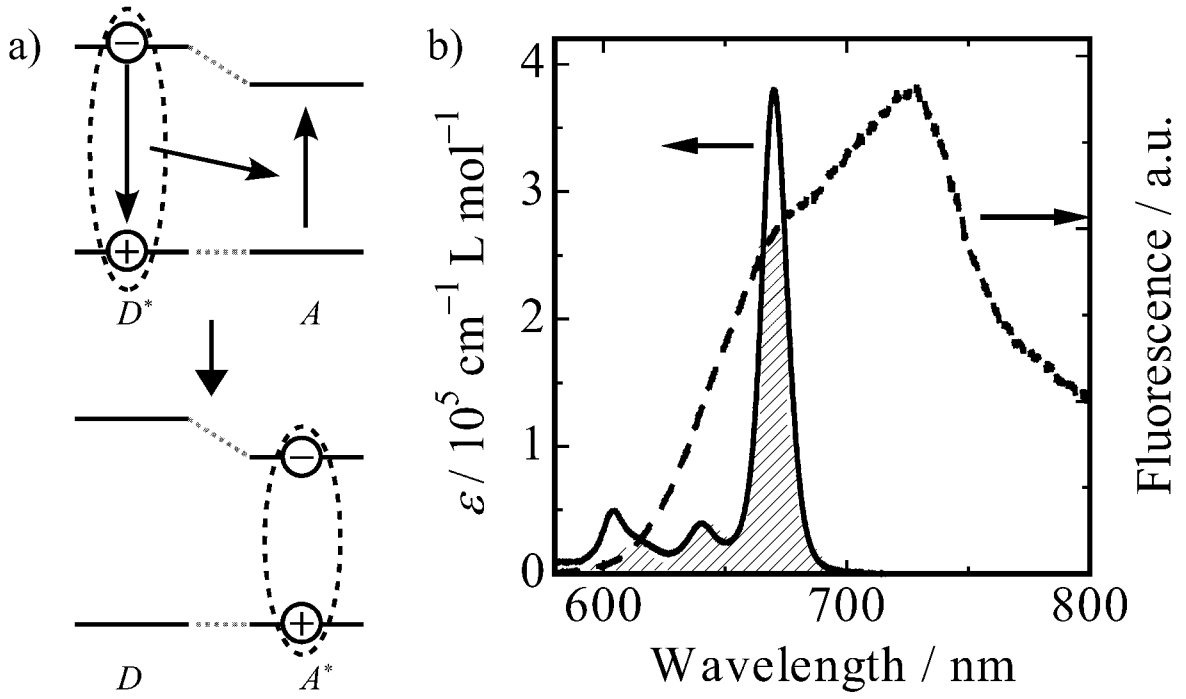


**Figure 1-8.** a) Schematic illustration of energy transfer. b) Absorption spectrum of phthalocyanine dyes (energy acceptor; solid line) and fluorescence spectrum of RR-P3HT (energy donor; broken line).

requirements for energy transfer between a donor and an acceptor are: 1) the energy of donor excited state should be higher than that of the acceptor excited state and 2) the rate of energy transfer should be more rapid than the decay rate of the donor excited state. Such energy transfer has attracted much interest in a number of emerging applications such as fluorescence imaging technologies,[113] molecular beacon biosencors,[114] electroluminescent devices,[115] and solar cells.[116,117] Energy transfer by point-dipole interaction is described by the Förster rate equation[118,119]

$$k_{\mathrm{EnT}} = \frac{1}{\tau_{\mathrm{D}}}\left(\frac{R_0}{R}\right)^6, \qquad (1-1)$$

$$R_0^6 = \frac{9000\,K^2 Q_{\mathrm{y}} \ln 10}{128\,\pi^5 n^4 N_A} \int \frac{f_D(\tilde{\nu})\epsilon_A(\tilde{\nu})}{\tilde{\nu}^4} d\,\tilde{\nu}, \qquad (1-2)$$

where $K^2$ is the orientation factor (= 0.67 for random situation), $Q_{\mathrm{y}}$ is the photoluminescence

quantum yield of the donor, $\tau_D$ is the photoluminescence lifetime of the donor, $n$ is the refractive index of the medium, $N_A$ is Avogadro's number, $R$ is the distance between the donor and the acceptor, $f_D(\tilde{\nu})$ is the peak-normalized fluorescence spectrum of the donor, $\varepsilon_A(\tilde{\nu})$ is the molar absorption coefficient of the acceptor, and $\tilde{\nu}$ is the wavenumber. The larger the overlap between the fluorescence spectrum of the donor and the absorption spectrum of the acceptor as shown in Figure 1-8b becomes, the faster the energy transfer rate becomes. $R_0$ is the critical transfer distance (Förster radius) at which the energy transfer rate is equal to the decay rate. For the donor with a high $Q_y$ and strong spectral overlap with the acceptor's absorbance, $R_0$ would typically be ~5 nm,[120–124] which is much longer than the scale of an electron transfer[125–129] and is comparable to the exciton diffusion length of the polymer excited state (~10 nm).[32–34] Therefore, it is noteworthy that the Förster radius is large enough to influence the photophysical processes in conjugated polymer based devices, such as EL devices and solar cells.

In the system of polymer solar cells based on donor:acceptor:dye ternary blends, NIR light-absorbing dye molecules doped into donor:acceptor matrices can collect energy of the polymer excited state by energy transfer because of a large spectrum overlap (Figure 1-8b). It was noted above that the dye molecules must be located at the donor/acceptor interface for efficient charge generation from the dye excitons. This is also true for the dye excitons generated by the energy transfer. Thus, the interfacial localization of the dye molecules is strongly required in donor:acceptor:dye ternary blend solar cells. After meeting such a requirement, the dye can act not only as a photosensitizer but also as an energy funnel at the donor/acceptor interface.

### *1.1.4. Ternary Blend Films*

In dye-sensitized polymer solar cells based on ternary blend films, the selective localization of dye molecules at the interface is essential for efficient dye sensitization and

energy collection as mentioned above. However, the ternary blend films consisting of three different materials show various phase separation, which is more complicated than that observed in binary blend films. The third material added can be located in one phase of the two original materials or at the interface of phases of original two materials as shown in Figures 1-9a–c. The surface free energy ($\gamma$) of materials can be considered as a key factor of selective localization. There are many reports in which the location of the third material added to the binary blend films is predicted by the surface energy of materials used in ternary blends. Sumita *et al.*[130] established a parameter of the wetting coefficient ($\omega_C$) to predict the location of material C in blends of materials A and B as follows. They considered the localization mechanism based on a simple model to minimize the total interfacial surface energy in the ternary blend system. Figure 1-9d is used to explain the wetting behavior of the particular component C at the interface of two phases (A and B). If the interfacial free energy at the interface is at minimum, the next equilibrium equation is valid:

$$\begin{aligned} \delta G &= \gamma_{C-A}\,\delta A_{C-A} + \gamma_{C-B}\,\delta A_{C-B} + \gamma_{A-B}\,\delta A_{A-B} \\ &= \gamma_{C-A}\,(2\pi r \sin\theta\, r\, \delta\theta) - \gamma_{C-B}\,(2\pi r \sin\theta\, r\, \delta\theta) + \gamma_{A-B}\,(2\pi r \sin\theta\, r\, \delta\theta) \\ &= 0\,, \end{aligned} \qquad (1-3)$$

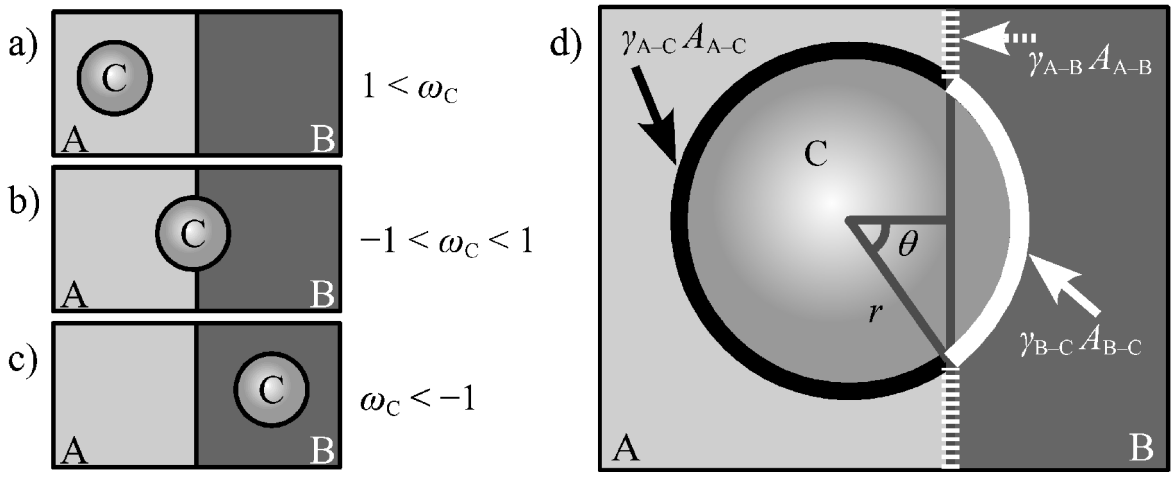


**Figure 1-9.** Schematic illustration of a-c) the location of thirdly added material C into A:B blends predicted by wetting coefficient $\omega_C$ and d) the wetting behavior of the particular component C at the interface of A/B.

where $r$ and $\theta$ are the radius and angle of material C as shown in Figure 1-9d and $A_{X-Y}$ and $\gamma_{X-Y}$ are the area and surface tension of X/Y interface, respectively. The $\gamma_{X-Y}$ can be calculated using the Neumann's equation

$$\gamma_{X-Y} = \gamma_X + \gamma_Y - 2\sqrt{\gamma_X \gamma_Y} \exp(-\beta(\gamma_X - \gamma_Y)^2), \quad (1-4)$$

where $\gamma_X$ is the surface energy of material X and $\beta$ = 0.000115 $m^4$ $mJ^{-2}$.[131] The wetting coefficient can be calculated from the interfacial surface energies in the system using Young's equation as follows:

$$\omega_C = \frac{\gamma_{C-B} - \gamma_{C-A}}{\gamma_{A-B}} \quad (1-5)$$

If $\omega_C$ is > 1, material C will be located in domain A. If $\omega_C < -1$, C will be located in domain B. If $-1 < \omega_C < 1$, C will be located at the interface between A and B, as shown in Figures 1-9a–c. This prediction of the materials doped into polymer blends has been attempted to various materials such as conductive carbon black particles,[130] carbon nanotubes,[132–134] $CaCO_3$ nanoparticles,[135] and polymers.[136] Such a prediction is adopted to the donor:acceptor:dye ternary blend films to determine the location of dyes.

## 1.2. Outline of This Thesis

The aim of this thesis is to develop the dye modification of the donor/acceptor interface in polymer solar cells and elucidate the influence of dye molecules on the device performance, film morphology, and photophysical dynamics. This thesis consists of six chapters. The first chapter describes the historical background and the motivation of this thesis. The following chapters are divided into three parts. The relationship of each chapter in this thesis is summarized in Figure 1-10.

In Part I (Chapter 2), the effect of the dye molecules located at the donor/acceptor interface are described before the attempt to construct more complicated dye-sensitized ternary blend

solar cells.

In Chapter 2, the dye modification at the interface of donor/acceptor with Ru-dye molecules in organic-inorganic hybrid solid solar cells is studied using double-layered cells consisting of RR-P3HT and a flat layer of dense $TiO_2$. The improvement of the photocurrent by dye molecules at the interface is discussed in terms of dye-sensitization and exciton-harvesting processes.

In Part II (Chapter 3–4), the author demonstrates the application of the dye sensitization to polymer:fullerene BHJ solar cells by the introduction of single or double NIR dyes.

In Chapter 3, the enhancement of the light-harvesting efficiency in RR-P3HT:PCBM BHJ solar cells is demonstrated by the introduction of phthalocyanine molecules as the third component at the RR-P3HT/PCBM interface. To examine the relationship between the device performance and the dye structure, which would affect the formation of dye aggregations in the blend film, the author employs two kinds of phthalocyanine dyes with different chemical structures as shown in Figure 1-10; a zinc phthalocyanine (ZnPc), which is easy to stack and aggregate together by an π–π interaction of phthalocyanine plane, and a silicon phthalocyanine (SiPc), which is difficult to stack each other by bulky substituents.[137,138] The improvement of light-harvesting efficiency and photocurrent by dye molecules are discussed in terms of the location of dye molecules and the light-harvesting mechanism based on the dye sensitization and the exciton harvesting.

In Chapter 4, multi-colored dye sensitization is examined for further enhancement of the sensitized window in the NIR regions. Silicon naphthalocyanine (SiNc), which also has bulky substituents perpendicular to the naphthalocyanine plane to inhibit the aggregation, is doped into RR-P3HT:PCBM blends in addition to SiPc to extend the photosensitivity up to 800 nm.

Part III (Chapter 5–6), provides more detailed information on the mechanism of dye

localization and light harvesting in dye-sensitized ternary blend films.

In Chapter 5, selective dye loading at the polymer/fullerene interface is studied for RR-P3HT:PCBM:SiPc ternary blend BHJ solar cells. The interfacial segregation of dye molecules in ternary blend films is discussed in terms of the surface energy of each component and the crystallization of P3HT enhanced by annealing.

In Chapter 6, the light-harvesting mechanism by dye molecules loaded into polymer:fullerene blends is comprehensively studied by transient absorption spectroscopy for ternary blend films of RR-P3HT:PCBM:SiPc. On the basis of quantitative analyses of transient absorption spectra and decay dynamics upon dye or polymer excitation, the fundamental photovoltaic conversion processes are demonstrated. Furthermore, the interfacial morphology of blend films is discussed through the annealing conditions and the dynamics to the charge separation.

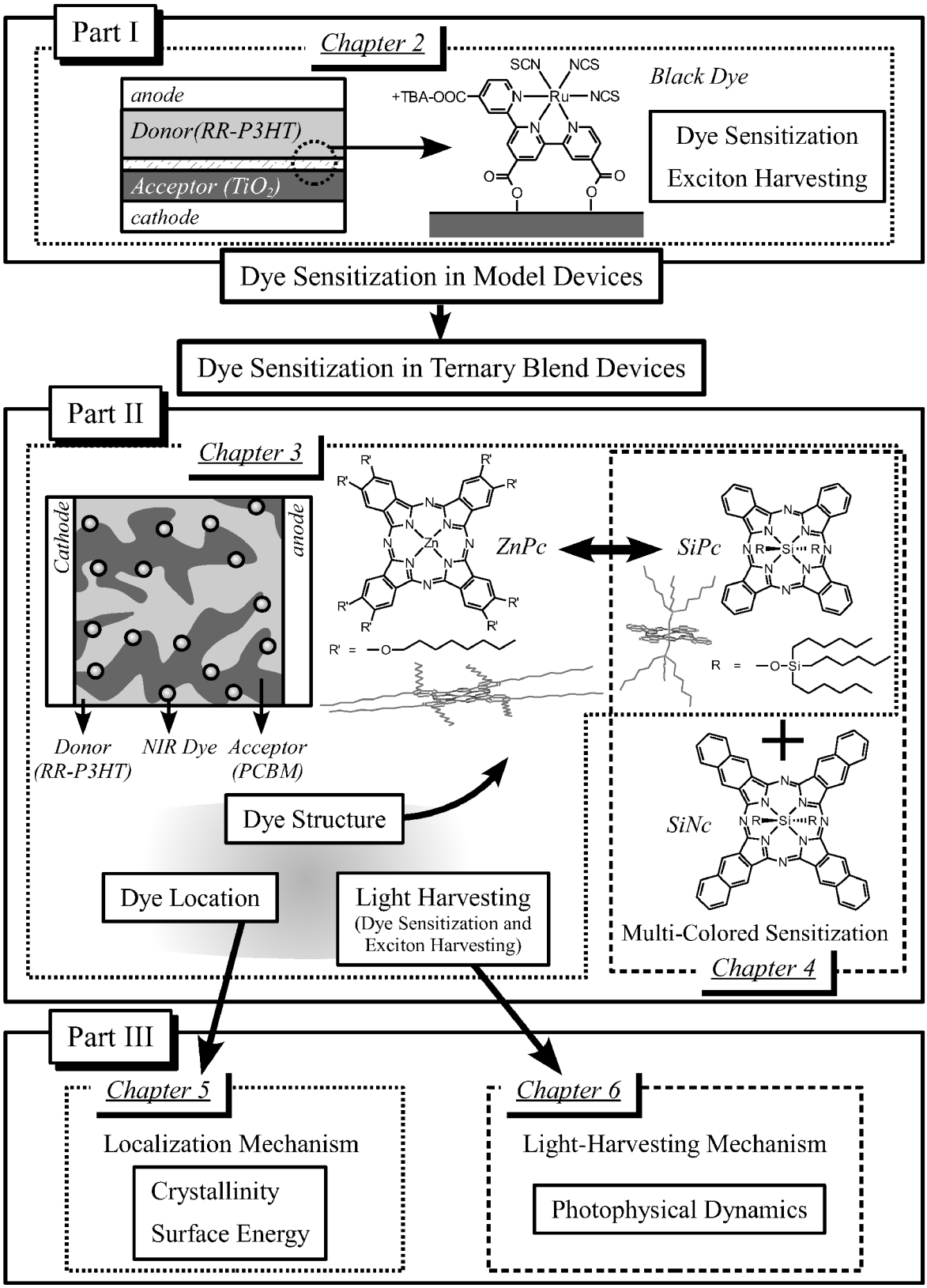


**Figure 1-10.** Relationship of each chapter in this thesis.

## References


(1) Chiang, C. K.; Fincher, C. R., Jr.; Park, Y. W.; Heeger, A. J.; Shirakawa, H.; Louis, E. J.; Gau, S. C.; MacDiarmid, A. G. *Phys. Rev. Lett.* **1977**, *39*, 1098–1101.

(2) Günes, S.; Neugebauer, H.; Sariciftci, N. S. *Chem. Rev.* **2007**, *107*, 1324–1338.

(3) Hoppe, H.; Sariciftci, N. S. *Adv. Polym. Sci.* **2008**, *214*, 1–86.

(4) Peet, J.; Heeger, A. J.; Bazan, G. C. *Acc. Chem. Res.* **2009**, *42*, 1700–1708.

(5) Krebs. F. C. *Solar Energy Mater. Solar Cells* **2009**, *93*, 394–412.

(6) Cheng, Y.-J.; Yang, S.-H.; Hsu, C.-S. *Chem. Rev.* **2009**, *109*, 5868–5923.

(7) Brabec, C. J.; Gowrisanker, S.; Halls, J. J. M.; Laird, D.; Jia, S.; Shawn P.; Williams, S. P. *Adv. Mater.* **2010**, *22*, 3839–3856.

(8) Deibel, C.; Dyakonov, V. *Rep. Prog. Phys.* **2010**, *73*, 096401.

(9) van Bavel, S.; Veenstra, S.; Loos, J. *Macromol. Rapid Commun.* **2010**, *31*, 1835–1845.

(10) Po, R.; Maggini, M.; Camaioni, N. *J. Phys. Chem. C* **2010**, *114*, 695–706.

(11) Delgado, J. L.; Bouit, P.-A.; Filippone, S.; Herranz, M. A.; Martín, N. *Chem. Commun.* **2010**, *46*, 4853–4865.

(12) Nielsen, T. D.; Cruickshank, C.; Foged, S.; Thorsen, J.; Krebs, F. C. *Solar Energy Mater. Solar Cells* **2010**, *94*, 1553–1571.

(13) Friend, R. H.; Gymer, R. W.; Holmes, A. B.; Burroughes, J. H.; Marks, R. N.; Taliani, C.; Bradley, D. D. C.; Santos, D. A. D.; Brédas, J. L.; Lögdlund, M.; Salaneck, W. R. *Nature* **1999**, *397*, 121–128.

(14) Gong, X.; Tong, M.; Xia, Y.; Cai, W.; Moon, J. S.; Cao, Y.; Yu, G.; Shieh, C.-L.; Nilsson, B.; Heeger, A. J. *Science* **2009**, *325*, 1665–1667.

(15) Stutzmann, N.; Friend, R. H.; Sirringhaus, H. *Science* **2003**, *299*, 1881–1884.

(16) Hide, F.; Díaz-García, M. A.; Schwartz, B. J.; Heeger, A. J. *Acc. Chem. Res.* **1997**, *30*, 430–436.

(17) McGehee, M. D.; Heeger, A. J. *Adv. Mater.* **2000**, *12*, 1655–1668.

(18) Thomas III, S. W.; Joly, G. D.; Swager, T. M. *Chem. Rev.* **2007**, *107*, 1339–1386.

(19) Jäkle, F. *Chem. Rev.* **2010**, *110*, 3985–4022.

(20) Herland, A.; Inganäs, O. *Macromol. Rapid Commun.* **2007**, *28*, 1703–1713.

(21) Szlufcik, J.; Sivoththaman, S.; Nlis, J. F.; Mertens, R. P.; Van Overstraeten, R. *Proc. IEEE*, **1997**, *85*, 711–730.

(22) Tanabe, K. *Energies* **2009**, *2*, 504–530.

(23) Morita, S.; Zakhidov, A. A.; Yoshino, K. *Solid State Commun.* **1992**, *82*, 249–252.

(24) Sariciftci, N. S.; Smilowitz, L.; Heeger, A. J.; Wudi, F. *Science* **1992**, *258*, 1474–1476.

(25) Peumans, P.; Yakimov, A.; Forrest, S. R. *J. Appl. Phys.* **2003**, *93*, 3693–3723.

(26) Goris, L.; Haenen, K.; Nesládek, M.; Wangner, P.; Vanderzande, D.; de Schepper, L.; D'Haen, J.; Lutsen, L.; Manca, J. V. *J. Mater. Sci.* **2005**, *40*, 1413–1418.

(27) Ameri, T.; Dennler, G.; Waldauf, C.; Denk, P.; Forberich, K.; Scharber, M. C.; Brabec, C. J.; Hingerl, K. *Appl. Phys. Lett.* **2008**, *103*, 084506.

(28) Dash, C. W.; Newman, R. *Phys. Rev.* **1955**, *99*, 1151–1155.

(29) Santbergen, R.; van Zolingen, R. J. C. *Solar Energy Mater. Solar Cells* **2008**, *92*, 432–444.

(30) Kübler, J. K. *Phys. Stat. Sol.* **1969**, *35*, 189–195.

(31) Knupfer, M. *Appl. Phys. A* **2003**, *77*, 623–626.

(32) Peumans, P.; Yakimov, A.; Forrest, S. R. *J. Appl. Phys.* **2004**, *93*, 3693–3723.

(33) Yang, L-G.; Chen, H-Z.; Wang, M. *Thin Solid Films* **2008**, *516*, 7701–7707.

(34) Lunt, R. R.; Giebink, N. C.; Belak, A. A.; Benziger, J. B.; Forrest, S. R. *J. Appl. Phys.* **2009**, *105*, 053711.

(35) Tang, C. W. *Appl. Phys. Lett.* **1986**, *48*, 183–185.

(36) Sariciftci, N. S.; Braun, D.; Zhang, C.; Srdanov, V. I.; Heeger, A. J.; Stucky, G.; Wudl,

F. *Appl. Phys. Lett.* **1993**, *62*, 585–587.

(37) Yu, G.; Gao, J.; Hummelen, J. C.; Wudi, F.; Heeger, A. J. *Science* **1995**, *270*, 1789–1791.

(38) Hiramoto, M.; Fujiwara, H.; Yokoyama, M. *Appl. Phys. Lett.* **1991**, *58*, 1062–1064.

(39) Yang, C. Y.; Heeger, A. J. *Synth. Met.* **1996**, *83*, 85–88.

(40) Halls, J. J. M.; Walsh, C. A.; Greenham, N. C.; Narseglia, E. A.; Friend, R. H.; Moratti, S. C.; Holmes, A. B. *Nature* **1995**, *376*, 498–500.

(41) Veenstra, A. C.; Verhees, W. J. H.; Kroon, J. M.; Koetse, M. M.; Sweelssen, J.; Bastiaansen, J. J. A. M.; Schoo, H. F. M.; Yang, X.; Alexeev, A.; Loos, J.; Schubert, U. S.; Wienk, M. M. *Chem. Mater.* **2004**, *16*, 2503–2508.

(42) Alam, M. M.; Jenekhe, S. A. *Chem. Mater.* **2004**, *16*, 4647–4656.

(43) Kim, Y.; Cook, S.; Choulis, S. A.; Nelson, J.; Durrant, J. R.; Bradley, D. D. C. *Chem. Mater.* **2004**, *16*, 4812–4818.

(44) Kietzke, T.; Hörhold, H.-H.; Neher, D. *Chem. Mater.* **2005**, *17*, 6532–6537.

(45) McNeill, C. R.; Abrusci, A.; Zaumseil, J.; Wilson, R.; McKiernan, M. J.; Burroughes, J. H.; Halls, J. J. M.; Greenham, N. C.; Friend, R. H. *Appl. Phys. Lett.* **2007**, *90*, 193506.

(46) Savenije, T. J.; Warman, J. M.; Goossens, A. *Chem. Phys. Lett.* **1998**, *287*, 148–153.

(47) Salafsky, J. S. *Phys. Rev. B* **1999**, *59*, 10885–10894.

(48) Arango, A. C.; Carter, S. A.; Brock, P. J. *Appl. Phys. Lett.* **1999**, *74*, 1698–1700.

(49) Ravirajan, P.; Haque, S. A.; Durrant, J. R.; Poplavskyy, D.; Bradley, D. D. C.; Nelson, J. *J. Appl. Phys.* **2004**, *95*, 1473–1480.

(50) Ohkita, H.; Shimazaki, Y.; Ohoka, M.; Ito, S. *Chem. Lett.* **2004**, *33*, 1598–1599.

(51) Ravirajan, P.; Peiró, A. M.; Nazeeruddin, M. K.; Grätzel, M.; Bradley, D. D. C.; Durrant, J. R.; Nelson, J. *J. Phys. Chem. B* **2006**, *110*, 7635–7639.

(52) Peiró, A. M.; Ravirajan, P.; Govender, K.; Boyle, D. S.; O'Brien, P.; Bradley, D. D. C.; Nelson, J.; Durrant J. R. *J. Mater. Chem.* **2006**, *16*, 2088–2096.

(53) Kudo, N.; Shimazaki, Y.; Ohkita, H.; Ohoka, M.; Ito, S. *Sol. Energy Sol Mater.* **2007**, *91*, 1243–1247.

(54) Goh, C.; Scully, S. R.; McGehee, M. D. *J. Appl. Phys.* **2007**, *101*, 114503.

(55) Halme, J.; Vahermaa , P.; Miettunen, K.; Lund, P. *Adv. Mater.* **2010**, *22*, E210–E234.

(56) Grätzel, M. *Chem. Lett.* **2005**, *34*, 8–13.

(57) Chiba, Y.; Islam, A.; Watanabe, Y.; Komiya, R.; Koide, N.; Han, L. Y. *Jpn. J. Appl. Phys., Part 2* **2006**, *45*, L638–L640.

(58) Camaioni, N.; Ridolfi, G.; Casalbore-Miceli, G.; Possamai, G.; Maggini, M. *Adv. Mater.* **2002**, *14*, 1735–1738.

(59) Camaioni, N.; Garlaschelli, L.; Geri, A.; Maggini, M.; Possamai, G.; Ridolfi, G. *J. Mater. Chem.* **2002**, *12*, 2065–2070.

(60) Prosa, T. J.; Winokur, M. J.; Moulton, J.; Smith, P.; Heeger, A. J. *Macromolecules* **1992**, *25*, 4364–4372.

(61) Ma, W.; Yang, C.; Gong, X.; Lee, K.; Heeger, A. J. *Adv. Funct. Mater.* **2005**, *15*, 1617–1622.

(62) Huang, J.; Li, G.; Yang, Y. *Appl. Phys. Lett.* **2005**, *87*, 112105.

(63) Savenije, T. J.; Kroeze, J. E.; Yang, X.; Loos, J. *Adv. Funct. Mater.* **2005**, *15*, 1260–1266.

(64) Mihailetchi, V. D.; Xie, H. X.; de Boer, B.; Koster L. J. A.; Blom, P. W. M. *Adv. Funct. Mater.* **2006**, *16*, 699–708.

(65) Li, G.; Shrotriya, V.; Huang, J.; Yao, Y.; Moriarty, T.; Emery, K.; Yang, Y. *Nat. Mater.* **2005**, *4*, 864–868.

(66) Kim, Y.; Cook, S.; Tuladhar, S. M.; Choulis, S. A.; Nelson, J.; Durrant, J. R.; Bradley,

D. D. C.; Giles, M.; McCulloch, I.; Ha, C.-S.; Ree, M. *Nat. Mater.* **2006**, *5*, 197–203.

(67) Schilinsky, P.; Asawapirom, U.; Scherf, U.; Biele, M.; Brabec, C. J. *Chem. Mater.* **2005**, *17*, 2175–2180.

(68) Hiorns, R. C.; de Bettignies, R.; Leroy, J.; Bailly, S.; Firon, M.; Sentein, C.; Khoukh, A.; Preud'homme, H.; Dagron-Lartigau, C. *Adv. Funct. Mater.* **2006**, *16*, 2263–2273.

(69) Kim, Y.; Choulis, S. A.; Nelson, J.; Bradley, D. D. C.; Cook, S.; Durrant, J. R. *Appl. Phys. Lett.* **2005**, *86*, 063502.

(70) Al-Ibrahim, M.; Ambacher, O.; Sensfuss, S.; Gobsch, G. *Appl. Phys. Lett.* **2005**, *86*, 201120.

(71) Park, J. H.; Kim, J. S.; Lee, J. H.; Lee, W. H.; Cho, K. *J. Phys. Chem. C* **2009**, *113*, 17579–17584.

(72) Lee, J. K.; Coates, N. E.; Cho, S.; Cho, N. S.; Moses, D.; Bazan, G. C.; Lee, K.; Heeger, A. J. *Appl. Phys. Lett.* **2008**, *92*, 243308.

(73) Yao, Y.; Hou, J.; Xu, Z.; Li, G.; Yang, Y. *Adv. Funct. Mater.* **2008**, *18*, 1783–1789.

(74) van Bavel, S. S.; Sourty, E.; de With, G.; Loos, J. *Nano Lett.* **2009**, *9*, 507–513.

(75) Groves, C.; Reid, O. G.; Ginger, D. S. *Acc. Chem. Res.* **2010**, *43*, 612–620.

(76) Spadafora, E. J.; Demadrille, R.; Ratier, B.; Grévin, B. *Nano Lett.* **2010**, *10*, 3337–3342.

(77) Andersson, B. V.; Herland, A.; Masich, S.; Inganäs, O. *Nano Lett.* **2009**, *9*, 853–855.

(78) van Bavel, S. S.; Bärenklau, M.; de With, G.; Hoppe, H.; Loos, J. *Adv. Funct. Mater.* **2010**, *20*, 1458–1463.

(79) Bundgaard, E.; Krebs, F. C. *Sol. Energy Mater. Sol. Cells* **2007**, *91*, 954–985.

(80) Kroon, R.; Lenes, M.; Hummelen, J. C.; Blom, P. W. M.; de Boer, B. *Polym. Rev.* **2008**, *48*, 531–582.

(81) Peet, J.; Kim, J. Y.; Coates, N. E.; Ma, W. L.; Moses, D.; Heeger, A. J.; Bazan, G. C.

*Nat. Mater.* **2007**, *6*, 497–500.

(82) Chen, H.-Y.; Hou, J.; Zhang, S.; Liang, Y.; Yang, G.; Yang, Y.; Yu, L.; Wu, Y.; Li, G.; *Nat. Photonics* **2009**, *3*, 649–653.

(83) Konarka Technologies, Inc. "Konarka News – Konarka Technologies" available from http://www.konarka.com/index.php/newsroom/press-release-list/ (accessed Dec. 8, 2010.)

(84) Peet, J.; Tamayo, A. B.; Dang, X.-D.; Seo, J. H.; Nguyen, T.-Q. *Appl. Phys. Lett.* **2008**, *93*, 163306.

(85) Ltaief, A.; Chaâbane, R. B.; Bouazizi, A.; Davenas, *J. Mater. Sci. Eng. C* **2006**, *26*, 344–347.

(86) Dastoor, P. C.; McNeill, C. R.; Frohne, H.; Foster, C. J.; Dean, B.; Fell, C. J.; Belcher, W. J.; Campbell, W. M.; Officer, D. L.; Blake, I. M.; Thordarson, P.; Crossley, M. J.; Hush, N. S.; Reimers, J. R. *J. Phys. Chem. C* **2007**, *111*, 15415–15426.

(87) Kaulach, I.; Muzikante, I.; Gerca, L.; Plotniece, M.; Roze, M.; Kalnachs, J.; Shlihta, G.; Shipkovs, P.; Kampars, V.; Tokmakov, *A. Eur. Phys. J. Appl. Phys.* **2007**, *40*, 169–173.

(88) Vogel, H. *Ber. Dtsch. Chem. Ges.* **1873**, *6*, 1302–1306.

(89) Moser, J. *Monatsh. Chem.* **1887**, *8*, 373.

(90) Gerischer, H.; Tributsch, H. *Ber. Bunsenges. Phys. Chem.* **1968**, *72*, 437–445.

(91) Tsubomura, H.; Matsumura, M.; Noyamura, Y.; Amamyiya, T. *Nature* **1976**, *261*, 402–403.

(92) Dare-Edwards, M. P.; Goodenough, J. B.; Hamnet, A.; Seddon, K. R.; Wright, R.D. *Faraday Disc., Chem. Soc.* **1980**, *70*, 285–298.

(93) O'Regan, B.; Grätzel, M. *Nature* **1991**, *353*, 737–740.

(94) Tachibana, Y.; Moser, J. E.; Grätzel, M.; Klug, D. R.; Durrant, J. R. *J. Phys. Chem.*

**1996**, *100*, 20056–20062.

(95) Asbury, J. B.; Hao, E.; Wang, Y.; Ghosh, H. N.; Lian, T. *J. Phys. Chem. B* **2001**, *105*, 4545–4557.

(96) Bauer, C.; Boschloo, G.; Mukhtar, E.; Hagfeldt, A. *J. Phys. Chem. B* **2001**, *105*, 5585–5588.

(97) Benkö, G.; Kallioinen, J.; Korppi-Tommola, J. E. I.; Yartsev, A. P.; Sundström, V. *J. Am. Chem. Soc.* **2002**, *124*, 489–493.

(98) Choi, H.; Kim, S.; Kang, S. O.; Ko, J.; Kang, M.-S.; Clifford, J. N.; Forneli, A.; Palomares, E.; Nazeeruddin, M. K.; Grätzel, M. *Angew. Chem., Int. Ed.* **2008**, *47*, 8259–8263.

(99) Inakazu, F.; Noma, Y.; Ogomi Y.; Hayase, S. *Appl. Phys. Lett.* **2008**, *93*, 093304.

(100) Lee, K.; Park, S. W.; Ko, M. J.; Kim, K.; Park, N.-G. *Nat. Mater.* **2009**, *8*, 665–671.

(101) Kroon, J. M.; Bakker, N. J.; Smit, H. J. P.; Liska, P.; Thampi, K. R.; Wang, P.; Zakeeruddin, S. M.; Grätzel, M.; Hinsch, A.; Hore, S.; Würfel, U.; Sastrawan, R.; Durrant, J. R.; Palomares, E.; Pettersson, H.; Gruszecki, T.; Walter, J.; Skupien, K.; Tulloch, G. E. *Prog. Photovolt.: Res. Appl.* **2007**, *15*, 1–18.

(102) Ogura, R. Y.; Nakane, S.; Morooka, M.; Orihashi, M.; Suzuki, Y.; Noda, K. *Appl. Phys. Lett.* **2009**, *94*, 073308.

(103) Darwent. J. R.; Douglas, P.; Harriman, A.; Porter, G.; Richoux, M.-C. *Coord. Chem. Rev.* **1982**, *44*, 83–126.

(104) Flora, W. H.; Hall, H. K.; Armstrong, N. R. *J. Phys. Chem. B* **2003**, *107*, 1142–1150.

(105) Calvete, M.; Yang, G. Y.; Hanack, M. *Synth. Met.* **2004**, *141*, 231–243.

(106) Chamberlain, G. A. *Solar Cells* **1983**, *8*, 47–83.

(107) Imahori, H.; Fukuzumi, S. *Adv. Funct. Mater.* **2004**, *14*, 525–536.

(108) Schlettwein, D.; Armstrong, N. R. *J. Phys. Chem.* **1994**, *98*, 11771–11779.

(109) Fox, J. P.; Goldberg, D. P. *Inorg. Chem.* **2003**, *42*, 8181–8191.

(110) Fukuda, T.; Homma, S.; Kobayashi, N. *Chem. Eur. J.* **2005**, *11*, 5205–5216.

(111) Li, R.; Zhang, X.; Zhu, P.; Ng, D. K. P.; Kobayashi, N.; Jiang, J. *Inorg. Chem.* **2006**, *45*, 2327–2334.

(112) Kao, P.-C.; Chu, S.-Y.; Liu, S.-J.; You, Z.-X.; Chuang, C.-A. *J. Electrochem. Soc.* **2006**, *153*, H122–H126.

(113) Jares-Erijman, E. A.; Jovin, T. M. *Nat. Biotech.* **2003**, *21*, 1387–1395.

(114) Medintz, I. L.; Clapp, A. R.; Mattoussi, H.; Goldman, E. R.; Fisher, B.; Mauro, J. M. *Nat. Mater.* **2003**, *2*, 630–638.

(115) Gong, X.; Wang, S.; Moses, D.; Bazan, G. C.; Heeger, A. J. *Adv. Mater.* **2005**, *17*, 2053–2058.

(116) Liu, Y.; Summers, M. A.; Edder, C.; Fréchet, J. M. J.; McGehee, M. D. *Adv. Mater.* **2005**, *17*, 2960–2969.

(117) Hardin, B. E.; Hoke, E. T.; Armstrong, P. B.; Yum, J.-H.; Comte, P.; Torres, T.; Fréchet, J. M. J.; Nazeeruddin, M. K.; Grätzel, M.; McGehee, M. D. *Nat. Photonics* **2009**, *3*, 406–411.

(118) Förster, T. *Discuss Faraday Soc.* **1959**, *27*, 7–17.

(119) Förster, T. in *Modern Quantum Chemistry, Vol. III*; Academic Press, New York, 1965.

(120) Ha, T.; Rasnik, I.; Cheng, W.; Babcock, H. P.; Gauss, G. H.; Lohman, T. M.; Chu, S. *Nature* **2002**, *419*, 638–641.

(121) Fan, C.; Wang, S.; Hong, J. W.; Bazan, G. C.; Plaxco, K. W.; Heeger, A. J. *Proc. Natl. Acad. Sci. USA* **2003**, *100*, 6297–6301.

(122) Hofkens, J.; Cotlet, M.; Vosch, T.; Tinnefeld, P.; Weston, K. D.; Ego, C.; Grimsdale, A.; Müllen, K.; Beljonne, D.; Brédas, J. L.; Jordens, S.; Schweitzer, G.; Sauer, M.; de Schryver, F. *Proc. Natl. Acad. Sci. USA* **2003**, *100*, 13146–13151.

(123) Scholes, G. D.; Andrews, D. L. *Phys. Rev. B* **2005**, *72*, 125331.

(124) Allan, G.; Delerue, C. *Phys. Rev. B* **2007**, *75*, 195311.

(125) Stynes, H. C.; Ibers, J. A. *Inorg. Chem.* **1971**, *10*, 2304–2308.

(126) Mauk, A. G.; Scott, R. A.; Gray, H. B. *J. Am. Chem. Soc.* **1980**, *102*, 4360–4363.

(127) Hush, N. S. *Coord. Chem. Rev.* **1985**, *64*, 135–157.

(128) Tsuchida, E.; Kaneko, M.; Nishide, H.; Hoshino, M. *J. Phys. Chem.* **1986**, *90*, 2283–2284.

(129) Lewis, F. D.; Wu, T.; Zhang, Y.; Letsinger, R. L.; Greenfield, S. R.; Wasielewski, M. R. *Science* **1997**, *277*, 673–676.

(130) Sumita, M.; Sakata, K.; Asai, S.; Miyasaka, K.; Nakagawa, H. *Polym. Bull.* **1991**, *25*, 265–271.

(131) Li, D.; Neumann, A. W. *J. Colloid Interface Sci.* **1990**, *137*, 304–307.

(132) Wu, M.; Shaw, L. *J. Appl. Polym. Sci.* **2006**, *99*, 477–488.

(133) Göldel, A.; Kasaliwal, G.; Pötschke, P. *Macromol. Rapid Commun.* **2009**, *30*, 423–429.

(134) Baudouin, A.-C.; Devaux, J.; Bailly, C. *Polymer* **2010**, *51*, 1341–1354.

(135) Ma, C. G.; Zhang, M. Q.; Rong, M. Z. *J. Appl. Polym. Sci.* **2007**, *103*, 1578–1584.

(136) Cheng, T. W.; Keskkula, H.; Paul, D. R. *Polymer* **1992**, *33*, 1606–1619.

(137) Li, H.; Jensen, T. J.; Fronczek, F. R.; Vicente, M. G. H. *J. Med. Chem.* **2008**, *51*, 502–511.

(138) Barger, W. R.; Hur, E.; Ferraudi, G.; Leznoff, C. C.; Nyokong, T.; Rosenthal, I.; Snow, A. W.; Stillman, M. J.; Wöhrle, D. In *Phthalocyanines, Properties and Applications*; VCH Publishers, Inc., New York, 1989; Vol. 1.

# *Part I*

# *Chapter 2*

# Improvement of Charge Injection Efficiency in Organic-Inorganic Hybrid Solar Cells by Chemical Modification of Metal Oxides with Organic Molecules

## 2.1. Introduction

Much attention has been focused on organic-inorganic hybrid solar cells with the expectation of producing materials integrating the advantages of the two materials: solution processability, high hole mobility, and photosensitivity of conjugated polymers and high electron mobility of inorganic semiconductors. However, the energy conversion efficiency ($\eta$) of the hybrid solar cells is still low (~1%)[1–4] owing to the poor interfacial contact between the organic and inorganic materials. Thus, much effort has been devoted to improve the electronic junction between the two materials by incorporating conjugated polymers into porous metal oxide[5,6] or controlling the blending morphology of the conjugated polymer and inorganic nanoparticles.[7] Previously, the author's group have reported that surface modification of $SnO_2$ nanoparticles with a fullerene derivative improves the cell performance.[8,9] This indicates that the chemical modification with organic molecules enhances the electron injection efficiency from a conjugated polymer to $SnO_2$ or improves the interfacial contact between them. Only recently there are some reports on similar improvement in the photocurrent by the chemical modification with ruthenium dyes,[10,11] although most studies have thus far focused on the photosensitizing effect of the dyes because they serve as an efficient photosensitizer for $TiO_2$ in dye-sensitized solar cells resulting in an

energy conversion efficiency of over 11%.[12,13] However, the mechanism for the improvement by the chemical modification is poorly understood. Here the author fabricates double layered hybrid solid solar cells consisting of regioregular-poly(3-hexylthiophene) (RR-P3HT) and a flat layer of dense $TiO_2$ (*d*-$TiO_2$) to address the effect of chemical modification of the metal oxide surface with organic dye molecules.

## 2.2. Experimental Methods

Double layered hybrid solar cells were fabricated as follows. A flat layer of *d*-$TiO_2$ (60 nm) was prepared on an indium tin oxide (ITO) substrate (10 Ω per square) by sol-gel method.[14] The substrate coated with *d*-$TiO_2$ was immersed in an ethanol solution of tris(isothiocyanato)ruthenium(II)-2,2′:6′,2″-terpyridine-4,4′,4″-tricarboxylic acid, tris-tetrrabutylammonium salt (Black Dye, Solaronix SA). A hole-transport layer (50 nm) was prepared on the *d*-$TiO_2$ layer by spin coating from a chlorobenzene solution of regioregular RR-P3HT (Aldrich, *Mw* = 87,000). Finally, the Au electrode (50 nm) was thermally deposited on the top of the polymer films at $2.5\times10^{-6}$ Torr. For nanoporous hybrid solar cells, a nanoporous $TiO_2$ layer (np-$TiO_2$, 180 nm) was prepared on the *d*-$TiO_2$ layer by spin coating from an aqueous solution of anatase $TiO_2$ nanoparticles with a diameter of 20 nm (Solaronix SA) and subsequently sintered at 150 °C for 30 min. Another ruthenium dye, *cis*-bis(isothiocyanato)bis(2,2′-bipyridyl-4,4′-dicarboxylato)ruthenium(II) (N3, Peccell), was also used for the nanoporous hybrid solar cells.

## 2.3. Results and Discussion

Figure 2-1 shows the current density–voltage (*J–V*) characteristics of nanoporous hybrid solar cells based on RR-P3HT and np-$TiO_2$ with and without N3 under simulated AM1.5G irradiation at an intensity of 100 mW $cm^{-2}$ in the air. Modifying the np-$TiO_2$ layer with N3, short-circuit current density ($J_{SC}$) of the hybrid solar cell reached 1.1 mA $cm^{-2}$, which was 2.2

times larger than that without N3. Nelson and co-workers have also reported on similar increases in the photocurrent for hybrid polymer-metal oxide solar cells modified with a ruthenium dye.[10,11] It seems plausible that the increased photocurrent is ascribed to the efficient photosensitizing effect of the dyes for metal oxide owing to the large absorption bands in the visible region and the effective electronic coupling through chemical bonding onto the metal oxide surface. Interestingly, similar improvement has been also observed for other hybrid solar cells based on poly(2-methoxy-5-(3′,7′-dimethyloctyloxy)-*p*-phenylenevinylene) (MDMO-PPV) and np-$SnO_2$ modified with $C_{60}C(COOH)_2$; $J_{SC}$ increases by a factor of 1.5 owing to the chemical modification (Table 2-1).[9] However, the 1.5-fold increase in $J_{SC}$ cannot be explained by the photosensitizing effect of $C_{60}C(COOH)_2$ because $C_{60}C(COOH)_2$ can capture only one-tenth photons compared with N3 owing to its small molar absorption coefficient. These results suggest that other mechanisms are involved in the increase in $J_{SC}$. As have been discussed in previous studies,[9–11] the chemical modification may improve electron injection efficiency in itself from the polymer to the metal oxide. However,

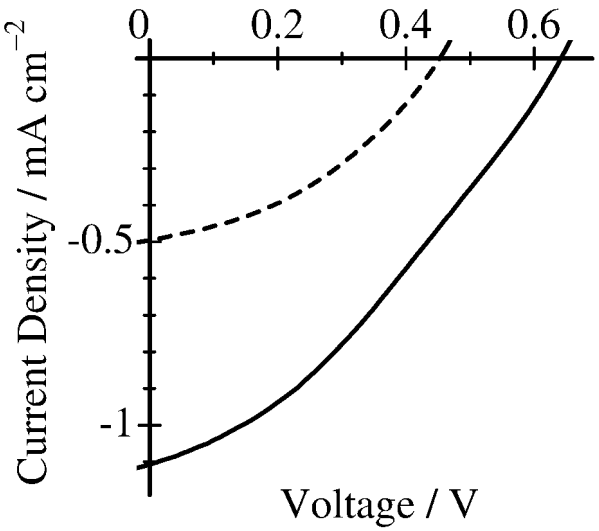


**Figure 2-1.** *J–V* characteristics of organic-inorganic hybrid solar cells with a layered structure of ITO|*d*-$TiO_2$ (60 nm)|np-$TiO_2$ (180 nm)/N3/RR-P3HT (50 nm)|Au cell (solid line) and ITO|*d*-$TiO_2$ (60 nm)|np-$TiO_2$ (180 nm)/RR-P3HT (50 nm)|Au cell (broken line).

**Table 2-1.** Cell performances of hybrid solar cells under the illumination of AM1.5G simulated solar light at an intensity of 100 mW cm$^{-2}$.

| Metal oxides | Modification molecules | Polymers | $J_{SC}$ / mA cm$^{-2}$ | $V_{OC}$ / V | FF | PCE / % | Ref. |
|---|---|---|---|---|---|---|---|
| np-$SnO_2$ | $C_{60}C(COOH)_2$ | MDMO-PPV | 0.32 | 0.63 | 0.42 | 0.085 | 9 |
| np-$SnO_2$ | ··· | MDMO-PPV | 0.22 | 0.57 | 0.52 | 0.064 | 9 |
| np-$TiO_2$[a] | N3 | RR-P3HT | 1.11 | 0.64 | 0.34 | 0.24 | This work |
| np-$TiO_2$[a] | ··· | RR-P3HT | 0.50 | 0.45 | 0.39 | 0.088 | This work |
| *d*-$TiO_2$ | Black Dye | RR-P3HT | 0.67 | 0.46 | 0.48 | 0.15 | This work |
| *d*-$TiO_2$ | ··· | RR-P3HT | 0.23 | 0.35 | 0.40 | 0.032 | This work |

[a]To prevent the direct contact between the ITO substrate and the overcoating conducting polymer, a flat layer of *d*-$TiO_2$ (60 nm) was prepared under the np-$TiO_2$ film.

the author cannot conclude that the electron injection efficiency is improved by the chemical modification because the modification could also improve the wetting of the oxide surface by the polymer resulting in the enlargement of the interfacial contact area where the charge separation will occur.

To determine the origin of the increase in $J_{SC}$, the author measured the action spectra of a double layered cell based on RR-P3HT and *d*-$TiO_2$ modified with ruthenium dyes. Here the author fabricated a flat layer of *d*-$TiO_2$ instead of the np-$TiO_2$ layer to eliminate the enlargement effect of the interfacial contact area by the chemical modification, and Black Dye was selected as a photosensitizer because of the large absorption band (up to ~900 nm), which is distinguishable from that of RR-P3HT. As shown in Figure 2-2, the double layered cell without Black Dye exhibited a photocurrent only at the absorption wavelengths of RR-P3HT (400–640 nm). On the other hand, the double layered cell with Black Dye exhibited a photocurrent not only at the absorption wavelengths of RR-P3HT around 400–640 nm but also at longer wavelengths of up to ~ 800 nm. The photocurrent action spectrum due to Black Dye was estimated from the absorption spectrum of Black Dye attached to the *d*-$TiO_2$ surface under the assumption that the internal quantum efficiency is unity, as shown by the solid line

in Figure 2-2. This was in good agreement with the photocurrent action spectrum at wavelengths longer than 650 nm, suggesting that the Black Dye contributed to the photocurrent generation. It is noteworthy that the photocurrent of around 500 nm is still almost twice as large as that expected from the sum (broken line) of the photocurrent for the double layered cell without Black Dye (open squares) and that estimated for the Black Dye (solid line). This enhancement is safely ascribable to the improvement in the charge injection efficiency from RR-P3HT to $TiO_2$, because the interfacial contact area does not change at all in the double layered cell. From the action spectra, furthermore, the increase in the photocurrent due to the improving efficiency of the charge injection was estimated to be more than three times that due to the photosensitizing effect of the dye. These findings suggest that the chemical modification with dye molecules can contribute not just to the photosensitization

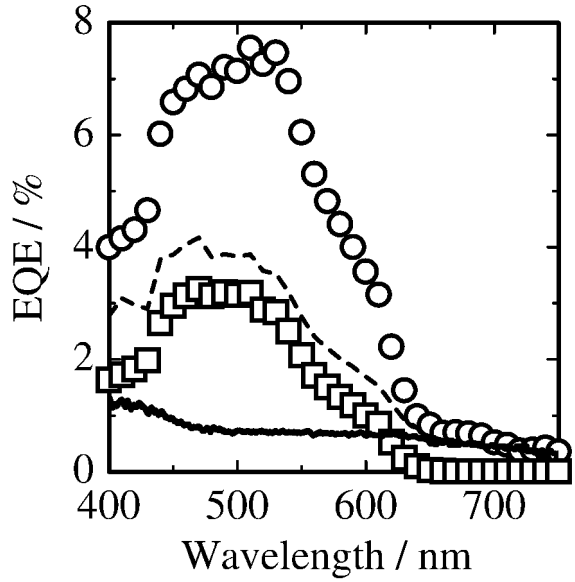


**Figure 2-2.** Photocurrent action spectra of ITO|*d*-$TiO_2$ (60 nm)|Black Dye|RR-P3HT (55 nm)|Au cell (open circles) and ITO|*d*-$TiO_2$ (60 nm)|RR-P3HT (55 nm)|Au cell (open squares). The solid line represents the photocurrent action spectrum of Black Dye estimated from the absorption spectrum of Black Dye under the assumption that the internal quantum efficiency is unity. The broken line represents the sum of the photocurrent for the double layered cell without Black Dye (open squares) and the estimated spectrum of Black Dye (solid line).

but mainly to the improvement in the charge injection efficiency in organic-inorganic hybrid solar cells.

A possible explanation for the increase in $J_{SC}$ is the light harvest effect based on excitation energy transfer from RR-P3HT to the dyes modified on the $TiO_2$ surface. The charge injection efficiency from the dyes to $TiO_2$ is considered to be much higher owing to the direct chemical bonding compared with that from RR-P3HT to $TiO_2$. As shown in Figure 2-3, the absorption of the dyes has a spectral overlap with the emission of RR-P3HT. Simple calculation assuming point dipoles gives a large Förster radius of beyond 2 nm for energy transfer from RR-P3HT excitons to dyes (Black Dye and N3), suggesting that the RR-P3HT exciton can efficiently transfer to the dyes bound to the $TiO_2$ surface where charge separation will occur efficiently. This is also the case for the hybrid cell of MDMO-PPV and $C_{60}C(COOH)_2$ because of the efficient emission of MDMO-PPV although $C_{60}C(COOH)_2$ has a much smaller molar absorption coefficient compared with ruthenium dyes. Indeed, the Förster radius has been calculated to be ~2 nm for MDMO-PPV and (1-(3-

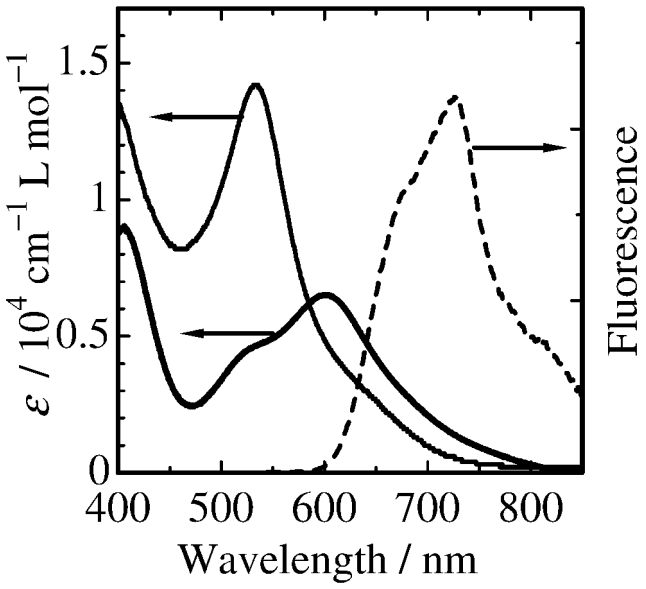


**Figure 2-3.** Molar absorption coefficient of N3 in ethanol (thin solid line) and Black Dye in ethanol (thick solid line) and emission spectrum of a RR-P3HT film on a glass substrate (broken line).

methoxycarbonyl)propyl-1-phenyl[6,6]methanofullerene (PCBM).[15] Furthermore, similar energy transfer from an emissive conjugated polymer to PCBM has been reported for blend films.[16] In the present $TiO_2$-RR-P3HT system, the energy transfer rate from RR-P3HT to Black Dye is estimated to be as fast as ~$5 \times 10^{11}$ $s^{-1}$ for a spatial separation of 1 nm, which is sevenfold the energy migration rate among polymers at the same spatial separation. The long distance and fast rate of energy transfer suggest that RR-P3HT excitons can be collected at the charge separation interface more efficiently through the direct energy transfer rather than successive energy migration among RR-P3HT moieties. A similar finding has been reported for a flat RR-P3HT/$TiO_2$ hybrid solar cell with a thin layer of a low band-gap polymer at the interface.[17] These light harvesting effects would contribute to the increase in $J_{SC}$.

Another explanation is the improvement of electronic junction at the interface of polymer and metal oxide. The modification of inorganic metal oxide with organic molecules made the metal oxide surface hydrophobic, resulting in better interfacial contact with the hydrophobic organic polymer. Indeed, the water contact angle of the *d*-$TiO_2$ surface increased from 14° to 30° after the chemical modification with N3. This improved contact enhances the electronic coupling between them because of the large orbital overlapping. Furthermore, electron transfer from RR-P3HT to $TiO_2$ through dyes is thermodynamically allowed because of the appropriate gradient of the lowest unoccupied molecular orbital or conduction band potential energy: 3.0 eV (RR-P3HT),[18] 3.9 eV (N3),[19] and 4.0 eV ($TiO_2$)[19] below vacuum level. As a result, the modification molecules serve as an electronic mediator that enhances the electron transfer efficiency from polymer to metal oxide. Efficient electron transfer through a mediator has been widely reported for other experimental systems, including photosynthetic reaction centers,[20] DNA,[21] and self-assembly monolayer systems.[22]

Finally, it should be noted that the chemical modification improved not only $J_{SC}$ but also open-circuit voltage ($V_{OC}$) as summarized in Table 2-1. The increase in $V_{OC}$ suggests that the

charge recombination is efficiently suppressed by the chemical modification. This is probably because the dyes at the interface separate the polymer from the metal oxide properly and prevent the direct contact between them, thereby suppressing the charge recombination between the holes in the polymer and the electrons injected into the metal oxide.

## 2.4. Conclusions

The effect of chemical modification of metal oxide surface with dye molecules in organic-inorganic hybrid solid solar cells was studied by using double layered cells consisting of RR-P3HT and a flat layer of *d*-$TiO_2$. The EQE measurements revealed that the chemical modification with dye molecules can serve not only as a photosensitizer but mainly as an energy funnel and/or an electronic mediator to significantly improve the electron injection efficiency from RR-P3HT to $TiO_2$.

## References


(1) Song, M. Y.; Kim, J. K.; Kim, K.-J.; Kim, D. Y. *Synth. Met.* **2003**, *137*, 1387–1388.

(2) Coakley, K. M.; Liu, Y.; Goh, C.; McGehee, M. D. *MRS Bull.* **2005**, *30*, 37–40.

(3) Beek, W. J. E.; Wienk, M. M.; Janssen, R. A. J. *J. Mater. Chem.* **2005**, *15*, 2985–2988.

(4) Lancelle-Beltran, E.; Prené, P.; Boscher, C.; Belleville, P.; Buvat, P.; Sanchez, C. *Adv. Mater.* **2006**, *18*, 2579–2582.

(5) Bartholomew, G. P.; Heeger, A. J. *Adv. Funct. Mater.* **2005**, *15*, 677–682.

(6) Coakley, K. M.; McGehee, M. D. *Appl. Phys. Lett.* **2003**, *83*, 3380–3382.

(7) Liu, J.; Tanaka, T.; Sivula, K.; Alivisatos, A. P.; Fréchet, J. M. J. *J. Am. Chem. Soc.* **2004**, *126*, 6550–6551.

(8) Ohkita, H.; Shimazaki, Y.; Ohoka, M.; Ito, S. *Chem. Lett.* **2004**, *33*, 1598–1599.

(9) Kudo, N.; Shimazaki, Y.; Ohkita, H.; Ohoka, M.; Ito, S. *Sol. Energy Mater. Sol. Cells* **2007**, *91*, 1243–1247.

(10) Peiró, A. M.; Ravirajan, P.; Govender, K.; Boyle, D. S.; O'Brien, P.; Bradley, D. D. C.; Nelson, J.; Durrant, J. R. *J. Mater. Chem.* **2006**, *16*, 2088–2096.

(11) Ravirajan, P.; Peiró, A. M.; Nazeeruddin, M. K.; Grätzel, M.; Bradley, D. D. C.; Durrant, J. R.; Nelson, J. *J. Phys. Chem. B* **2006**, *110*, 7635–7639.

(12) Grätzel, M. *Chem. Lett.* **2005**, *34*, 8–13.

(13) Chiba, Y.; Islam, A.; Watanabe, Y.; Komiya, R.; Koide, N.; Han, L. Y. *Jpn. J. Appl. Phys., Part 2* **2006**, *45*, L638–L640.

(14) Grant, C. D.; Schwartzberg, A. M.; Smestad, G. P.; Kowalik, J.; Tolbert, L. M.; Zhang, J. Z. *Synth. Met.* **2003**, *132*, 197–204.

(15) Scully, S. R.; McGehee, M. D. *J. Appl. Phys.* **2006**, *100*, 034907.

(16) Cook, S.; Ohkita, H.; Durrant, J. R.; Kim, Y.; Benson-Smith, J. J.; Nelson, J.; Bradley, D. D. C. *Appl. Phys. Lett.* **2006**, *89*, 101128.

(17) Liu, Y.; Summers, M. A.; Edder, C.; Fréchet, J. M. J.; McGehee, M. D. *Adv. Mater.* **2005**, *17*, 2960–2964.

(18) Kim, Y.; Choulis, S. A.; Nelson, J.; Bradley, D. D. C.; Cook, S.; Durrant, J. R. *Appl. Phys. Lett.* **2005**, *86*, 063502.

(19) Hagfeldt, A.; Grätzel, M. *Chem. Rev.* **1995**, *95*, 49–68.

(20) Bixon, M.; Jortner, J.; Michelbeyerle, M. E. *Biochim. Biophys. Acta* **1991**, *1056*, 301–315.

(21) Voityuk, A. A.; Rösch, N.; Bixon, M.; Jortner, J. *J. Phys. Chem. B* **2000**, *104*, 9740–9745.

(22) Imahori, H.; Yamada, H.; Nishimura, Y.; Yamazaki, I.; Sakata, Y. *J. Phys. Chem. B* **2000**, *104*, 2099–2108.

# *Part II*

# *Chapter 3*

# Improvement of the Light-Harvesting Efficiency in Polymer/Fullerene Bulk Heterojunction Solar Cells by Interfacial Dye Modification

## 3.1. Introduction

Polymer:fullerene bulk heterojunction (BHJ) solar cells have attracted much attention because they are considered to be a promising candidate for a lightweight, flexible, cost-effective, large-area, and renewable energy source.[1–9] Since the 1990s, power conversion efficiencies (PCEs) of polymer:fullerene solar cells have been steadily improved, and in recent years, operational stabilities of such devices have also been studied for practical application.[10–15] Currently, the most effective materials employed in polymer:fullerene BHJ solar cells are regioregular poly(3-hexylthiophene) (RR-P3HT; Figure 3-1a) as the donor and 1-(3-methoxycarbonyl)propyl-1-phenyl[6,6]methanofullerene (PCBM; Figure 3-1b) as the acceptor. Recently, PCEs approaching 5% have been reported by several groups for this donor/acceptor combination.[16–19] Furthermore, short-circuit external quantum efficiencies (EQEs) exceed 70% for such devices,[18,19] suggesting that most excitons can contribute to the photocurrent generation although photoluminescence (PL) from RR-P3HT is still observed after thermal annealing.[18] In other words, it can safely be said that there is little room for significant improvement in the short-circuit current density ($J_{SC}$) for BHJ solar cells based on only RR-P3HT and PCBM.

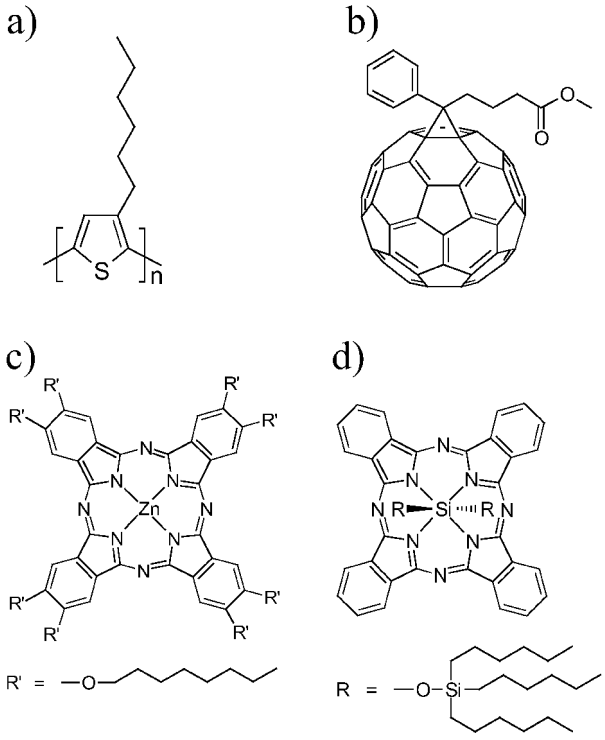


**Figure 3-1.** Chemical structures of (a) the donor material RR-P3HT, (b) the acceptor material PCBM, and the near-infrared dyes (c) ZnPc and (d) SiPc. The ZnPc molecule is a planar structure, while the SiPc molecule is a bulky structure with bis(trihexylsilyl oxide) groups in the axial direction perpendicular to the phthalocyanine plane.

To collect the solar light more efficiently, a variety of low-band-gap polymers have been developed over the last several years[20–23] because RR-P3HT can absorb only ~25% of the total number of photons in the solar light.[9] It is striking that a PCE of over 5% has been reported for blend films of a low-band-gap polymer and the $C_{70}$ derivative of PCBM.[23,24] At this moment, however, there are few successful reports on low-band-gap polymer-based solar cells, partly because it is difficult to synthesize low-band-gap polymers with a high charge mobility.[25] On the other hand, dye sensitization is another approach to improving the light-harvesting efficiency, but there have been few successful reports for improving the light-harvesting efficiency in polymer BHJ solar cells. Only recently, the dye-sensitization effect has been demonstrated for polymer:fullerene BHJ solar cells.[26] In general, dye molecules are

simply blended as the third component to absorb the solar light at longer wavelengths that the original donor and acceptor materials cannot harvest. This is a simple and versatile method, and therefore various dye molecules are available. In most cases, however, dye introduction rarely improved but rather degraded the device performance. This is considered to be due to the formation of dye aggregations in blend films, which would reduce the absorption efficiency or the charge mobility of the active layer.[27–29]

Herein the author reports the photovoltaic properties of BHJ solar cells based on RR-P3HT:PCBM blends incorporated with a dye molecule. To examine the relationship between the device performance and the formation of dye aggregations in the blend film, the author employs two near-infrared dye molecules with different structures: one is zinc 2,3,9,10,16,17,23,24-octakis(octyloxy)-29*H*,31*H*-phthalocyanine (ZnPc; Figure 3-1c), and the other is silicon phthalocyanine bis(trihexylsilyl oxide) (SiPc; Figure 3-1d). The improvement of light-harvesting efficiency and hence photocurrent by dye molecules are discussed in terms of the location of dye molecules and the light-harvesting mechanism based on the dye sensitization and the exciton harvesting.

## 3.2. Experimental Methods

All devices were fabricated as follows: indium tin oxide (ITO)-coated glass substrates (10 Ω per square) were washed by ultrasonication in toluene, acetone, and ethanol for 15 min, dried with $N_2$, and then cleaned with a UV–$O_3$ cleaner (Nippon Laser & Electronics NL-UV253S) for 30 min. A thin layer (ca. 40 nm) of poly(3,4-ethylenedioxythiophene) oxidized with poly(4-styrenesulfonate) (PEDOT:PSS; H. C. Starck PH500) was spin-coated onto the cleaned substrates at a spin rate of 3000 rpm, and the layer was dried at 140 °C for 10 min in air. A blend layer of RR-P3HT:PCBM:dye (100 nm) was spin-coated from a chlorobenzene solution on the PEDOT:PSS film at 1200 rpm for 60 s. The blend solution was prepared as follows: RR-P3HT (Plextronics, regioregularity > 98%, number-average molecular weight,

$M_n$ ~ 45,000−65,000 g mol$^{-1}$) was dissolved in chlorobenzene (10 mg mL$^{-1}$), and the solution was stirred at 40 °C overnight. To the solution were added PCBM (Frontier Carbon; 10 mg mL$^{-1}$) and dye (Aldrich, ZnPc or SiPc; 0.7 mg mL$^{-1}$). Note that the dye concentration was optimized in the range from 0.1 to 2.0 mg mL$^{-1}$. The blend solution was filtered with a 0.45-μm poly(tetrafluoroethylene) filter before the spin coating. The active layer was thermally annealed at 150 °C for 30 min in a $N_2$-filled glovebox. A thin layer of $TiO_x$ (<10 nm) was prepared by the spin coating from a dehydrated ethanol solution of titanium isopropoxide (Aldrich) at 2000 rpm for 60 s.[30] Finally, the aluminum electrode (70 nm) was thermally deposited on top of the $TiO_x$ layer at 2.5 × 10$^{-4}$ Pa. For comparison, RR-P3HT:PCBM control devices without dye were also prepared separately under the same conditions to give the same active layer thickness.

Absorption and PL spectra were measured with a spectrophotometer (Hitachi model U-3500) and a spectrofluorometer (Jasco model FP-6600), respectively. The film thickness was evaluated with an atomic force microscope (Shimadzu model SPM-9500J) in the contact mode at room temperature. The *J*−*V* characteristics were measured with a direct-current voltage and a current source/monitor (Advantest model R6243) in the dark and under illumination with AM1.5G simulated solar light with 100 mW cm$^{-2}$. The light intensity was corrected with a calibrated silicon photodiode reference cell (Peccell model PECSI01). The photocurrent action spectra were measured with a digital electrometer (Advantest model R8252) under monochromatic light illumination from a 500-W xenon lamp (Thermo Oriel model 66921) with optical cut filters and a monochromator (Thermo Oriel, UV−visible Cornerstone). The active area of the device was 0.07 cm$^{-2}$. The illumination was carried out from the ITO side in air. At least 10 devices were fabricated to ensure reproducibility of the *J*−*V* characteristics.

## 3.3. Results

### *3.3.1. Absorption Spectra*

The author first compares the absorption spectra of the two dye molecules in solutions and in blend films before and after annealing. In blend solutions, as shown in parts a and b of Figure 3-2, a large and broad absorption and a small and sharp absorption were observed at around 460 and 670 nm, which are ascribable to RR-P3HT and dye (ZnPc or SiPc), respectively. The absorption spectrum of each blend solution is a simple superposition of the RR-P3HT and dye spectra because of little contribution of PCBM in the same wavelength range, indicating homogeneous mixing and no interaction in the ground state. On the other hand, the blend films showed different absorption spectra between ZnPc and SiPc. As shown in parts c and d of Figure 3-2, the RR-P3HT:PCBM:ZnPc blend film exhibits a distinct absorption band of RR-P3HT at around 500 nm and a significantly broadened and decreased absorption band of ZnPc at around 670 nm, while the RR-P3HT:PCBM:SiPc blend film exhibits distinct absorption bands of RR-P3HT and SiPc at around 500 and 670 nm, respectively, as with the blend solution. Note that ZnPc molecules certainly exist in the blend film because the ZnPc absorption was observed for a solution prepared by dissolving the blend film again. Therefore, the decrease in the absorption of ZnPc indicates the formation of dye aggregations in the film, which would reduce the effective absorption coefficient.[31,32] As shown in parts e and f of Figure 3-2, a similar tendency was observed for the blend films after annealing: the ZnPc absorption was still negligible, but the SiPc absorption remained the same as that before annealing. It is noteworthy that the RR-P3HT:PCBM:SiPc blend film exhibits a large absorption of RR-P3HT with a distinct shoulder at around 600 nm comparable to those for the control device without SiPc, which are indicative of crystallization of RR-P3HT,[33,34] while the RR-P3HT:PCBM:ZnPc blend film exhibits relatively smaller changes in

the absorption of RR-P3HT. This difference suggests that ZnPc molecules disturb the crystallization of RR-P3HT, while SiPc molecules do not at all. These spectral differences are discussed later in terms of molecular structures.

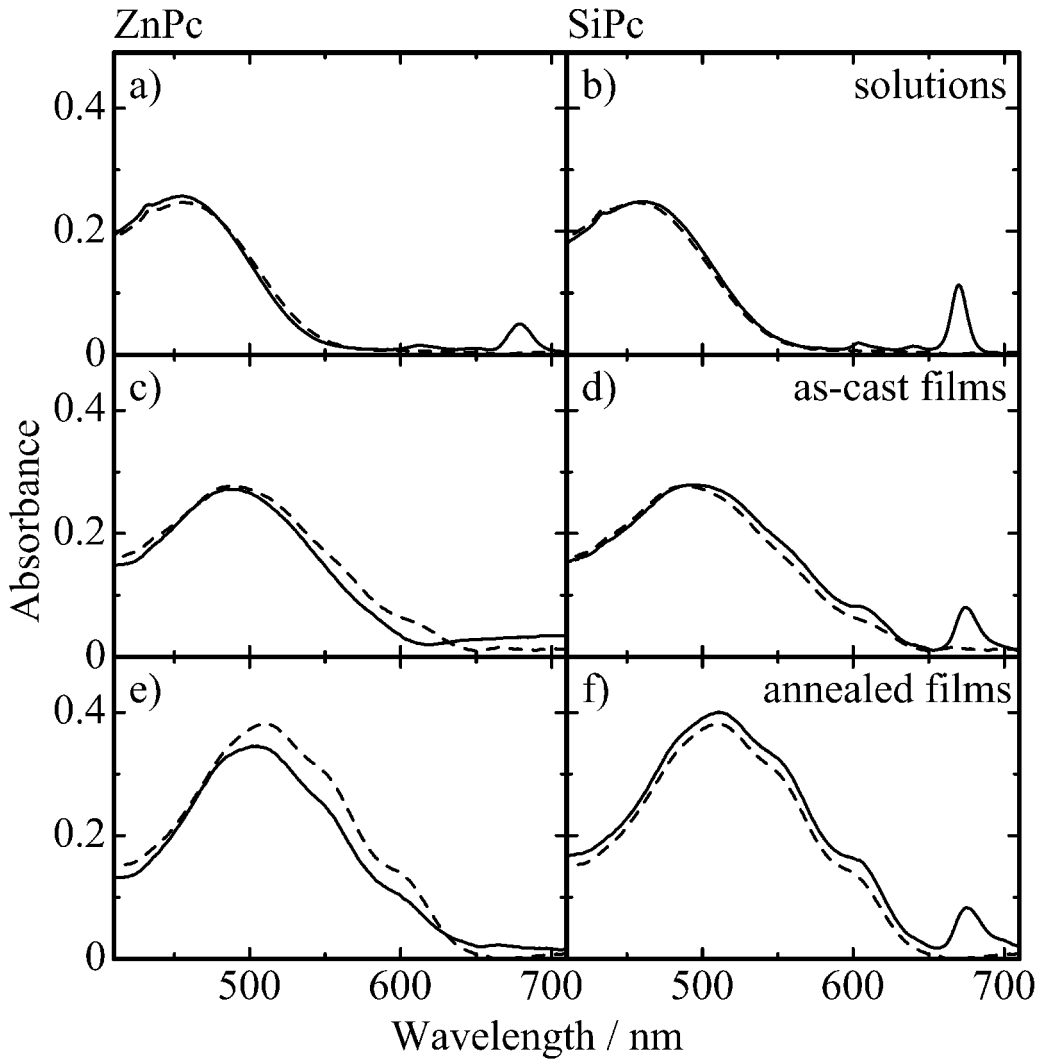


**Figure 3-2.** Absorption spectra of blend solutions, as-cast films, and annealed films with (solid lines) and without dye molecules (broken lines): (a) RR-P3HT:PCBM:ZnPc solutions, (b) RR-P3HT:PCBM:SiPc solutions, (c) RR-P3HT:PCBM:ZnPc as-cast films, (d) RR-P3HT:PCBM:SiPc as-cast films, (e) RR-P3HT:PCBM:ZnPc annealed films, and (f) RR-P3HT:PCBM:SiPc annealed films.

### *3.3.2. J–V Characteristics*

The author turns now to the device performance of these two blend films with different dye molecules. Figure 3-3a shows the *J*−*V* characteristics of RR-P3HT:PCBM:ZnPc solar cells and RR-P3HT:PCBM control cells before and after annealing under AM1.5G illumination from a calibrated solar simulator with an intensity of 100 mA $cm^{-2}$. The averaged device parameters of these cells are summarized in Table 3-1. Before the thermal annealing, the *J*−*V* curve (thin solid line) was almost the same as that for the control cell without ZnPc (thin broken line). After the thermal annealing, $J_{SC}$ significantly increased and was comparable to that for the control cell without ZnPc (thick broken lines), while the fill factor (FF) was much smaller than that for the control cell. As a result, the introduction of ZnPc decreased PCE from 2.2 to 1.1%. Such a poorer performance can be ascribed to the formation of dye aggregations in blend films. In particular, the *J*−*V* curve with an inflection point has been occasionally seen for organic solar cells, indicating that there is a transport-limiting interface close to the aluminum electrode.[35,36] Therefore, aggregations of ZnPc molecules are also likely to limit the transport of photogenerated charges at the interface. On the other hand, as shown in Figure 3-3b and Table 3-1, the RR-P3HT:PCBM:SiPc device exhibits a distinguished increase in $J_{SC}$ to 7.9 mA $cm^{-2}$ after the thermal annealing, which is even higher than that for the control device (6.5 mA $cm^{-2}$). It should be noted that FF remained the same as that for the control device without SiPc even after the thermal annealing, which would induce the formation of dye aggregations. As a result, the overall performance improved to PCE = 2.7%. This finding suggests that the appropriate selection of dye molecules is crucial for improving the device performance effectively.

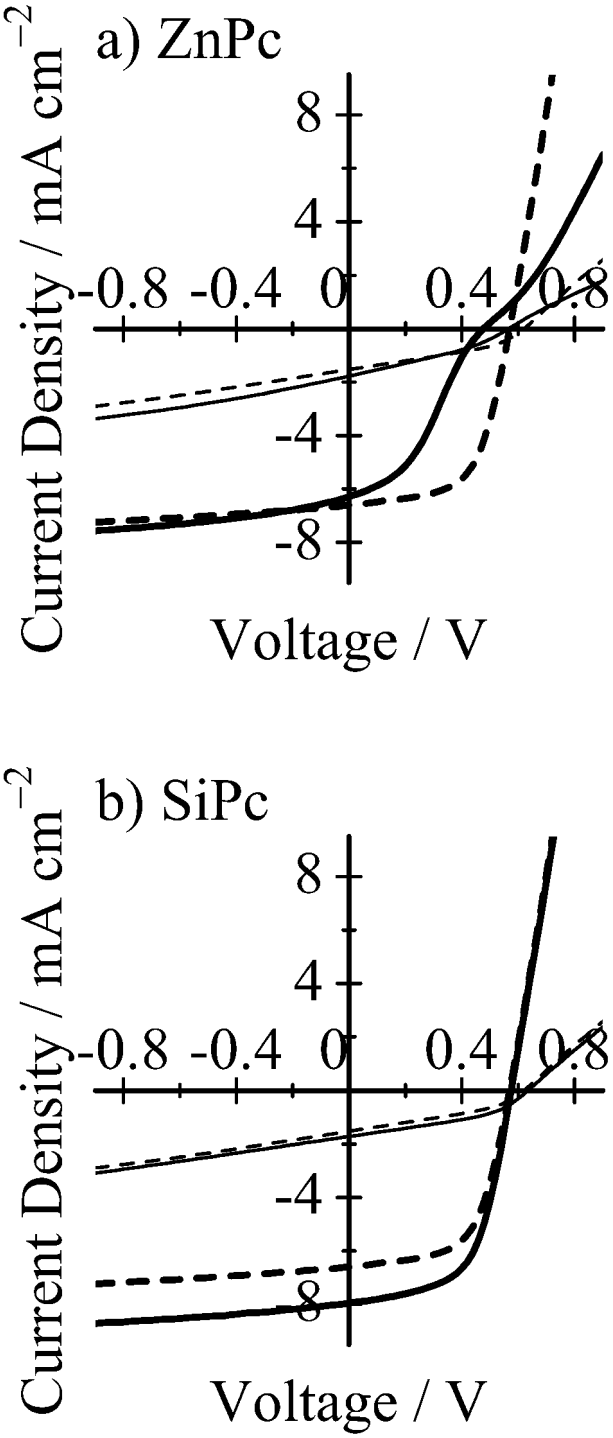


**Figure 3-3.** *J*−*V* characteristics of RR-P3HT:PCBM blend films with (solid lines) and without dye (broken lines) before (thin lines) and after annealing (thick lines): (a) RR-P3HT:PCBM:ZnPc; (b) RR-P3HT:PCBM:SiPc.

**Table 3-1.** Averaged device parameters of RR-P3HT:PCBM solar cells with and without dye.[a]

| | $J_{SC}$ / mA cm$^{-2}$ | $V_{OC}$ / V | FF | PCE / % |
|---|---|---|---|---|
| RR-P3HT:PCBM | 1.5 | 0.60 | 0.33 | 0.30 |
| RR-P3HT:PCBM:ZnPc | 1.9 | 0.58 | 0.32 | 0.35 |
| RR-P3HT:PCBM:SiPc | 2.1 | 0.64 | 0.43 | 0.58 |
| RR-P3HT:PCBM (annealed) | 6.5 | 0.58 | 0.59 | 2.2 |
| RR-P3HT:PCBM:ZnPc (annealed) | 6.2 | 0.48 | 0.37 | 1.1 |
| RR-P3HT:PCBM:SiPc (annealed) | 7.9 | 0.58 | 0.59 | 2.7 |

[a]All of the parameters are averaged valiues for at lease 10 devices.

### *3.3.3. EQE Spectra*

In order to address the origin of the increase in $J_{SC}$ by the addition of SiPc, the author measured the EQE spectra of RR-P3HT:PCBM:SiPc and RR-P3HT:PCBM:ZnPc devices for comparison. In the EQE spectra of the RR-P3HT:PCBM:ZnPc devices, as shown in Figure 3-4a, the photocurrent peak was observed only in the wavelength range (400−600 nm) of the RR-P3HT absorption and no photocurrent signal was observed in the wavelength range (650−700 nm) of the ZnPc absorption, which is in agreement with the absorption spectra mentioned before. On the other hand, as shown in Figure 3-4b, the RR-P3HT:PCBM:SiPc devices exhibit two EQE peaks in the wavelength range of the RR-P3HT absorption and also in the longer wavelength range (650−700 nm) of the SiPc absorption. Before the thermal annealing, the EQE corresponding to the RR-P3HT absorption (470−600 nm) was comparable to that for the control device without SiPc (20%). The EQE corresponding to the SiPc absorption (650−700 nm) was as high as 10%, which is clear evidence that direct photoexcitation of SiPc does contribute to photocurrent generation. After the thermal annealing, the EQE corresponding to direct photoexcitation of SiPc (650−700 nm) increased up to 20% compared to that before annealing (10%), suggesting that the thermal annealing results in an increase in the number of SiPc molecules that can directly contribute to the

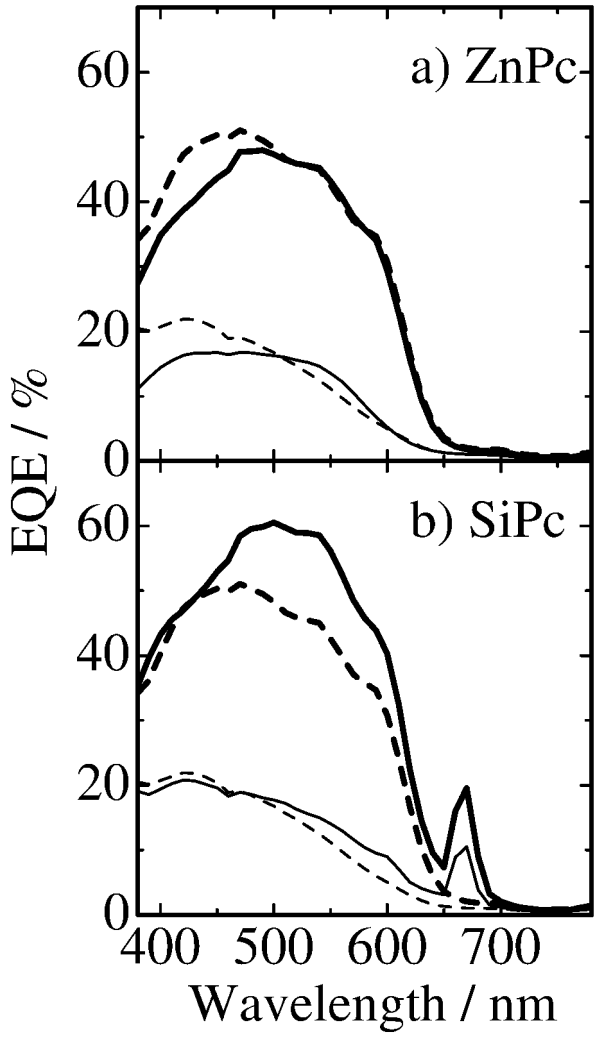


**Figure 3-4.** EQE spectra of RR-P3HT:PCBM blend films with (solid lines) and without dye (broken lines) before (thin lines) and after annealing (thick lines): (a) RR-P3HT:PCBM:ZnPc; (b) RR-P3HT:PCBM:SiPc.

photocurrent. More interestingly, the EQE corresponding to the RR-P3HT absorption (470−600 nm) also increased to 60% compared to that for the control device without SiPc (50%), suggesting that SiPc molecules are not directly involved in the photoabsorption but, nonetheless, promote charge generation from RR-P3HT excitons indirectly. In other words, there are two origins for the increase in $J_{SC}$ by the addition of SiPc molecules: one is that the direct contribution of SiPc to the photocurrent results from photoexcitation of the incorporated SiPc itself, and the other is that the indirect contribution of SiPc to the photocurrent results from the improvement in the charge generation from RR-P3HT excitons

in the presence of SiPc. From the EQE spectra, the contribution of each mechanism to the increase in $J_{SC}$ was evaluated to be 0.4 mA cm$^{-2}$ for the direct mechanism and 1.0 mA cm$^{-2}$ for the indirect mechanism. Therefore, the increase in $J_{SC}$ is mainly due to the indirect contribution of SiPc to the improvement in the charge generation from RR-P3HT excitons rather than the direct photoabsorption of SiPc molecules. The author will discuss each mechanism later in detail.

### *3.3.4. PL Quenching*

The author furthermore measured the PL efficiency of RR-P3HT in blend films with acceptor materials (PCBM or SiPc) to obtain an in-depth understanding of the quenching mechanism of RR-P3HT excitons in the ternary blends. The PL efficiency was evaluated as the ratio of the PL intensity at 700 nm of the blend films to that of the pristine RR-P3HT film when RR-P3HT was selectively excited at 550 nm. Before the thermal annealing, as shown in Figure 3-5, the PL efficiency was lower than 8% for both RR-P3HT:PCBM and RR-P3HT:PCBM:SiPc blend films. The low PL efficiency suggests that most of the RR-P3HT excitons can arrive at the interface because of the homogeneous mixture of RR-P3HT and

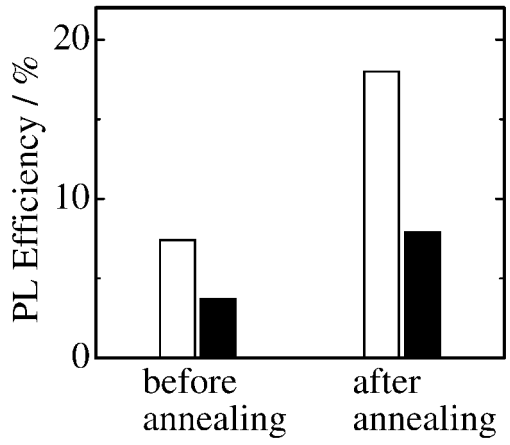


**Figure 3-5.** PL efficiency of RR-P3HT:PCBM:SiPc (closed bars) and RR-P3HT:PCBM (open bars) blend films before and after annealing. The efficiency was evaluated as the ratio of the PL intensity of blend films to that of a RR-P3HT pristine film when RR-P3HT was selectively excited at 550 nm. The PL intensity observed at 700 nm was corrected by variation of the absorption at the excitation wavelength.

PCBM in blend films. After the thermal annealing, the PL efficiency of the RR-P3HT:PCBM blend increased to 18%, which is consistent with previous reports.[18,37] The increase in the PL efficiency suggests that fewer RR-P3HT excitons can arrive at the interface after the thermal annealing, which is ascribable to enlargement of the RR-P3HT domain because of crystallization. On the other hand, the PL efficiency of the RR-P3HT:PCBM:SiPc film was as low as 8% even after annealing, which is comparable to that of the RR-P3HT:PCBM film before annealing. As mentioned before, the introduction of SiPc molecules does not disturb the crystallization of RR-P3HT. Therefore, these results suggest that there is an efficient exciton-harvesting mechanism in the RR-P3HT:PCBM:SiPc ternary blend films.

## 3.4. Discussion

The author starts off the discussion by considering the difference in the absorption spectra and the device performance between the two dye molecules (ZnPc and SiPc) with different structures. The ZnPc dye can be regarded as a planar molecule and is therefore likely to stack in the direction normal to the phthalocyanine plane, resulting in the formation of dye aggregations. On the other hand, the SiPc dye has two bulky groups in the axial direction perpendicular to the phthalocyanine plane, which probably inhibit effective stacking of the π-conjugation plane and hence suppress the formation of dye aggregations. As mentioned before, the difference in the absorption spectra and the device performance can be explained in terms of the formation of dye aggregations in blend films. In previous reports on BHJ solar cells incorporated with dye molecules, planar dye molecules such as ZnPc have been generally employed and hence the formation of dye aggregations has been the main obstacle to improving the device performance.[28,29] The author therefore concludes that the selection of bulky dyes such as SiPc is key to the development of ternary BHJ solar cells without the formation of dye aggregations.

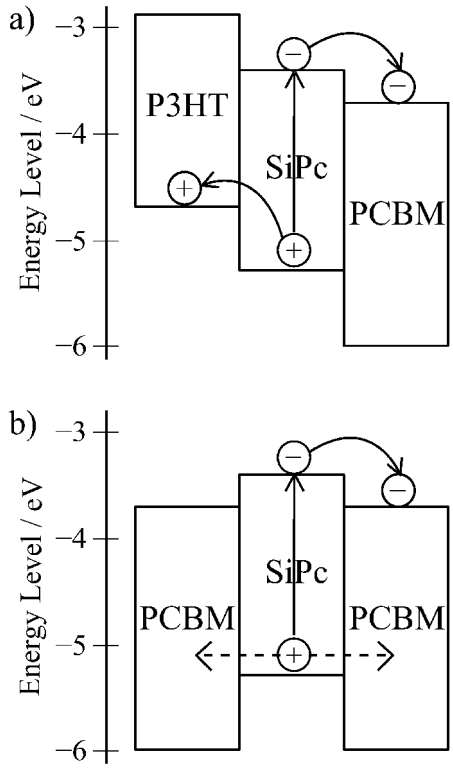


**Figure 3-6.** Energy diagrams of SiPc molecules and the surrounding materials: (a) SiPc located at the interface between P3HT and PCBM; (b) SiPc located in the PCBM domain.

Next, the author discusses the location of SiPc dye molecules in blend films. As shown in Figure 3-6a, SiPc excitons located at the interface of RR-P3HT/PCBM can inject an electron into PCBM and a hole into P3HT, because there are energetic cascades in both the lowest unoccupied molecular orbital (LUMO) and highest occupied molecular orbital (HOMO) levels.[38–41] This energetic cascade is essential for dye sensitization at the interface. On the other hand, SiPc excitons located in a PCBM domain, as shown in Figure 3-6b, can inject an electron into the PCBM domain but cannot inject a hole into the surrounding PCBM domain because of the lower HOMO level of PCBM. Much the same is true for SiPc excitons located in a P3HT domain. In other words, only SiPc molecules located at the interface of P3HT/PCBM can contribute to the photocurrent generation. Therefore, the observation of the photocurrent originating from the SiPc absorption indicates that some SiPc molecules are

located at the P3HT/PCBM interface even before the thermal annealing. Furthermore, it can be said that more SiPc molecules contribute to the photocurrent after the thermal annealing, because as mentioned before the EQE at 670 nm increased from 10 to 20% while the absorbance remained the same. This is probably because the charge collection efficiency is improved by the formation of interpenetrating networks of RR-P3HT and PCBM by the thermal annealing. In addition, it is possible that the number of SiPc molecules located at the RR-P3HT/PCBM interface, which can contribute to the photocurrent generation, is simply increased by the thermal annealing. The EQE after the thermal annealing (~20%) is comparable to the absorption at the same wavelength 670 nm, suggesting that the majority of SiPc molecules incorporated are localized at the interface. The author speculates that the localization of SiPc molecules at the interface is due to crystallization of RR-P3HT and aggregation of nanocrystalline PCBM domains upon annealing as reported previously.[33,42] In other words, SiPc molecules located in RR-P3HT or PCBM domains could be expelled from each domain into the interface by crystallization of RR-P3HT and aggregation of nanocrystalline PCBM domains. The author therefore emphasizes that the selection of crystalline materials such as RR-P3HT and PCBM as a matrix is crucial for the localization of dye molecules at the interface where the charge separation can occur efficiently, which is also key to the development of interfacial dye modification in ternary BHJ solar cells.

Finally, the author discusses the mechanism of dye sensitization in RR-P3HT:PCBM:SiPc ternary blends. As mentioned before, there are two mechanisms for the increase in $J_{SC}$ by the addition of SiPc molecules. One is that the additional absorption of SiPc molecules contributes to the increase in $J_{SC}$ directly. In the present study, this direct contribution is not so large because of the narrow absorption band of SiPc molecules, which can harvest the solar light only at a limited spectral window. Dye molecules with a wider absorption band would provide a larger photocurrent. The other mechanism is that SiPc molecules promote the

charge separation from RR-P3HT excitons at the interface, although they do not absorb photons directly. As described in Chapter 2, the author reported a similar result for a RR-P3HT/$TiO_2$ bilayered hybrid solar cell with chemical modification of the $TiO_2$ surface with a ruthenium complex dye.[43] In the hybrid cell, the EQE originating from RR-P3HT increased by the introduction of dye molecules at the interface, which can be explained in terms of Förster energy transfer from RR-P3HT to the ruthenium complex. Such efficient light harvesting by using energy transfer has also been reported for another hybrid solar cell.[44,45] The same is true for the present system. Simple calculation assuming point dipoles gives a large Förster radius of beyond 3 nm for energy transfer from RR-P3HT to SiPc. The energy transfer rate from RR-P3HT to SiPc is estimated to be as fast as $\sim 8 \times 10^{12}$ $s^{-1}$ for a spatial separation of 1 nm, which is over a 100 times faster than the energy migration rate among RR-P3HT at the same spatial separation. As shown in Figure 3-7c, therefore, the efficient long-range Förster energy transfer can collect RR-P3HT excitons that could not reach the interface only by repetition of short-range excitation energy hoppings (Figure 3-7b). Furthermore, the Förster energy transfer is not random diffusion but directional transport from a donor to an acceptor molecule and thereby can harvest RR-P3HT donor excitons more efficiently into the SiPc acceptor at the interface. In other words, the efficient long-range Förster energy transfer can increase the effective exciton diffusion length, which can explain the lower PL efficiency of the RR-P3HT:PCBM:SiPc ternary blend film (Figure 3-5). The highly efficient Förster energy transfer from RR-P3HT to SiPc supports the author's estimation that the majority of SiPc molecules are located at the interface because SiPc molecules in RR-P3HT domains would quench RR-P3HT excitons efficiently and cause a decrease in $J_{SC}$, but this is not the case. Note that the advantage of the Förster energy transfer would be undistinguished if RR-P3HT and PCBM were well mixed so that most excitons could arrive at the interface even without dye molecules, as shown in Figure 3-7a. This

situation can apply to the ternary blend before annealing because the EQE originating from RR-P3HT and the PL efficiency were comparable to those for RR-P3HT:PCBM blends without dye (Figures 3-4 and 3-5). From these results, the author concludes that the exciton harvesting in polymer BHJ solar cells can be efficiently improved by the long-range energy transfer of incorporated dye molecules with a large spectral overlap with donor materials.

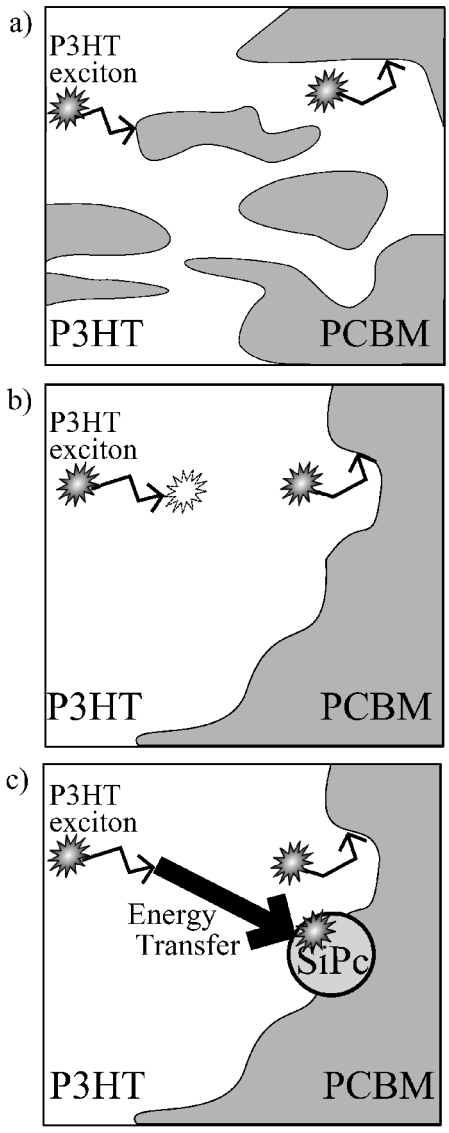


**Figure 3-7.** Schematic illustrations of the donor/acceptor interface: (a) before annealing, each domain is so small that most excitons can reach the interface; (b) after annealing, some excitons cannot reach the interface because of the larger domain size; (c) after annealing and in the presence of SiPc, even excitons generated far away can reach the interface by energy transfer to the SiPc molecule.

## 3.5. Conclusions

In summary, the author has shown dye-sensitized polymer/fullerene BHJ solar cells with the improved photocurrent and PCE compared to control BHJ cells without the dye. The key to the improvement is the allocation of dye molecules at the donor/acceptor interface without the formation of dye aggregations. Such dye molecules located at the interface can contribute to the photocurrent generation by direct photoexcitation and also harvest excitons more efficiently through long-range energy transfer to the dye molecule. The author demonstrated that the key requirement can be achieved by following two appropriate selections of device materials. One is the selection of dyes with bulky groups such as SiPc to suppress the formation of dye aggregations, which would reduce the effective absorption coefficient. Of course, it is essential for dye sensitization that there are energetic cascades at the interface in both the LUMO and HOMO levels. A large spectral overlap between the dye absorption and the donor fluorescence is also beneficial for efficient long-range energy transfer. The other is the selection of matrix materials likely to be crystallized such as RR-P3HT and PCBM, which results in the localization of dye molecules at the interface where the charge separation can occur efficiently. The selection of these materials is important for the design of dye-sensitized BHJ solar cells.

## References and Notes

(1) Hoppe, H.; Sariciftci, N. S. *J. Mater. Chem.* **2006**, *16*, 45–61.

(2) Günes, S.; Neugebauer, H.; Sariciftci, N. S. *Chem. Rev.* **2007**, *107*, 1324–1338.

(3) Brabec, C. J.; Durrant, J. R. *MRS Bull.* **2008**, *33*, 670–675.

(4) Thompson, B. C.; Fréchet, J. M. J. *Angew. Chem., Int. Ed.* **2008**, *47*, 58–77.

(5) Krebs, F. C.; Alstrup, J.; Spanggard, H.; Larsenb, K.; Kold, E. *Sol. Energy Mater. Sol. Cells* **2004**, *83*, 293–300.

(6) Dennler, G.; Lungenschmied, C.; Neugebauer, H.; Sariciftci, N. S.; Labouret, A. J. *Mater. Res.* **2005**, *20*, 3224–3233.

(7) Lungenschmied, C.; Dennler, G.; Neugebauer, H.; Sariciftci, N. S.; Glatthaar, M.; Meyer, T.; Meyer, A. *Sol. Energy Mater. Sol. Cells* **2007**, *91*, 379–384.

(8) Krebs, F. C.; Spanggard, H.; Kjær, T.; Biancardo, M.; Alstrup, J. *Mater. Sci. Eng. B* **2007**, *138*, 106–111.

(9) Smestad, G. P.; Krebs, F. C.; Lampert, C. M.; Granqvist, C. G.; Chopra, K. L.; Mathew, X.; Takakura, H. *Sol. Energy Mater. Sol. Cells* **2008**, *92*, 371–373.

(10) Krebs, F. C.; Spanggard, H. *Chem. Mater.* **2005**, *17*, 5235–5237.

(11) Katz, E. A.; Gevorgyan, S.; Orynbayev, M. S.; Krebs, F. C. *Eur. Phys. J. Appl. Phys.* **2007**, *36*, 307–311.

(12) Jørgensen, M.; Norrman, K.; Krebs, F. C. *Sol. Energy Mater. Sol. Cells* **2008**, *92*, 686–714.

(13) Hauch, J. A.; Schilinsky, P.; Choulis, S. A.; Childers, R.; Biele, M.; Brabec, C. J. *Sol. Energy Mater. Sol. Cells* **2008**, *92*, 727–731.

(14) Krebs, F. C. *Sol. Energy Mater. Sol. Cells* **2008**, *92*, 715–726.

(15) Gevorgyan, S. A.; Krebs, F. C. *Chem. Mater.* **2008**, *20*, 4386–4390.

(16) Ma, W.; Yang, C.; Gong, X.; Lee, K.; Heeger, A. J. *Adv. Funct. Mater.* **2005**, *15*, 1617–

1622.

(17) Li, G.; Shrotriya, V.; Huang, J.; Yao, Y.; Moriarty, T.; Emery, K.; Yang, Y. *Nat. Mater.* **2005**, *4*, 864–868.

(18) Kim, Y.; Cook, S.; Tuladhar, S. M.; Choulis, S. A.; Nelson, J.; Durrant, J. R.; Bradley, D. D. C.; Giles, M.; McCulloch, I.; Ha, C.-S.; Ree, M. *Nat. Mater.* **2006**, *5*, 197–203.

(19) Kim, J. Y.; Kim, S. H.; Lee, H.-H.; Lee, K.; Ma, W.; Gong, X.; Heeger, A. J. *Adv. Mater.* **2006**, *18*, 572–576.

(20) Bundgaard, E.; Krebs, F. C. *Sol. Energy Mater. Sol. Cells* **2007**, *91*, 954–985.

(21) Shaheen, S. E.; Vangeneugden, D.; Kiebooms, R.; Vanderzande, D.; Fromherz, T.; Padinger, F.; Brabec, C. J.; Sariciftci, N. S. *Synth. Met.* **2001**, *121*, 1583–1584.

(22) Yao, Y.; Shi, C.; Li, G.; Shrotriya, V.; Pei, Q.; Yang, Y. *Appl. Phys. Lett.* **2006**, *89*, 153507.

(23) Peet, J.; Kim, J. Y.; Coates, N. E.; Ma, W. L.; Moses, D.; Heeger, A. J.; Bazan, G. C. *Nat. Mater.* **2007**, *6*, 497–500.

(24) Lee, J. K.; Ma, W. L.; Brabec, C. J.; Yuen, J.; Moon, J. S.; Kim, J. Y.; Lee, K.; Bazan, G. C.; Heeger, A. J. *J. Am. Chem. Soc.* **2008**, *130*, 3619–3623.

(25) Mühlbacher, D.; Scharber, M.; Morana, M.; Zhu, Z.; Waller, D.; Gaudiana, R.; Brabec, C. *Adv. Mater.* **2006**, *18*, 2884–2889.

(26) Peet, J.; Tamayo, A. B.; Dang, X.-D.; Seo, J. H.; Nguyen, T.-Q. *Appl. Phys. Lett.* **2008**, *93*, 163306.

(27) Ltaief, A.; Chaâbane, R. B.; Bouazizi, A.; Davenas, J. *Mater. Sci. Eng. C* **2006**, *26*, 344–347.

(28) Dastoor, P. C.; McNeill, C. R.; Frohne, H.; Foster, C. J.; Dean, B.; Fell, C. J.; Belcher, W. J.; Campbell, W. M.; Officer, D. L.; Blake, I. M.; Thordarson, P.; Crossley, M. J.; Hush, N. S.; Reimers, J. R. *J. Phys. Chem. C* **2007**, *111*, 15415–15426.

(29) Kaulach, I.; Muzikante, I.; Gerca, L.; Plotniece, M.; Roze, M.; Kalnachs, J.; Shlihta, G.; Shipkovs, P.; Kampars, V.; Tokmakov, A. *Eur. Phys. J. Appl. Phys.* **2007**, *40*, 169–173.

(30) Hayakawa, A.; Yoshikawa, O.; Fujieda, T.; Uehara, K.; Yoshikawa, S. *Appl. Phys. Lett.* **2007**, *90*, 163517.

(31) Li, H.; Jensen, T. J.; Fronczek, F. R.; Vicente, M. G. H. *J. Med. Chem.* **2008**, *51*, 502–511.

(32) Barger, W. R.; Hur, E.; Ferraudi, G.; Leznoff, C. C.; Nyokong, T.; Rosenthal, I.; Snow, A. W.; Stillman, M. J.; Whrle, D. In *Phthalocyanines, Properties and Applications*; Leznoff, C. C.; Lever, A. B. P.; Eds.; VCH Publishers, Inc.: New York, 1989; Vol. 1.

(33) Erb, T.; Zhokhavets, U.; Gobsch, G.; Raleva, S.; Sthn, B.; Schilinsky, P.; Waldauf, C.; Brabec, C. J. *Adv. Funct. Mater.* **2005**, *15*, 1193–1196.

(34) Brown, P. J.; Thomas, D. S.; Khler, A.; Wilson, J. S.; Kim, J.-S.; Ramsdale, C. M.; Sirringhaus, H.; Friend, R. H. *Phys. Rev. B* **2003**, *67* 064203.

(35) Vogel, M.; Doka, S.; Breyer, Ch.; Lux-Steiner, M. Ch.; Fostiropoulos, K. *Appl. Phys. Lett.* **2006**, *89*, 163501.

(36) Glatthaar, M.; Riede, M.; Keegan, N.; Sylvester-Hvid, K.; Zimmermann, B.; Niggemann, M.; Hinsch, A.; Gombert, A. *Sol. Energy Mater. Sol. Cells* **2007**, *91*, 390–393.

(37) Li, G.; Yao, Y.; Yang, H.; Shrotriya, V.; Yang, G.; Yang, Y. *Adv. Funct. Mater.* **2007**, *17*, 1636–1644.

(38) The HOMO and LUMO levels are taken from several references: $HOMO_{SiPc}$ = 5.3 eV, $LUMO_{SiPc}$ = 3.4 eV (ref 39), $HOMO_{RR\text{-}P3HT}$ = 4.7 eV (ref 40), and $LUMO_{PCBM}$ = 3.7 eV (ref 41).

(39) Cheng, G.; Peng, X.; Hao, G.; Kennedy, V. O.; Ivanov, I. N.; Knappenberger, K.; Hill,

T. J.; Rodgers, M. A. J.; Kenney, M. E. *J. Phys. Chem. A* **2003**, *107*, 3503–3514.

(40) Onoda, M.; Tada, K.; Nakayama, H. *J. Appl. Phys.* **1999**, *86*, 2110–2115.

(41) Brabec, C. J.; Cravino, A.; Meissner, D.; Sariciftci, N. S.; Fromherz, T.; Rispens, M. T.; Sanchez, L.; Hummelen, J. C. *Adv. Funct. Mater.* **2001**, *11*, 374–380.

(42) Yang, X.; Loos, J.; Veenstra, S. C.; Verhees, W. J. H.; Wienk, M. M.; Kroon, J. M.; Michels, M. A. J.; Janssen, R. A. J. *Nano Lett.* **2005**, *5*, 579–583.

(43) Kudo, N.; Honda, S.; Shimazaki, Y.; Ohkita, H.; Ito, S.; Benten, H. *Appl. Phys. Lett.* **2007**, *90*, 183513.

(44) Liu, Y.; Summers, M. A.; Edder, C.; Fréchet, J. M. J.; McGehee, M. D. *Adv. Mater.* **2005**, *17*, 2960–2964.

(45) Scully, S. R.; Armstrong, P. B.; Edder, C.; Fréchet, J. M. J.; McGehee, M. D. *Adv. Mater.* **2007**, *19*, 2961–2966.

# *Chapter 4*

# Multi-Colored Dye Sensitization of Polymer/Fullerene Bulk Heterojunction Solar Cells

## 4.1. Introduction

Bulk heterojunction (BHJ) solar cells based on polymer/fullerene blends have attracted much attention because of their potential advantages.[1–4] Among them, the most thoroughly studied materials for the active layer are blends of regioregular poly(3-hexylthiophene) (RR-P3HT, Figure 4-1a) and 1-(3-methoxycarbonyl)propyl-1-phenyl[6,6]methanofullerene (PCBM, Figure 4-1a). The RR-P3HT:PCBM solar cells exhibit reproducible power conversion efficiency (PCE) of around 4–5% with high fill factor (FF) and external quantum efficiency (EQE).[5,6] Such device parameters are still the highest in organic solar cells. However, RR-P3HT can absorb only a quarter of the total photons in the solar light.[7,8] Consequently, a variety of low band-gap polymers have been developed to absorb a broad range of the solar light.[3,4] On the other hand, dye sensitization based on ternary blends of polymer:fullerene:dye has been recently reported as another approach to improve the light-harvesting efficiency in BHJ polymer solar cells.[5,6]

In ternary blend bulk heterojunction (BHJ) solar cells, dye molecules are simply blended into the polymer:fullerene matrix as the third component to harvest solar photons at wavelengths longer than the original donor and acceptor materials can collect. This is a simple and versatile method and therefore various dye molecules are applicable. In Chapter 3, the author has demonstrated that silicon phthalocyanine bis(trihexylsilyl oxide) (SiPc,

Figure 4-1a) can effectively harvest the longer wavelength light that RR-P3HT:PCBM cannot absorb.[13] Considering the large photocurrent due to dye molecules and the cascaded energy levels of RR-P3HT, PCBM, and SiPc, as shown in Figure 4-1b,[14–16] the author speculated that the majority of dye molecules are located at the donor/acceptor interface by the crystallization of both RR-P3HT and PCBM domains.[13] For further improvement, multiple dye loading would expand the light-harvesting window and hence boost the photocurrent effectively. Such multi-colored dye sensitization has been reported for $TiO_2$-based solar cells.[17] In most cases, however, unfavorable interactions between different dye molecules often cause degradation in the device performance. Limited successful reports have demonstrated that this problem can be avoided by constructing a dye-bilayer structure stained with two different dyes[18,19] or by selecting a suitable co-adsorbing material[20,21] to inhibit dye aggregation. However, such strategy would be difficult and inappropriate for polymer solar cells because they are typically fabricated by simple spin-coating method.

Herein the author reports multi-colored dye sensitization of P3HT:PCBM solar cells fabricated by simple spin-coating. In addition to SiPc, silicon naphthalocyanine bis(trihexylsilyl oxide) (SiNc, Figure 4-1a) is employed as the fourth component, which has complementary spectral absorption at longer wavelengths than SiPc and meets an energetic requirement of the cascaded energy levels of RR-P3HT, SiNc, and PCBM as shown in Figure 4-1b.[14–16]

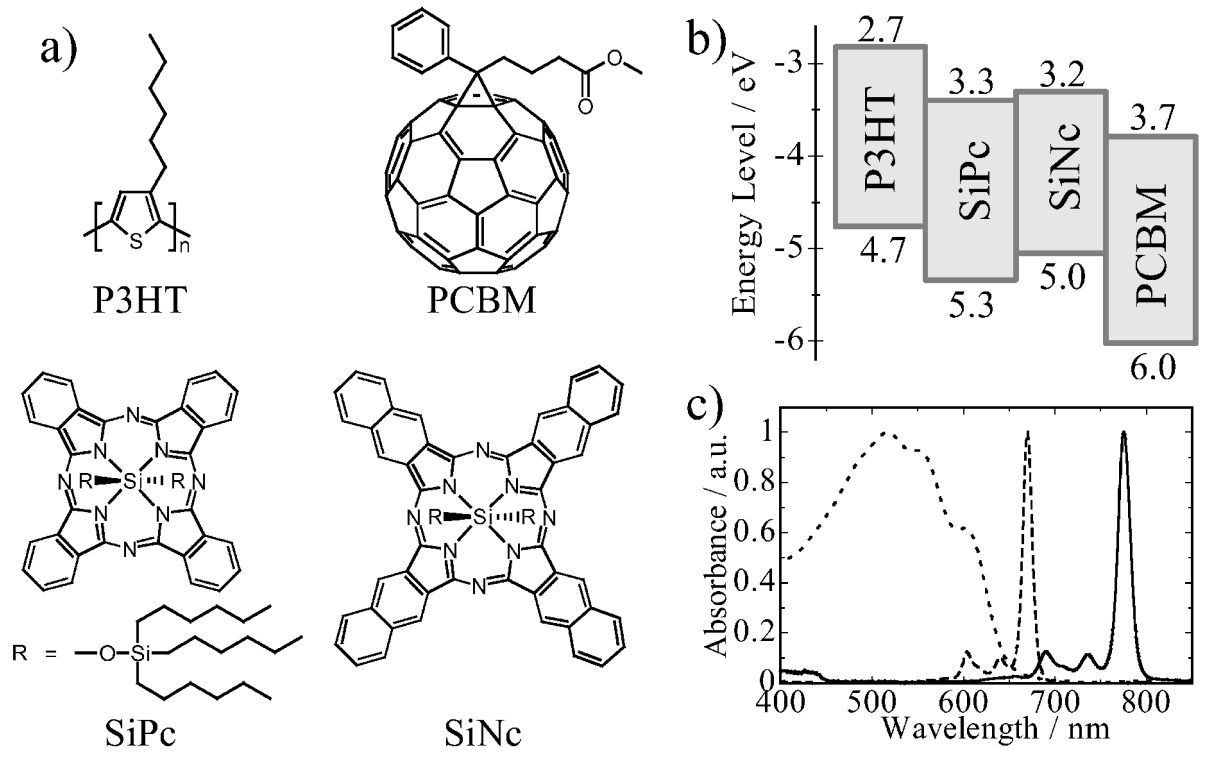


**Figure 4-1.** a) Chemical structures, b) energy diagrams of RR-P3HT, PCBM, SiPc, and SiNc. c) Absorption spectra of the RR-P3HT:PCBM film (dotted line), SiPc (broken line), and SiNc (solid line) in solution.

## 4.2. Experimental Methods

Figure 4-2a shows the device configuration of ITO|PEDOT:PSS|P3HT:PCBM:SiPc:SiNc|Ca|Al solar cell. Devices were fabricated as follows. A thin layer (*ca.* 40 nm) of poly(3,4-ethylenedioxythiophene) oxidized with poly(4-styrenesulfonate) (PEDOT:PSS, H.C.Starck, PH500) was spin-coated onto the cleaned indium tin oxide (ITO)-coated glass substrates (10 Ω per square) at a spin rate of 3000 rpm and dried at 140 °C for 10 min in air. A blend layer of RR-P3HT:PCBM:SiPc:SiNc (*ca.* 200 nm) was spin-coated from an *o*-dichlorobenzene solution (1:1:0.1:0.03) on the PEDOT:PSS film at 600 rpm for 60 s. Then, the wet film was dried in covered glass petri dishes for 60 min. Finally, the Ca/Al electrode (20/80 nm) was thermally deposited on top of the active layer at $2.5 \times 10^{-4}$ Pa. The dye concentrations were

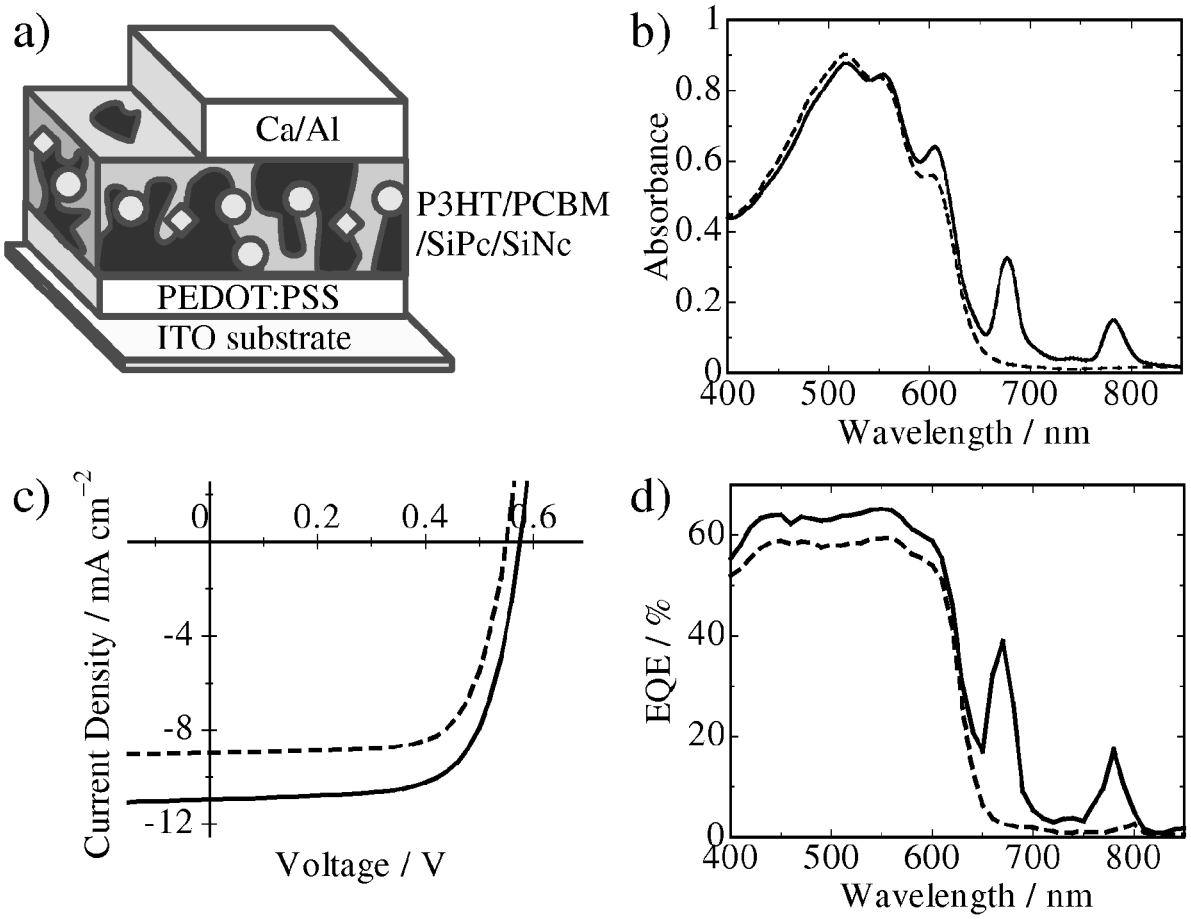


**Figure 4-2.** a) Device configuration of the quaternary blend solar cell. b) Absorption spectra of the RR-P3HT:PCBM:SiPc(4.8 wt%):SiNc(1.5 wt%) blend (solid line) and RR-P3HT:PCBM blend film (broken line). c) *J–V* characteristics and d) EQE spectra of the ITO|PEDOT:PSS|RR-P3HT:PCBM:SiPc:SiNc|Ca|Al (solid lines) and the ITO|PEDOT:PSS|RR-P3HT:PCBM|Ca|Al device (broken lines).

4.8 wt% for SiPc and 1.5 wt% for SiNc, which were optimized for the RR-P3HT:PCBM:dye ternary blend solar cells with SiPc or SiNc.

## 4.3. Results and Discussion

The absorption spectra of the active layers are shown in Figure 4-2b. The quaternary blend films exhibited sharp and intense absorption bands at around 670 and 780 nm,[22] which are ascribable to SiPc and SiNc absorption, respectively, in addition to the absorption of RR-P3HT:PCBM at around 400–600 nm (Figure 4-1c). Interestingly, the vibrational band at

around 600 nm, which is indicative of the crystallization of P3HT,[23] was clearly observed even in the presence of SiPc and SiNc molecules, suggesting that the crystallization of P3HT is not disturbed by the addition of dyes.[24]

Figure 4-2c shows the *J–V* characteristics of the RR-P3HT:PCBM:SiPc:SiNc quaternary blend solar cells and the corresponding RR-P3HT:PCBM binary blend control solar cells under AM1.5G illumination from a calibrated solar simulator with an intensity of 100 mW $cm^{-2}$. The P3HT:PCBM:SiPc:SiNc quaternary blend solar cells exhibited a substantially improved performance compared to the binary blend control cells: a short-circuit current density of $J_{SC}$ = 10.9 mA $cm^{-2}$, an open-circuit voltage of $V_{OC}$ = 0.57 V, a fill factor of FF = 0.69, and PCE = 4.3% (Table 4-1). Compared to the binary blend control solar cells, as shown in Figure 4-2d, the quaternary blend solar cells exhibited an improved external quantum efficiency (EQE) peak at 400–600 nm and two sharp EQE peaks at 670 and 780 nm, corresponding to the absorption of SiPc and SiNc (Figure 4-1c), respectively. The EQE peaks at 670 and 780 nm indicate that both SiPc and SiNc act as sensitizers in the RR-P3HT:PCBM matrix. The EQE at 400–600 nm suggests that the charge separation is as efficient at the interface of RR-P3HT/dye/PCBM as at the interface of RR-P3HT/PCBM. Furthermore, as reported in Chapter 3, the improved EQE is ascribed to the efficient P3HT exciton harvesting to the interface of RR-P3HT/PCBM by the energy transfer from P3HT to dye molecules located at the interface. Such efficient light harvesting based on energy transfer has also been

**Table 4-1.** Device performances for the RR-P3HT:PCBM:SiPc:SiNc quaternary blend solar cells

| SiPc / wt% | SiNc / wt% | $J_{SC}$ / mA $cm^{-2}$ | $V_{OC}$ / V | FF | PCE / % |
|---|---|---|---|---|---|
| 0 | 0 | 8.96 | 0.55 | 0.71 | 3.5 |
| 4.8 | 0 | 10.3 | 0.57 | 0.69 | 4.1 |
| 0 | 1.5 | 9.94 | 0.55 | 0.68 | 3.7 |
| 4.8 | 1.5 | 10.9 | 0.57 | 0.69 | 4.3 |

reported for organic/inorganic hybrid solar cells and dye-sensitized $TiO_2$ solar cells.[25–27] To evaluate the dye contribution efficiency, which is the probability that dye molecules can contribute to the photocurrent generation, the author calculated the absorption efficiency of dye molecules in the quaternary blend solar cells with 4.8 wt% SiPc and 1.5 wt% SiNc molecules by the transfer matrix method.[28] As a result, the absorption efficiency was estimated to be 62% at 670 nm and 33% at 780 nm. From the ratio of the EQE to the absorption efficiency, the dye contribution efficiency is estimated to be 63% at 670 nm (SiPc) and 52% at 780 nm (SiNc). As the author have discussed in Chapter 3, only dye molecules located at the interface of RR-P3HT/PCBM can contribute to the photocurrent generation. The author therefore concludes that the majority of both dye molecules are selectively located at the interface of RR-P3HT/PCBM and thus effectively contribute to the photocurrent generation.

Furthermore, as summarized in Table 4-1, the PCE of the quaternary blend solar cells is higher than that of the individual ternary blend solar cells with a single dye. This is mainly due to the increase in $J_{SC}$. For the individual ternary blend solar cells, the addition of SiPc or SiNc increased $J_{SC}$ from ~9 to ~10 mA $cm^{-2}$ by ~1 mA $cm^{-2}$. For the quaternary blend solar cells, the addition of SiPc and SiNc increased $J_{SC}$ from ~9 to ~11 mA $cm^{-2}$ by ~2 mA $cm^{-2}$. In other words, the increase of $J_{SC}$ in the quaternary blend solar cells is equal to a simple sum of that in the individual ternary blend solar cells. This result indicates that both SiPc and SiNc molecules are located at the interface in the quaternary blends and can contribute to the photocurrent generation effectively without unfavorable interactions between the two dye molecules. Indeed, as mentioned above, SiPc and SiNc contributed as efficiently in the quaternary blend solar cells as in the ternary blend solar cells.

## 4.4. Conclusions

The author's multi-colored dye-sensitized blend solar cells based on quaternary blends of

polymer and fullerene with two different dyes having complementary spectral absorption in the near-IR region are highly efficient. The photocurrent is increased ~10% in the individual ternary blend solar cells and is simply doubled to ~20% in the quaternary blend solar cells. This is probably because both dye molecules are located at the interface without unfavorable aggregation. In other words, the device performance of polymer solar cells can be easily improved by multi-colored dye-sensitization with suitable selection of near-IR dyes and concentration of dyes. An appropriate combination of more than two dyes with different absorption bands or dyes with wider absorption bands compared to phthalocyanines and naphthalocyanines employed in this study could increase PCE to more than 5%. Moreover, this method is simple and versatile and therefore can be easily applied not only to various material combinations but also directly in the existing industrial processes. Thus, this approach could boost the photocurrent generation even for highly efficient polymer solar cells based on low-bandgap polymer and fullerene with PCE > 7%.[10]

## References and Notes

(1) Dennler, G.; Scharber, M. C.; Brabec, C. J. *Adv. Mater.* **2009**, *21*, 1323–1338.

(2) Krebs, F. C.; Gevorgyan S. A.; Alstrup, J. *J. Mater. Chem.*, **2009**, *19*, 5442–5451.

(3) Helgesen, M.; Søndergaard, R.; Krebs, F. C. *J. Mater. Chem.* **2010**, *20*, 36–60.

(4) Krebs, F. C.; T. Tromholt, T.; Jørgensen, M. *Nanoscale*, **2010**, *2*, 873–886.

(5) Li, G.; Shrotriya, V.; Huang, J.; Yao, Y.; Moriarty, T.; Emery, K.; Yang, Y. *Nat. Mater.* **2005**, *4*, 864–868.

(6) Kim, Y.; Cook, S.; Tuladhar, S. M.; Choulis, S. A.; Nelson, J.; Durrant, J. R.; Bradley, D. D. C.; Giles, M.; McCulloch, I.; Ha, C.-S.; Ree, M. *Nat. Mater.* **2006**, *5*, 197–203.

(7) Bundgaard, E.; Krebs, F. C. *Sol. Energy Mater. Sol. Cells* **2007**, *91*, 954–985.

(8) Kroon, R.; Lenes, M.; Hummelen, J. C.; Blom, P. W. M.; de Boer, B. *Polym. Rev.* **2008**, *48*, 531–582.

(9) Peet, J.; Kim, J. Y.; Coates, N. E.; Ma, W. L.; Moses, D.; Heeger, A. J.; Bazan, G. C. *Nat. Mater.* **2007**, *6*, 497–500.

(10) Chen, H.-Y.; Hou, J.; Zhang, S.; Liang, Y.; Yang, G.; Yang, Y.; Yu, L.; Wu, Y.; Li, G.; *Nat. Photonics* **2009**, *3*, 649–653.

(11) Peet, J.; Tamayo, A. B.; Dang, X.-D.; Seo, J. H.; Nguyen, T.-Q. *Appl. Phys. Lett.* **2008**, *93*, 163306.

(12) Suresh, P.; Balraju, P.; Sharma, G. D.; Mikroyannidis, J. A.; Stylianakis, M. M. *ACS Appl. Mater. Interfaces* **2009**, *1*, 1370–1374.

(13) Honda, S.; Nogami, T.; Ohkita, H.; Benten, H.; Ito, S. *ACS Appl. Mater. Interfaces* **2009**, *1*, 804–810.

(14) Flora, W. H.; Hall, H. K.; Armstrong, N. R. *J. Phys. Chem. B* **2003**, *107*, 1142–1150.

(15) Onoda, M.; Tada, K.; Nakayama, H. *J. Appl. Phys.* **1999**, *86*, 2110–2115.

(16) Brabec, C. J.; Cravino, A.; Meissner, D.; Sariciftci, N. S.; Fromherz, T.; Rispens, M.

T.; Sanchez, L.; Hummelen, J. C. *Adv. Funct. Mater.* **2001**, *11*, 374–380.

(17) Choi, H.; Kim, S.; Kang, S. O.; Ko, J.; Kang, M.-S.; Clifford, J. N.; Forneli, A.; Palomares, E.; Nazeeruddin, M. K.; Grätzel, M. *Angew. Chem., Int. Ed.* **2008**, *47*, 8259–8263.

(18) Inakazu, F.; Noma, Y.; Ogomi Y.; Hayase, S. *Appl. Phys. Lett.* **2008**, *93*, 093304.

(19) Lee, K.; Park, S. W.; Ko, M. J.; Kim, K.; Park, N.-G. *Nat. Mater.* **2009**, *8*, 665–671.

(20) Kroon, J. M.; Bakker, N. J.; Smit, H. J. P.; Liska, P.; Thampi, K. R.; Wang, P.; Zakeeruddin, S. M.; Grätzel, M.; Hinsch, A.; Hore, S.; Würfel, U.; Sastrawan, R.; Durrant, J. R.; Palomares, E.; Pettersson, H.; Gruszecki, T.; Walter, J.; Skupien, K.; Tulloch, G. E. *Prog. Photovolt.: Res. Appl.* **2007**, *15*, 1–18.

(21) Ogura, R. Y.; Nakane, S.; Morooka, M.; Orihashi, M.; Suzuki, Y.; Noda, K. *Appl. Phys. Lett.* **2009**, *94*, 073308.

(22) The HOMO and LUMO levels of SiPc and SiNc shown in Figure 4-1b are obtained from $E_{Ox}$ and $E_{Red}$ measured by cyclic voltammetry reported in ref. 14. The bandgaps in Figure 4-1b are a little wider than those estimated from the optical bandgaps of SiPc (1.8 eV) and SiNc (1.6 eV). However, even if these values are changed to latter values, there are still the cascaded energy levels among P3HT, PCBM, and dyes (SiPc and SiNc) as shown in Figure 4-1b.

(23) Erb, T.; Zhokhavets, U.; Gobsch, G.; Raleva, S.; Stühn, B.; Schilinsky, P.; Waldauf, C.; Brabec, C. J. *Adv. Funct. Mater.* **2005**, *15*, 1193–1196.

(24) The vibrational band at 600 nm in Figure 4-2b is slightly larger for the P3HT:PCBM:SiPc:SiNc blends than for the P3HT:PCBM blends because of a small vibrational band of SiPc at 600 nm as shown in Figure 4-1d.

(25) Kudo, N.; Honda, S.; Shimazaki, Y.; Ohkita, H.; Ito, S.; Benten, H. *Appl. Phys. Lett.* **2007**, *90*, 183513.

(26) Liu, Y.; Summers, M. A.; Edder, C.; Fréchet, J. M. J.; McGehee, M. D. *Adv. Mater.*, **2005**, *17*, 2960–2964.

(27) Hardin, B. E.; Hoke, E. T.; Armstrong, P. B.; Yum, J.-H.; Comte, P.; Torres, T.; Fréchet, J. M. J.; Nazeeruddin, M. K.; Grätzel, M.;McGehee, M.D. *Nat. Photonics*, **2009**, *3*, 406–411.

(28) Peumans, P.; Yakimov, A.; Forrest, S. R. *J. Appl. Phys.* **2003**, *93*, 3693–3723.

# *Part III*

# *Chapter 5*

# Selective Dye Loading at the Heterojunction in Polymer/Fullerene Solar Cells

## 5.1. Introduction

Bulk heterojunction solar cells based on polymer:fullerene blends have attracted much attention because they have potential advantages.[1–4] Recently, polymer solar cells based on a blend of regioregular poly(3-hexylthiophene) (RR-P3HT) and 1-(3-methoxycarbonyl)propyl-1-phenyl[6,6]methanofullerene (PCBM) have been widely studied, because they exhibit a relatively high external quantum efficiency (EQE) of more than 70% and high fill factor of up to ~0.7. These device parameters are still the highest reported for polymer solar cells. The performance of this polymer solar cell can be improved by annealing of the active layer such as thermal annealing and solvent annealing.[5–9] The thermal annealing has been reported to enhance the formation of RR-P3HT crystal domains and PCBM aggregates. The solvent annealing has been reported to enhance the formation of well-ordered RR-P3HT nanofibrils but suppress the formation of PCBM large aggregates.[9] After such annealing treatments, power conversion efficiency (PCE) can be improved to 4–5%. For further improvement, more efficient light-harvesting is required because RR-P3HT can absorb only a quarter of the total photons in the solar light.[10,11] Consequently, various low band-gap polymers have been developed to absorb a broad range of the solar light.[10–14] On the other hand, dye sensitization has been recently reported as another way to improve the light-harvesting efficiency in polymer solar cells by several groups.[15–18]

In dye-sensitized polymer solar cells, dye molecules are simply blended as the third component to harvest solar photons at longer wavelengths that the original donor and acceptor materials cannot collect. This is a simple and versatile method and therefore various dye molecules can be employed. However, the dye aggregation hinders the efficient light harvesting in ternary blends. In Chapter 3, the author reported that an appropriate selection of dyes with bulky groups, silicon phthalocyanine bis(trihexylsilyl oxide) (SiPc), can effectively suppress the formation of dye aggregates and consequently improve the light-harvesting efficiency. Furthermore, in Chapter 4, the author demonstrated that this method is applicable even to multi-colored sensitization with different dye molecules. Considering the large photocurrent due to dye molecules, the author speculated that most of the dye molecules are segregated to the donor/acceptor interface because of the crystallinity of matrix polymers and fullerenes. Such interfacial segregation of dye molecules is also the key to the improvement. However, there remains a fundamental question of why dye molecules are spontaneously segregated into the interface only by spin-coating from blend solutions.

Segregations of a component material can be found in various blends. For various binary blends such as polymer:fullerene, polymer:polymer, or phthalocyanine:fullerene, surface segregation has been recently reported.[19–24] These studies suggested that the material with a lower surface energy is likely to be segregated into the air/film interface while the material with a higher surface energy is segregated to the film/electrode interface, indicating that the vertical phase separation is strongly dependent on the surface energy of each material. For ternary blend films i which a third material is added to binary blends, the location of the third component has been studied for various materials such as conductive carbon black particles,[25] carbon nanotubes,[26–28] $CaCO_3$ nanoparticles,[29] and polymers.[30] These studies indicated that the location of the third component can be predicted in terms of the surface energy of each component in ternary blends, which is in good agreement with the observation of transmission

electron microscopy (TEM) images. In other words, surface energy plays a crucial role in segregation of each material in blends, which has significant impact on the phase-separated structures.

Herein the author reports the selective localization of SiPc molecules at the RR-P3HT/PCBM interface in ternary blends, which can improve the device performance of the ternary blend solar cells by the efficient dye sensitization as mentioned above. To address the origin of such selective localization, the author carefully measured the absorption spectra of SiPc doped into various films and the surface energy of pristine films of RR-P3HT, PCBM, and SiPc, and blend films of RR-P3HT:SiPc and PCBM:SiPc. On the basis of these detailed analyses, the selective localization of dye molecules is explained in terms of the crystallization of the matrix material and the surface energy of each component. Furthermore, the relevance of the device performance of the ternary blend solar cells to the dye localization by annealing conditions is also discussed.

## 5.2. Experimental Methods

### *5.2.1. Sample Preparation*

Ternary blend solar cells of RR-P3HT:PCBM:SiPc were fabricated as follows. Indium tin oxide (ITO)-coated glass substrates (10 Ω per square) were washed by ultrasonication in toluene, acetone, and ethanol for 15 min, dried with $N_2$, and then cleaned with a UV–$O_3$ cleaner for 30 min. A thin layer (ca. 40 nm) of poly(3,4-ethylenedioxythiophene) with poly(4-styrenesulfonate) (PEDOT:PSS, H.C.Starck, PH500) was spin-coated onto the cleaned ITO-coated substrates at a spin rate of 3000 rpm and the layer was dried at 140 °C for 10 min in air. For the thermal-annealed device, a blend layer of RR-P3HT:PCBM:SiPc (ca. 100 nm) was spin-coated from a chlorobenzene solution on the PEDOT:PSS film at 1200 rpm for 60 s and the film was annealed at 150 °C for 30 min in a $N_2$-filled glove box. For the solvent-

annealed device, a blend layer of RR-P3HT:PCBM:SiPc (ca. 200 nm) was spin-coated from an *o*-dichlorobenzene solution on the PEDOT:PSS film at 600 rpm for 60 s. Then, the wet film was dried in covered glass petri dishes for 60 min. Finally, the Ca/Al electrode (20/80 nm) was thermally deposited on top of the active layer at $2.5 \times 10^{-4}$ Pa. The blend solution was prepared as follows: RR-P3HT (Plextronics, regioregularity > 98%, $M_n$ = ~45,000–65,000 g mol$^{-1}$) and PCBM (Frontier Carbon) were dissolved in chlorobenzene (10 and 10 mg mL$^{-1}$) or *o*-dichlorobenzene (17 and 17 mg mL$^{-1}$), the solution was stirred at 40 °C overnight, and then SiPc (Aldrich) was dissolved in the solution at room temperature. Note that the dye composition was varied from 1.5 to 17 wt% in the ternary blend films. For comparison, RR-P3HT:PCBM control devices without dyes were also prepared separately under the same condition to give the same active layer thickness.

For contact angle measurements, neat films of RR-P3HT, regiorandom P3HT (RRa-P3HT, Aldrich, head-to-head : head-to-tail = 1 : 1, $M_w$ = 90,600), PCBM, SiPc, polystyrene (PSt, Scientific Polymer Products, $M_w$ = 22,000), and poly(methyl methacrylate) (PMMA, Scientific Polymer Products, $M_w$ = 380,000) and blend films of RR-P3HT:SiPc and PCBM:SiPc with various dye compositions were prepared by spin-coating on glass substrates previously cleaned as described above from chlorobenzene solutions (10–30 mg mL$^{-1}$).

For the model system of ternary blend films, RR-P3HT:PSt:SiPc and PMMA:PSt:SiPc blend films were prepared by spin-coating on glass substrates previously cleaned as described above from chrolobenzene solutions with RR-P3HT:PSt:SiPc (10:10:5 mg mL$^{-1}$) and PMMA:PSt:SiPc (10:10:5 mg mL$^{-1}$).

For absorption spectra measurements, RRa-P3HT, RRa-P3HT:PCBM, and RR-P3HT:PCBM (before and after thermal annealing) films doped with SiPc were prepared by spin-coating on glass substrates previously cleaned as described above from chrolobenzene solutions: RRa-P3HT, RRa-P3HT:PCBM, and RR-P3HT:PCBM were separately dissolved in

chlorobenzene at a concentration of 10 mg $mL^{-1}$ and then SiPc was dissolved in the solution to give various dye compositions of 1–100 wt% in the final films. The RR-P3HT:PCBM blend film was annealed at 150 °C for 30 min in a $N_2$-filled glove box.

### *5.2.2. Measurements*

Absorption spectra were measured with a spectrophotometer (Hitachi, U-3500). The *J–V* characteristics were measured with a DC voltage and current source/monitor (Advantest, R6243) in the dark and under the illumination with AM1.5G simulated solar light with 100 mW $cm^{-2}$. The light intensity was corrected with a calibrated silicon photodiode reference cell (Bunkoh-Keiki, BS-520). The photocurrent action spectra were measured with a digital electrometer (Advantest, R8252) under monochromatic light illumination from a 500-W xenon lamp (Thermo Oriel, Model 66921) with optical cut filters and a monochromator (Thermo Oriel, UV–visible Cornerstone). The active area of the device was 0.07 $cm^2$. The illumination was carried out from the ITO side under $N_2$ atmosphere. At least 3 devices were fabricated to ensure the reproducibility of the *J–V* characteristics.

Contact angles $\theta_X$ using ultrapure water were measured on a spin-coated film of material X at room temperature. The surface energy $\gamma_X$ of the material X was evaluated from $\theta_X$ by the Neumann's equation combined with Young's equation.[31] The interfacial energy $\gamma_{A-B}$ between materials A and B was evaluated from $\gamma_A$ and $\gamma_B$ by the Neumann's equation.[31] The wetting coefficient $\omega_C$ of material C in a blend of materials A and B was evaluated by Young's equation.[25]

Film morphology and thickness were measured with an atomic force microscope (Shimadzu, SPM-9600) in the contact mode. The AFM images were obtained for as-cast films, SiPc-removed films by immersing the as-cast films into pentane (Wako) for 1 min, and PSt-removed films after by immersing the SiPc-removed films into cyclohexane (Nacalai Tesque) for 5 min. The film thickness was evaluated from the step height across a scratch

made on the films.

## 5.3. Results

### *5.3.1. Device Performances*

Figure 5-1 shows the *J–V* characteristics of RR-P3HT:PCBM:SiPc ternary blend solar cells and the corresponding control solar cells of RR-P3HT:PCBM binary blends with solvent annealing (Figure 5-1a) or thermal annealing (Figure 5-1b) under AM1.5G simulated solar

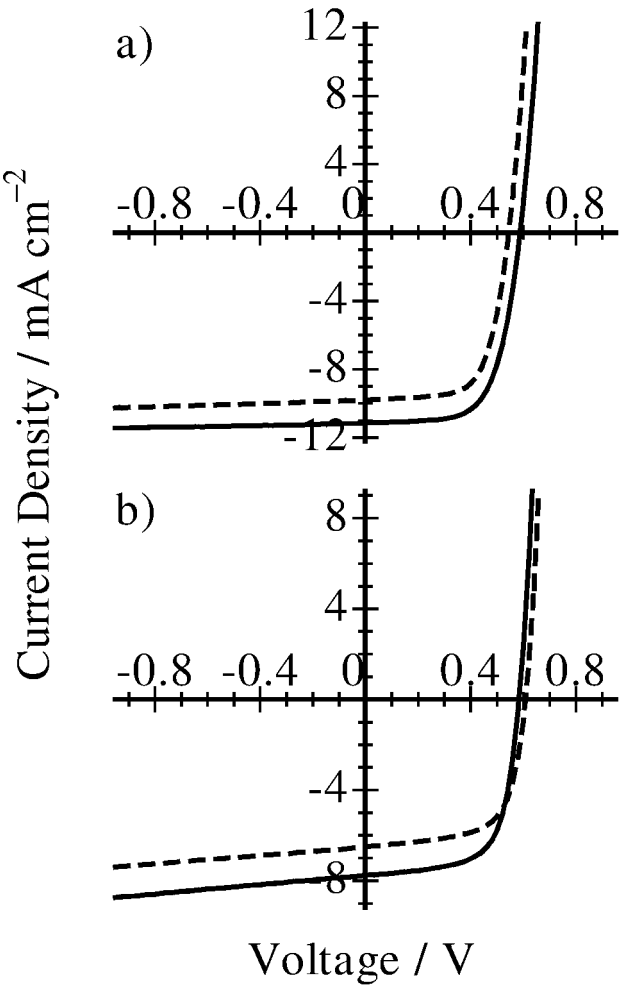


**Figure 5-1.** *J–V* characteristics of RR-P3HT:PCBM:SiPc (1:1:0.1) ternary blend (solid lines) and RR-P3HT:PCBM (1:1) binary blend solar cells (broken lines) after a) solvent and b) thermal annealing.

illumination at an intensity of 100 mW $cm^{-2}$. In the ternary blend solar cells, RR-P3HT is employed as a donor material, PCBM as an acceptor material, and SiPc as a light-harvesting dye that has an absorption band at longer wavelengths than RR-P3HT. The active layer was annealed under two different conditions: thermal annealing at 150 °C and solvent annealing under *o*-dichlorobenzene vapor. The dye composition was fixed to 4.8 wt% for both annealing conditions. For the solvent-annealed cells, as shown in Figure 5-1a, the short-circuit current density was improved by ~15% from $J_{SC}$ = 9.69 mA $cm^{-2}$ for the binary blend control cell to $J_{SC}$ = 11.1 mA $cm^{-2}$ for the ternary blend solar cell. The open-circuit voltage was also improved by ~5% from $V_{OC}$ = 0.55 V to 0.58 V. Consequently, power conversion efficiency was improved by ~20% from PCE = 3.5% to 4.2% because of the dye addition. Similarly, as shown in Figure 5-1b, the short-circuit current density of the thermal-annealed device was also improved by ~15% from $J_{SC}$ = 6.73 mA $cm^{-2}$ for the binary blend control cell to $J_{SC}$ = 7.83 mA $cm^{-2}$ for the ternary blend solar cell. The open-circuit voltage slightly decreased by the dye addition. Overall, PCE was improved by ~10% from PCE = 2.6% to 2.9%. These results are consistent with the results shown in Chapter 3. The difference in PCE is simply ascribed to the different thickness of the active layer. In other words, the dye addition can improve $J_{SC}$ mainly and thus enhance PCE by more than 10% under either annealing condition.

Figure 5-2 shows the dye-composition dependence of device performances of RR-P3HT:PCBM:SiPc ternary blend solar cells under different annealing conditions. For the solvent-annealed device, $J_{SC}$ increased with the increase in dye composition below 4.8 wt% and then kept constant up to 17 wt%. The other parameters slightly decreased with the increase in dye composition above 4.8 wt%. For the thermal-annealed device, on the other hand, $J_{SC}$ and FF slightly increased with the increase in the dye composition below 4.8 wt% but significantly decreased at a high dye composition of 17 wt%. Consequently, as mentioned

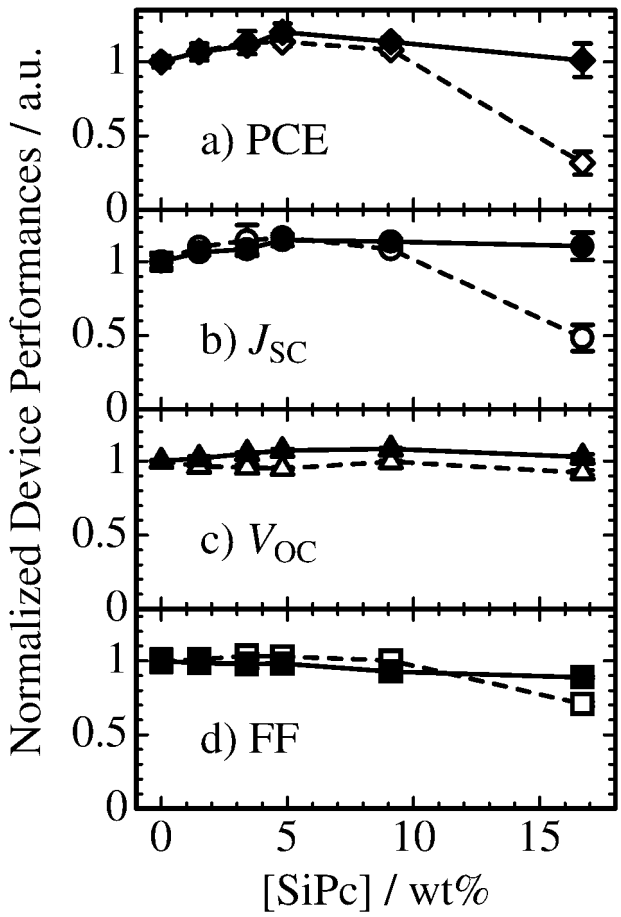


**Figure 5-2.** Normalized device performances of RR-P3HT:PCBM:SiPc blend solar cells after solvent (closed symbols) and thermal annealing (open symbols) plotted against a composition of SiPc: a) PCE, b) $J_{SC}$, c) $V_{OC}$, and d) FF.

above, the best performance was obtained at a dye composition of 4.8 wt% under both annealing conditions. The device parameters of RR-P3HT:PCBM:SiPc ternary blend solar cells are summarized in the Appendix.

To address the origin of the decrease in the photocurrent at high compositions of SiPc, the author measured the external quantum efficiency (EQE) spectra of ternary blend solar cells with different dye compositions. At a dye composition of 4.8 wt%, as shown in Figure 5-3a, EQE peaks increased at 400–600 nm (P3HT absorption) and 670 nm (SiPc absorption) under either annealing condition, compared to the binary blend control devices. As reported in Chapter 3, the improvement in the EQE peak at 400–600 nm is ascribed to the efficient P3HT

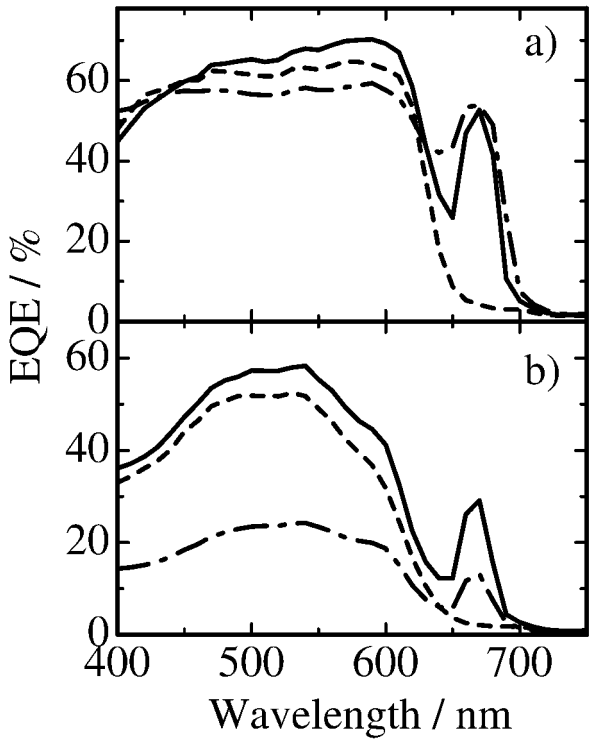


**Figure 5-3.** EQE spectra of RR-P3HT:PCBM:SiPc ternary blend with 4.8 wt% SiPc (solid lines) and 17 wt% SiPc (dashed–dotted lines) and RR-P3HT:PCBM (1:1) binary blend solar cells (broken lines) after a) solvent and b) thermal annealing.

exciton harvesting to the interface of P3HT/PCBM by the energy transfer from P3HT to SiPc located at the interface, and the improvement at 670 nm is ascribed to the direct absorption of SiPc. The exciton harvesting by energy transfer has also been reported for organic/inorganic hybrid solar cells and dye-sensitized $TiO_2$ solar cells.[32–35] At a dye composition of 17 wt%, on the other hand, EQE peaks slightly decreased at 400–600 nm and remained the same at 670 nm for the solvent-annealed cells while whole the EQE spectra decreased uniformly for the thermal-annealed cells. This finding suggests that the origin of the decrease in the photocurrent is dependent on the annealing conditions as discussed later.

To estimate how many dyes can contribute to the photocurrent generation quantitatively, the author evaluated the internal conversion efficiency (IQE) at the dye absorption, which is a lower limit of the dye contribution efficiency to the photocurrent. For the ternary blend

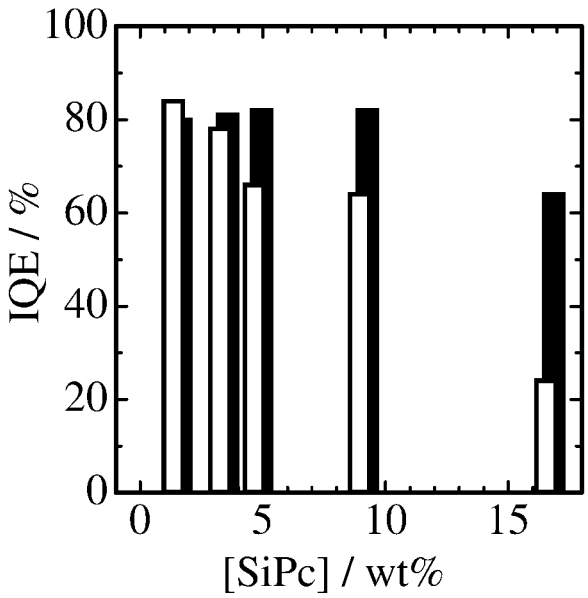


**Figure 5-4.** IQE at 670 nm of RR-P3HT:PCBM:SiPc ternary blend solar cells after solvent (closed bars) and thermal annealing (open bars) plotted against a composition of SiPc.

devices with 4.8 wt% SiPc, the absorption efficiency at 670 nm was calculated to be 65% for the solvent-annealed device and 44% for the thermal-annealed device by the transfer matrix method.[36] As shown in Figure 5-3, the EQE at 670 nm was 53% for the solvent-annealed device and 29% for the thermal-annealed device. Therefore, the IQE at 670 nm was estimated to be as high as 82% for the solvent-annealed device and 66% for the thermal-annealed device. Figure 5-4 shows the dependence of the IQE at 670 nm for RR-P3HT:PCBM:SiPc devices on the dye composition. For the solvent-annealed devices, the IQE is as high as ~80% at dye compositions of <10 wt% and still higher than 60% at 17 wt%. For the thermal-annealed devices, on the other hand, the IQE kept higher than 60% up to 9.1 wt% but decreased to ~20% at a dye composition of 17 wt%. Considering the cascaded energy levels, as the author has discussed in Chapter 3, only dye molecules located at the P3HT/PCBM interface can contribute to the photocurrent generation. Therefore, such a high IQE suggests that the majority of dye molecules are selectively located at the interfacial area and thus effectively contribute to the photocurrent generation.

### *5.3.2. Absorption Spectra*

Figure 5-5 shows typical absorption spectra of ternary and binary blend films. As shown in Figure 5-5, the solvent-annealed ternary blend film of RR-P3HT:PCBM:SiPc(4.8 wt%) exhibited more distinguished vibrational bands at around 500–600 nm, which are indicative of the crystallization of P3HT,[37] than the thermal-annealed ternary blend film. Interestingly, the vibrational bands were clearly observed even in the presence of SiPc molecules under both annealing conditions, suggesting that the crystallization of P3HT is not disturbed by the addition of SiPc molecules. The peak wavelength of the SiPc absorption was observed at 676 nm for the solvent-annealed ternary blends and for 677 nm for the thermal-annealed ternary blends. These bands were slightly red-shifted compared to the peak wavelength of SiPc dissolved in solution (669 nm),[38] suggesting that SiPc molecules are not as homogeneously

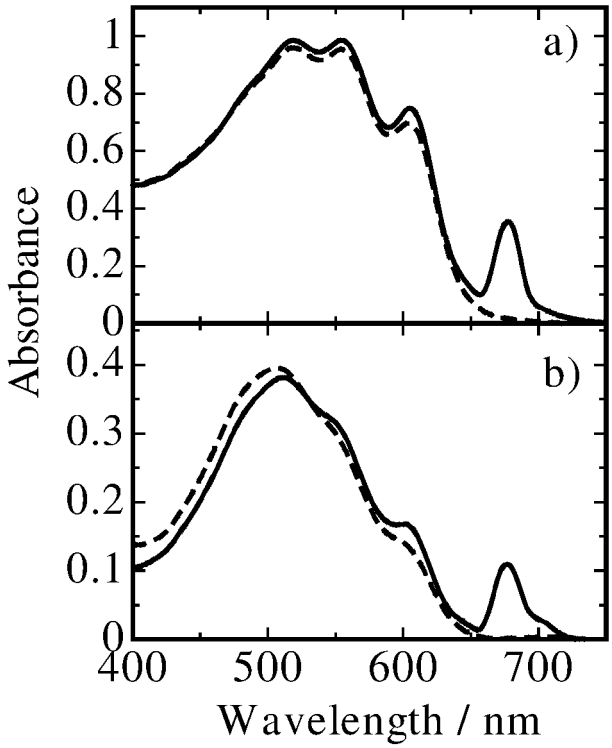


**Figure 5-5.** Absorption spectra of RR-P3HT:PCBM:SiPc (1:1:0.1) ternary blend (solid lines) and RR-P3HT:PCBM (1:1) binary blend solar cells (broken lines) after a) solvent and b) thermal annealing.

dispersed in blend films as in solution but probably more concentrated in blend films as described below.

To understand how the majority of dye molecules are dispersed in blend films, the author carefully examines the dependence of absorption spectra on the dye composition in details. As shown by the open triangles in Figure 5-6, the absorption peak wavelength of SiPc ($\lambda_{max}$) in RR-P3HT films was red-shifted monotonically from 670 nm (1 wt% SiPc) to 687 nm (100 wt % SiPc). On the other hand, the absorption peak in PCBM films was significantly red-shifted to 679 nm even at a low dye composition of 1 wt%, suggesting the ground-state interaction between SiPc and PCBM. The peak was further red-shifted to 696 nm up to 20 wt%, but blue-shifted to 687 nm above 20 wt%. These red-shifts observed for both blends are indicative of the increase in the local concentration of dye molecules. The blue-shift observed for PCBM films with >20wt% SiPc is due to the surface segregation of SiPc as described

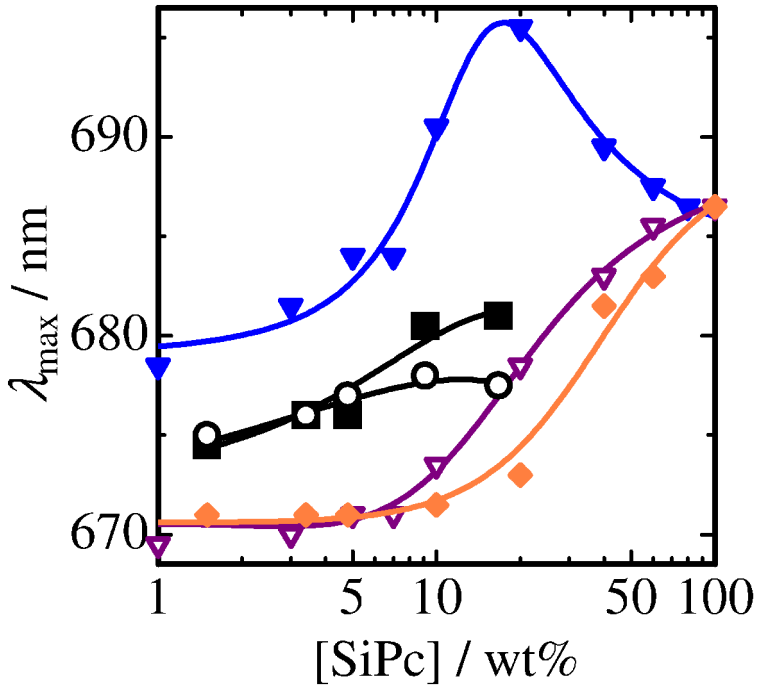


**Figure 5-6.** Peak wavelengths of the SiPc absorption in RRa-P3HT (closed diamonds), RR-P3HT (open triangles), PCBM (closed triangles), and RR-P3HT:PCBM matrix with solvent (closed squares) and thermal annealing (open circles) plotted against a composition of SiPc. The solid lines are guided to the eye for SiPc doped in each matrix film.

later, which would decrease the interaction between SiPc and PCBM. On the other hand, the absorption peak of SiPc in RR-P3HT:PCBM blend films is located about midway between them. If the majority of SiPc molecules were located at each pure domain in ternary blend films, the absorption peak should be close to that observed for SiPc in RR-P3HT or PCBM films. The intermediate absorption peak of ternary blend films suggests that the majority of SiPc molecules are located at the interface of RR-P3HT and PCBM. Here the author tentatively ascribes the primary location of SiPc in ternary blend films to disordered P3HT domains located at the interface, because SiPc molecules are likely to be located in RR-P3HT rather than in PCBM as described in the next section. Thus, the red-shifted absorption compared to binary blend films can be ascribed to the increase in the local concentration of SiPc at disordered P3HT domains in ternary blend films.

In order to evaluate the local concentration of SiPc at disordered P3HT domains, the author measured the absorption spectra of SiPc molecules doped in RRa-P3HT amorphous films with different dye concentrations. As shown by the closed diamonds in Figure 5-6, the peak wavelength was gradually red-shifted from 671 to 687 nm with increasing dye concentration from 1 to 100 wt%. This trend is consistent with a previous report.[39] A similar result was observed for SiPc doped into PSt amorphous films (see the Appendix), indicating that the peak shift is not due to the interaction with the matrix but can be ascribed to the increase in the local concentration of SiPc molecules in the matrix. Interestingly, the absorption peak of SiPc in RR-P3HT films was almost the same as that in RRa-P3HT at dye compositions <10 wt% but was red-shifted at higher compositions >10 wt%. This suggests that the local concentration in RR-P3HT is almost the same as in RRa-P3HT films at <10 wt% but higher than in RRa-P3HT films at >10 wt%. This is probably related to the crystallization of RR-P3HT as discussed later.

To examine the effect of the crystallization of RR-P3HT on the local concentration of dye

molecules, the author compared the absorption peaks of SiPc doped in various matrices with different crystallinity at a dye composition fixed to 3.4 wt%. In Chapters 3 and 4, the author speculated that the crystallization of matrix materials would expel dye molecules into the interface of P3HT/PCBM. If the crystallization were the only driving force for dye molecules to be selectively located at the interface, the absorption peak of SiPc in RRa-P3HT:PCBM blend films should be the same as that in RRa-P3HT films. However, the absorption peak of SiPc was actually more red-shifted in RRa-P3HT:PCBM blend films (674 nm) than in RRa-P3HT films (671 nm). This finding shows that there is another driving force for the selective localization of dye molecules into the interface, which will be described in the next section. Furthermore, the absorption peak of SiPc was red-shifted to 675 nm for RR-P3HT:PCBM blend films before thermal annealing and more red-shifted to 676 nm for RR-P3HT:PCBM blend films after thermal annealing. Details are summarized in the Appendix. The crystallinity of P3HT increased in the order of RRa-P3HT:PCBM, RR-P3HT:PCBM before thermal annealing, and after thermal annealing, because vibrational bands at around 500–600 nm were more distinguished in the same order (see the Appendix). Thus, the red-shifts observed for RR-P3HT:PCBM blend films are ascribable to the crystallization of P3HT, which can induce the interfacial segregation of dye molecules.

### *5.3.3. Surface Energy*

As mentioned in the Introduction, the difference in surface energy between RR-P3HT and PCBM has been reported to be one of the driving forces for the vertical phase-separation in RR-P3HT:PCBM binary blend films.[19–21] Here the author focuses on the surface energy of materials as another driving force of the selective dye localization in ternary blend films. The surface energy of material A ($\gamma_A$) was estimated from the contact angle of ultrapure water on spin-coated films of material A.[31] The surface energy of RR-P3HT ($\gamma_{RR\text{-}P3HT}$ = 20 mJ m$^{-2}$) was lower than that of PCBM ($\gamma_{PCBM}$ = 29 mJ m$^{-2}$), which are consistent with previous reports.[40,41]

The surface energy of RRa-P3HT ($\gamma_{RRa\text{-}P3HT}$ = 21 mJ m$^{-2}$) was almost the same as that of RR-P3HT. On the other hand, the surface energy of SiPc was $\gamma_{SiPc}$ = 23 mJ m$^{-2}$, which is relatively close to that of RR-P3HT but is an intermediate value between those of RR-P3HT and PCBM. The surface energy of each material employed in this study is summarized in Table 5-1.

Before considering ternary blends, the author first examined the location of dye molecules in binary blend films of RR-P3HT:SiPc or PCBM:SiPc. Figure 5-7 shows the surface energy of the binary blend films with various compositions of SiPc. For RR-P3HT:SiPc blends, the surface energy $\gamma_{RR\text{-}P3HT:SiPc}$ was the same as $\gamma_{RR\text{-}P3HT}$ up to 40 wt% SiPc. For PCBM:SiPc blends, on the other hand, the surface energy $\gamma_{PCBM:SiPc}$ steeply decreased from $\gamma_{PCBM}$ = 29 mJ m$^{-2}$ at 0 wt% to 24 mJ m$^{-2}$ even at 10 wt% SiPc, which is already comparable to $\gamma_{SiPc}$ = 23 mJ m$^{-2}$. These findings suggest that SiPc molecules are likely to be embedded in RR-P3HT matrix but to be segregated at the air/film interface of the PCBM film. This difference can be rationally explained in terms of the surface energy: the component with the lowest surface energy (RR-P3HT for RR-P3HT:SiPc blends and SiPc for PCBM:SiPc blends) is segregated into the air/film interface to decrease the total energy of the system. These results suggest that SiPc molecules are located in P3HT rather than in PCBM.

**Table 5-1.** Contact angles and surface energy for various films.

| Materials | Contact angle / deg | Surface energy / mJ m$^{-2}$ |
|---|---|---|
| RR-P3HT | 105 | 20 |
| RRa-P3HT | 103 | 21 |
| SiPc | 100 | 23 |
| PSt | 95 | 26 |
| PCBM | 91 | 29 |
| PMMA | 67 | 44 |

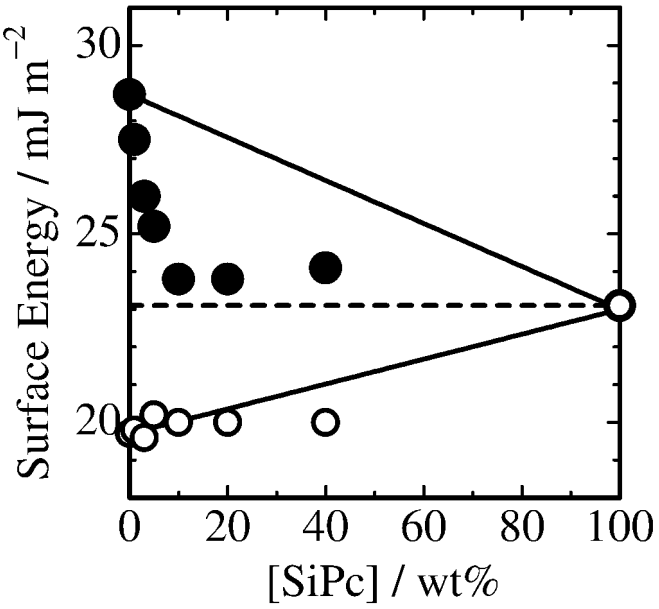


**Figure 5-7.** Surface energy, which is estimated by the contact angles of ultrapure water on films, of RR-P3HT:SiPc (open circles) and PCBM:SiPc (closed circles) blend films plotted against a composition of SiPc. The broken line represents the surface energy of SiPc (23 mJ $m^{-2}$). The solid lines represent the surface energy of RR-P3HT:SiPc or PCBM:SiPc predicted on the assumption of homogeneous dispersion of SiPc molecules in blend films.

Next, the author considered the location of dye molecules in ternary blends of RR-P3HT:PCBM:SiPc on the basis of the interfacial surface energy. Here, the author estimated the wetting coefficient for ternary blends to predict the location of dyes in blend films. This method has been applied to polymer blends doped with various materials such as conductive carbon black particles,[25] carbon nanotubes,[26–28] $CaCO_3$ nanoparticles,[29] and polymers.[30] The wetting coefficient of material C ($\omega_C$) in blends of materials A and B can be calculated by the Young's equation as follows: $\omega_C = (\gamma_{C-B} - \gamma_{C-A})/\gamma_{A-B}$ where $\gamma_{X-Y}$ is the interfacial surface energy between X and Y.[25] The interfacial surface energy can be calculated by the Neumann's equation as follows: $\gamma_{X-Y} = \gamma_X + \gamma_Y - 2\,(\gamma_X\,\gamma_Y)^{0.5} \exp\,[-\beta\,(\gamma_X - \gamma_Y)^2]$, where $\beta = 0.000115$ $m^4$ $mJ^{-2}$.[31] If the wetting coefficient is larger than unity ($\omega_C > 1$), the material C will be located in the domain A. If $\omega_C < -1$, C will be located in the domain B. If $-1 < \omega_C < 1$, C will be

located in the interface between A and B. The wetting coefficient of SiPc in RR-P3HT:PCBM blends was calculated to be 0.32 on the basis of the above equation, suggesting that SiPc molecules are located at the P3HT/PCBM interface. This is true for SiPc doped into RRa-P3HT:PCBM blends because RRa-P3HT has almost the same surface energy as RR-P3HT. It should be noted that this evaluation is valid for ternary blends in the thermodynamically equilibrium state. Originally, it was considered for the addition of particle components, for example carbon black particles.[25] In other words, it is not clear if the wetting coefficient can be applied to RRa-P3HT:PCBM blend films doped with dye molecules prepared by spin-coating that results in the thermodynamically non-equilibrium state.

The author thus prepared two model systems to demonstrate the validity of this evaluation to the author's ternary blend films. One is RR-P3HT:PSt:SiPc and the other is PMMA:PSt:SiPc blends. The RR-P3HT:PSt:SiPc blend film is a model of $-1 < \omega_C < 1$ where dye molecules are considered to be located at the interface of P3HT/PSt. This is similar to RR-P3HT:PCBM:SiPc blends. Instead of PCBM, PSt is employed because of the following three reasons: (i) RR-P3HT:PSt blends show large phase separation of P3HT-rich domains and PSt-rich domains, which can be observed by atomic force microscopy (AFM),[42] and (ii) the surface energy of PSt ($\gamma_{PSt}$ = 26 mJ m$^{-2}$) is similar to that of PCBM and higher than that of RR-P3HT and SiPc, resulting in a wetting coefficient of SiPc in the RR-P3HT:PSt blend ($\omega_C$

**Table 5-2.** Wetting coefficients and predicted location of SiPc doped into various blend matrices.

| Matrices | Wetting coefficient ($\omega_C$) | Predicted location of dyes in the blends |
|---|---|---|
| RR-P3HT:PCBM | 0.32 | interface |
| RRa-P3HT:PCBM | 0.49 | interface |
| RR-P3HT:PSt | 0.60 | interface |
| PMMA:PSt | −1.3 | in PSt |

= 0.60) similar to that of RR-P3HT:PCBM:SiPc blends, as shown in Table 5-2, and (iii) the components in ternary blend films can be assigned by sequential removal of materials: first, SiPc can be removed by immersing the films into pentane that can dissolve SiPc but cannot dissolve RR-P3HT or PSt, and then PSt can be removed by immersing the films into cyclohexane that can dissolve PSt but cannot dissolve RR-P3HT.[43] On the other hand, the PMMA:PSt:SiPc blend film is studied as a model of $\omega_C < -1$ where dye molecules are considered to be located at PSt domains because of the high surface energy of PMMA ($\gamma_{PMMA}$ = 44 mJ $m^{-2}$). This blend also shows a large phase separation of PMMA domains and PSt domains,[44] and each domain can be assigned because PMMA cannot dissolve in pentane or cyclohexane.[43]

Figure 5-8 shows the AFM images of RR-P3HT:PSt:SiPc ternary blend films before and after successive dissolving of SiPc and PSt. For as-cast films of RR-P3HT:PSt:SiPc, as shown in Figure 5-8a, sea–island phase-separated structures were observed with a ring projection at the interface between sea and island domains. After immersing in pentane to remove SiPc, as shown in Figure 5-8c, the ring projection changed to the ring hollow although the sea–island phase-separated structure remained the same. After immersing in cyclohexane to remove PSt, as shown in Figure 5-8e, only the island domains were observed on substrates. Thus, the sea and island domains can be assigned to PSt and RR-P3HT domains, respectively. These results show that the majority of SiPc molecules are located at the interface of RR-P3HT/PSt in RR-P3HT:PSt:SiPc ternary blends. This dye location is in good agreement with the prediction based on a wetting coefficient of $-1 < \omega_C = 0.60 < 1$.

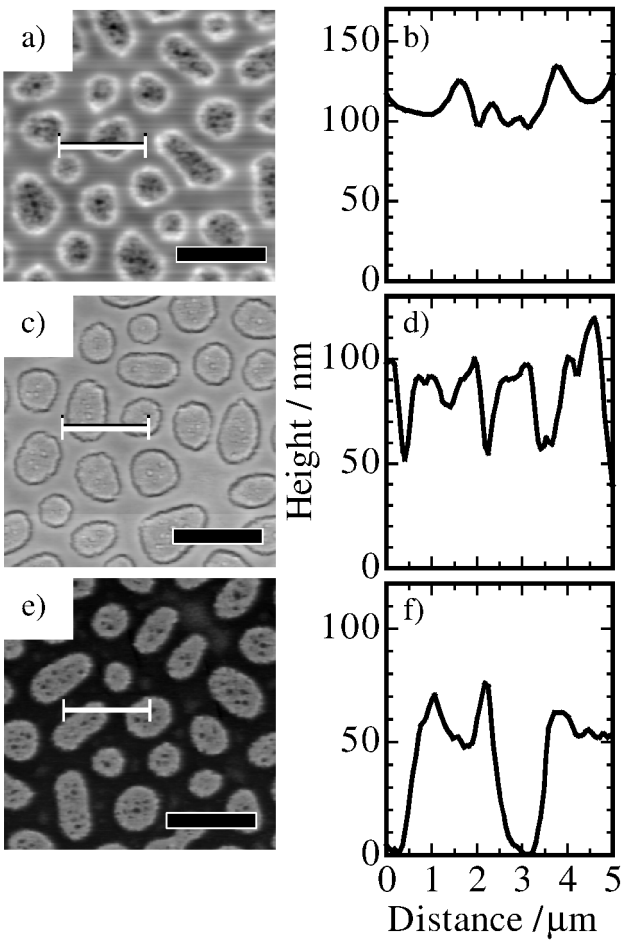


**Figure 5-8.** AFM images of RR-P3HT:PSt:SiPc (10:10:5) blend films: a) as-cast films, c) SiPc-removed films by immersing in pentane for 1 min, e) PSt-removed films by immersing in cyclohexane for 5 min. The right figures b), d), and f) represent line profiles at the white bars shown in a), c), and e), respectively. The black scale bars shown in a), c), and e) are 5 μm.

On the other hand, Figure 5-9 shows the AFM images of PMMA:PSt:SiPc ternary blends. Similarly, as shown in Figure 5-9a, sea–island phase-separated structures were observed for as-cast films of the ternary blend, but no ring projection or hollow was observed at the interface between the sea and island domains. After removing SiPc, as shown in Figure 5-9c, no ring hollow was observed in contrast to RR-P3HT:PSt:SiPc blends film after removal of SiPc. Instead, the height of the sea domains decreased by ~20%, which is consistent with the weight fraction of SiPc. After removing PSt, as shown in Figure 5-9e, only the island

domains were observed. Thus, the sea and island domains can be assigned to PSt and PMMA domains, respectively. These results show that the majority of SiPc molecules are located in the sea domains of PSt in PMMA:PSt:SiPc ternary blend films, which is again in good agreement with the prediction by the wetting coefficient, as summarized in Table 5-2. All these findings show that the dye location in ternary blend films can be well predicted on the basis of the wetting coefficient.

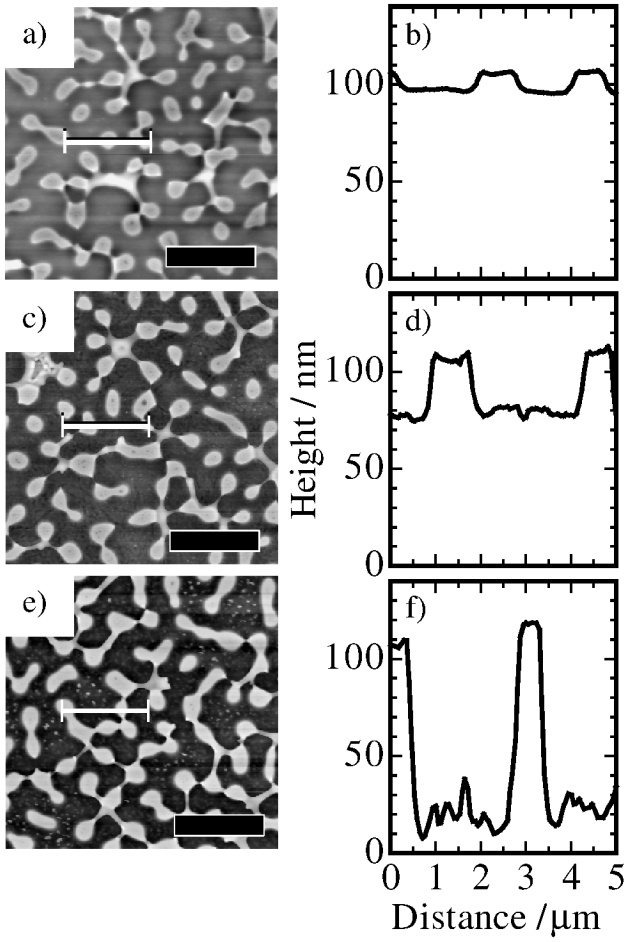


**Figure 5-9.** AFM images of PMMA:PSt:SiPc (10:10:5) blend films: a) as-cast films, c) SiPc-removed films by immersing in pentane for 1 min, e) PSt-removed films by immersing in cyclohexane for 5 min. The right figures b), d), and f) represent line profiles at the white bars shown in a), c), and e), respectively. The black scale bars shown in a), c), and e) are 5 μm.

### *5.3.4. Blend Morphology*

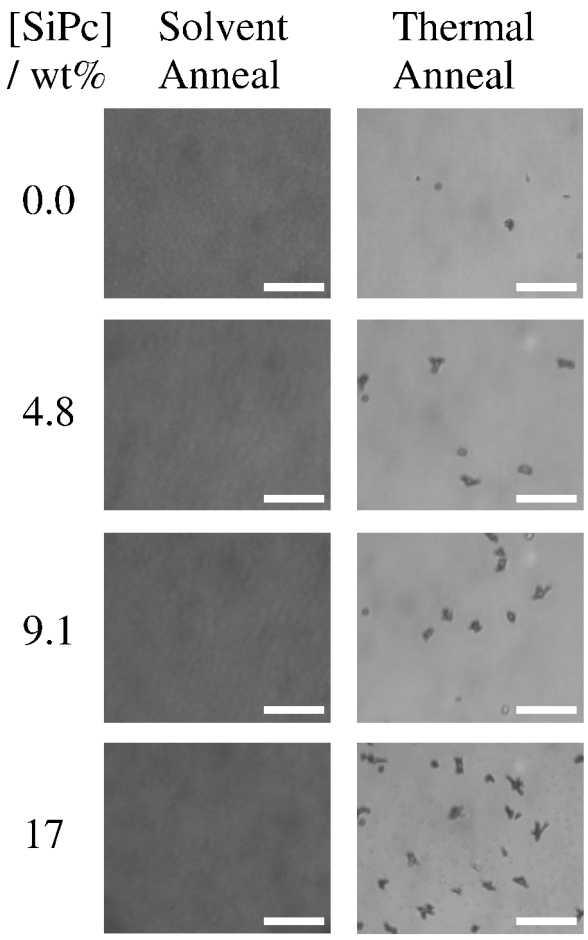


**Figure 5-10.** Optical microscope images of RR-P3HT:PCBM:SiPc ternary blend films after solvent and thermal annealing. The composition of SiPc is shown on the left. The white scale bars show 50 μm.

Finally, the author examines the film morphology under the different annealing conditions by the optical microscopy to discuss the relationship between the device performance and the film morphology. As shown in Figure 5-10, micrometer-sized clusters were observed for RR-P3HT:PCBM binary blend films after thermal annealing at 150 °C for 30 min. As reported previously, these clusters are ascribable to PCBM: the thermal annealing would enhance the diffusion of small molecules such as PCBM and consequently induce the formation of PCBM aggregates.[45] Upon the addition of dye molecules, the number and size of PCBM clusters

increased with increasing dye composition. A lot of needle-like PCBM clusters were observed for the films with 17 wt% SiPc. On the other hand, no cluster was observed for the solvent-annealed blend films with or without dye molecules. This is consistent with a previous report on RR-P3HT:PCBM binary blends.[9] These results suggest that the addition of SiPc molecules can enhance the diffusion of PCBM molecules to cause the formation of PCBM aggregates for thermal-annealed films but has little effect on the morphology of solvent-annealed films. Such a difference in blend morphology under different annealing conditions must have significant impact on the device performance as discussed later.

## 5.4. Discussion

### *5.4.1. Location of Dye Molecules*

First, the author discusses the location of SiPc molecules in ternary blend films. In binary blend films of PCBM:SiPc, as mentioned before, SiPc molecules are likely to be segregated into the air/film interface of the PCBM film. If SiPc molecules were homogeneously dispersed in the PCBM film, the surface energy would decrease linearly with increasing dye compositions as shown by the solid line in Figure 5-7. Considering the thickness of the PCBM film (35 nm), 3 wt% of SiPc would be enough to cover whole the film surface. In other words, 1 wt% of SiPc molecules would cover 33% of the PCBM surface if all of them were segregated into the surface. From the straight line, the surface concentration of SiPc is estimated to be ~20% at 1 wt% SiPc and ~60% at 3 wt% SiPc. Both estimations demonstrate that 60% of SiPc molecules are not in the PCBM bulk but segregated into the film surface even without thermal annealing. In binary blend films of P3HT:SiPc, on the other hand, most SiPc molecules are embedded in the P3HT bulk as shown in Figure 5-7. These results suggest that most SiPc molecules are located in the P3HT domains rather than in the PCBM domains in ternary blends. This is consistent with the prediction based on the wetting coefficient for

ternary blends of RR-P3HT:PCBM:SiPc; the positive wetting coefficient ($\omega_C = 0.32$) suggests that SiPc molecules are likely to be located at P3HT rather than PCBM even at the interface. On the other hand, the addition of dye molecules has no impact on the crystallization of P3HT as shown in Figure 5-5. This suggests that dye molecules are not located in the P3HT crystalline domains. Furthermore, the high IQE observed at the dye absorption as shown in Figure 5-4 shows that SiPc molecules would be close to both P3HT and PCBM domains to generate photocurrent efficiently. The author concludes that the majority of SiPc molecules are located at disordered P3HT domains at the interface of P3HT/PCBM as shown by previous morphological studies based on TEM.[46–48]

### *5.4.2. Localization Driving Force*

The author next discusses the localization mechanism of dyes in ternary blend films. The author estimates the local concentration of SiPc ($[SiPc]_{Local}$) in blend films from the peak wavelength of the dye absorption $\lambda_{max}$ in P3HT:PCBM blend films. As a reference, the author employs the absorption peak of SiPc in RRa-P3HT amorphous films, assuming that $[SiPc]_{Local}$ is the same as the dye composition [SiPc], that is, SiPc molecules are homogeneously dispersed. Figure 5-11a shows $[SiPc]_{Local}$ in P3HT:PCBM blend films estimated from the dye absorption $\lambda_{max}$. Here the author focuses on the difference in $[SiPc]_{Local}$ for various blend films at a fixed dye composition of 3.4 wt%. For RRa-P3HT:PCBM films, if SiPc molecules were homogeneously dispersed only in RRa-P3HT amorphous domains because the majority of them are not located in the PCBM domains, $[SiPc]_{Local}$ would be double the original dye composition. However, $[SiPc]_{Local}$ was estimated to be as high as 14 wt%, suggesting the localization of dye molecules at the interface instead of a homogeneous distribution. This localization is not ascribed to the crystallization of P3HT because of amorphous films but is rather consistent with the wetting coefficient ($\omega_C = 0.49$). In other words, this localization can be explained in terms of the surface energy. For RR-P3HT:PCBM films, $[SiPc]_{Local}$ increased

to 20 wt% even before thermal annealing and to 25 wt% after thermal annealing. As mentioned before, there is no difference in the surface energy between RRa-P3HT and RR-P3HT. The author ascribes this increase in $[SiPc]_{Local}$ to the crystallization of P3HT, which would expel dye molecules into the interface. The author concludes that there are two driving forces to localize SiPc molecules at the interface in ternary blend films of P3HT:PCBM:SiPc; one is the surface energy balance and the other is the crystallization of P3HT. Furthermore, the increase ratio in $[SiPc]_{Local}$ is larger from RRa-P3HT to RRa-P3HT:PCBM, which is due to

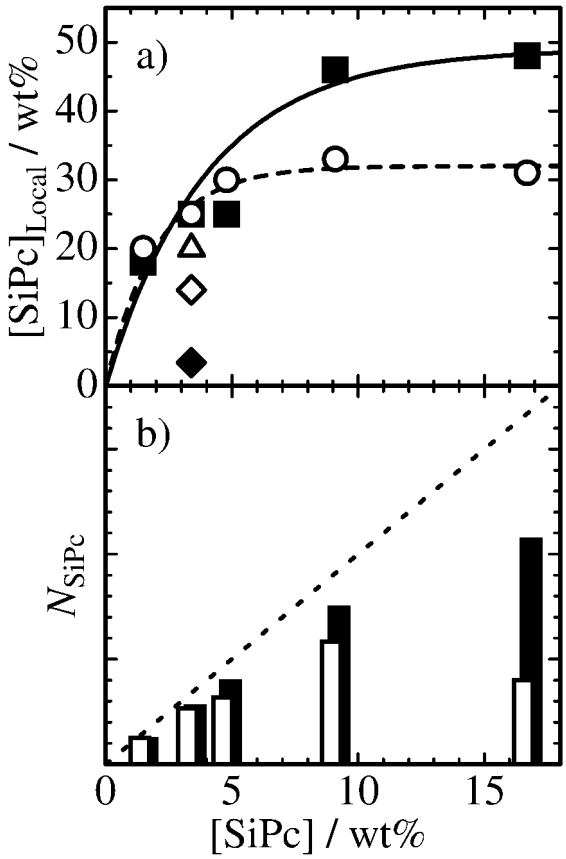


**Figure 5-11.** a) Local concentrations of SiPc in RRa-P3HT (closed diamond) RRa-P3HT:PCBM (open diamond), and RR-P3HT:PCBM before (open triangle) and after thermal annealing (open circles) and solvent (closed squares) plotted against a composition of SiPc. The solid and broken lines are guided to the eye for solvent and thermal annealing, respectively. b) The number of SiPc molecules contributing to the photocurrent generation in RR-P3HT:PCBM after thermal (open bars) and solvent annealing (closed bars) plotted against a composition of SiPc. The broken line represents the total number of SiPc molecules loaded into RR-P3HT:PCBM blends.

the surface energy, than from RRa-P3HT:PCBM to RR-P3HT:PCBM after thermal annealing, which is due to the crystallization of P3HT. In other words, the surface energy is the primary driving force to localize SiPc molecules at the interface for thermal-annealed films of RR-P3HT:PCBM although the crystallization can also assist the localization.

### *5.4.3. Annealing Effect on Dye Localization*

The author finally discusses the difference in $[SiPc]_{Local}$ for ternary blend films with various dye composition from 3.4 to 17 wt% under two annealing conditions. As shown in Figure 5-11a, $[SiPc]_{Local}$ increases with the increase in dye compositions and is saturated at >10 wt%. The saturated $[SiPc]_{Local}$ is as high as ~50 wt% for solvent annealing and ~30 wt% for thermal annealing. This saturation indicates that the majority of SiPc molecules are selectively loaded at the interfacial disordered domains up to 10 wt% but a part of them overflow from the interface over 10 wt%. To discuss the relationship between such dye distribution and photocurrent, the author estimates the number of dye molecules contributing to the photocurrent generation ($N_{SiPc}$), which is proportional to the product of the IQE at 670 nm and [SiPc]. The broken line in Figure 5-11b represents the total number of SiPc molecules loaded into the blend films. As shown in Figure 5-11b, $N_{SiPc}$ is close to the dye composition below 10 wt% for both annealing conditions, suggesting that most of the dyes loaded can contribute to the photocurrent generation. At 17 wt%, on the other hand, $N_{SiPc}$ deviates from the broken line for both annealing conditions, but still increases for the solvent-annealed device (closed bar) but decreases for the thermal-annealed device (open bar). For the solvent-annealed device with 17 wt% SiPc, as shown in Figure 5-3a, the decrease in EQE was observed only at the absorption band of P3HT. The author concludes that excess SiPc molecules at 17 wt% overflow into P3HT domains and thus quench P3HT excitons. For the thermal-annealed device with 17 wt% SiPc, as shown in Figure 5-3b, the decrease in EQE was observed over the whole wavelength although $[SiPc]_{Local}$ was still as high as ~30 wt%. As shown in Figure

5-10, many PCBM clusters were observed at 17 wt%, suggesting the presence of PCBM diffusion in the film from the disordered domain at the interface to the PCBM domain. Note that PCBM is more likely to diffuse in the presence of SiPc. This suggests that SiPc molecules serve as a plasticizer at the interface. Considering the molecular size, SiPc also could diffuse just as PCBM under the thermal annealing condition. However, this is not the case as shown in Figure 5-11. This is probably because SiPc molecules cannot diffuse into P3HT crystalline domains with a lower surface energy or into PCBM domains with a higher surface energy even at a high temperature. The author concludes that SiPc molecules still remain in the disordered domain but PCBM molecules escape from the disordered domain to the PCBM domain by thermal diffusion at a high temperature. Such decrease in the local concentration of PCBM ($[PCBM]_{Local}$) in the disordered domain results in the significant decrease in EQEs not only at the absorption band of SiPc because of the large distance between SiPc and PCBM in the disordered domain but also at the absorption band of P3HT because of efficient energy transfer from P3HT to SiPc. Note that $[SiPc]_{Local}$ is higher for the solvent-annealed device than for the thermal-annealed device at dye compositions of >5 wt%. This indicates that a part of SiPc molecules escape from the interface by thermal diffusion. In other words, both annealing treatments can enhance the local concentration of SiPc at the interface, which would affect the device performance. In particular, the solvent annealing can enhance $[SiPc]_{Local}$ without the decrease in $[PCBM]_{Local}$ at the interface and consequently improve the device performance more effectively.

## 5.5. Conclusions

The author has studied the selective localization of dye molecules at the interface of polymer and fullerene domains in polymer:fullerene:dye ternary blend solar cells. Compared to the control devices without dyes, the RR-P3HT:PCBM:SiPc ternary blend solar cells with a

dye composition of 4.8 wt% exhibited an increase of 15–20% in $J_{SC}$ and PCE because of the selective localization of dye molecules at the interface. Detailed analyses of the surface energy and the absorption spectra revealed the following two driving forces for the interfacial dye localization: the surface energy of each material and the crystallization of the matrix material. The surface energy measurements showed that SiPc molecules in PCBM:SiPc blend films are segregated into the air/film interface because of the lower surface energy of SiPc and that in RR-P3HT:SiPc blends are embedded into the films. Furthermore SiPc molecules have no impact on the crystallization of RR-P3HT in the ternary blend films. The author concludes that SiPc molecules can be localized in disordered P3HT phases at the interface of P3HT/PCBM rather than in the PCBM and crystal RR-P3HT domains. This is in good agreement with the prediction based on the wetting coefficient, suggesting that the surface energy has critical impact on such interfacial segregation. For the quantitative discussion of the dye localization at the interface of P3HT/PCBM in ternary blend films, the local concentration of SiPc ($[SiPc]_{Local}$) was estimated from the peak wavelength of the SiPc absorption band. Interestingly, $[SiPc]_{Local}$ is as high as 14 wt% even for RRa-P3HT:PCBM:SiPc blends, which is much higher than the original dye composition of 3.4 wt %. Thus, this increase is ascribable to the effect of the surface energy. For RR-P3HT:PCBM:SiPc blends, $[SiPc]_{Local}$ increased to 20 wt% even before thermal annealing and to 25 wt% after thermal annealing. This is rather ascribable to the crystallization of P3HT because the surface energy of RR-P3HT is the same as that of RRa-P3HT. The increase ratio of $[SiPc]_{Local}$ due to the surface energy is larger than that due to the crystallization of P3HT. The author concludes that the surface energy is the primary driving force to localize SiPc molecules at the interface for thermal-annealed films of RR-P3HT:PCBM although the crystallization can also assist the localization. As the dye-composition increases, $[SiPc]_{Local}$ also increases and then is saturated at 10 wt%. The saturated $[SiPc]_{Local}$ is as high as ~50 wt%

for solvent annealing and ~30 wt% for thermal annealing. As the dye-composition increases further up to 17 wt%, the solvent-annealed device keeps a high $J_{SC}$ but the thermal-annealed device exhibits a significant decrease in $J_{SC}$ due to the formation of large clusters of PCBM. Such formation of PCBM clusters is enhanced by the addition of dye molecules, suggesting that dye molecules located at the interface serve as a plasticizer and hence assist the diffusion of PCBM molecules at a high temperature, resulting in the formation of PCBM aggregates. On the other hand, the solvent annealing does not enhance such diffusion of small molecules and consequently the dye molecules still remain at the interface. In other words, the solvent-annealed devices can load much more dye molecules at the interface without changing the blend morphology, resulting in the higher efficiencies even with the high composition of dye molecules. The author concludes that the dye-sensitized polymer solar cells with ternary blends can be rationally designed by careful consideration of the crystallization of the matrix and the surface energy of each material and also the annealing condition for the active layer.

## 5.6. Appendix

### *5.6.1. Device Performances*

Table 5-A1 summarizes the device performances of RR-P3HT:PCBM:SiPc ternary blend solar cells with different dye composition under solvent and thermal annealing conditions.

**Table 5-A1.** Device performances for RR-P3HT:PCBM:SiPc ternary blend solar cells with solvent and thermal annealing.

| Anneal | SiPc / wt% | $J_{SC}$ / mA cm$^{-2}$ | $V_{OC}$ / V | FF | PCE / % |
|---|---|---|---|---|---|
| Solvent | 0.0 | 9.69 | 0.55 | 0.66 | 3.5 |
| | 1.5 | 10.3 | 0.56 | 0.65 | 3.8 |
| | 3.4 | 10.5 | 0.57 | 0.65 | 3.9 |
| | 4.8 | 11.1 | 0.58 | 0.65 | 4.2 |
| | 9.1 | 11.0 | 0.59 | 0.62 | 4.0 |
| | 17 | 10.7 | 0.56 | 0.59 | 3.6 |
| Thermal | 0.0 | 6.73 | 0.61 | 0.63 | 2.6 |
| | 1.5 | 7.40 | 0.58 | 0.64 | 2.8 |
| | 3.4 | 7.69 | 0.58 | 0.66 | 2.9 |
| | 4.8 | 7.83 | 0.58 | 0.65 | 2.9 |
| | 9.1 | 7.29 | 0.60 | 0.63 | 2.8 |
| | 17 | 3.26 | 0.56 | 0.45 | 0.82 |

### *5.6.2. Dependence of Peak Wavelengths of SiPc on Dye Composition*

Figure 5-A1 shows the peak wavelengths of SiPc ($\lambda_{max}$) doped into amorphous polymer matrices. In RRa-P3HT films, the $\lambda_{max}$ was gradually red-shifted from 671 to 687 nm with increasing dye concentration from 1 to 100 wt%. As shown by the open squares in Figure 5-A1, almost the same result was observed for SiPc doped into polystyrene (PSt) amorphous films. These results indicate that the peak shift is not due to the interaction with the matrix but can be ascribed to the increase in the local concentration of SiPc molecules in the matrix.

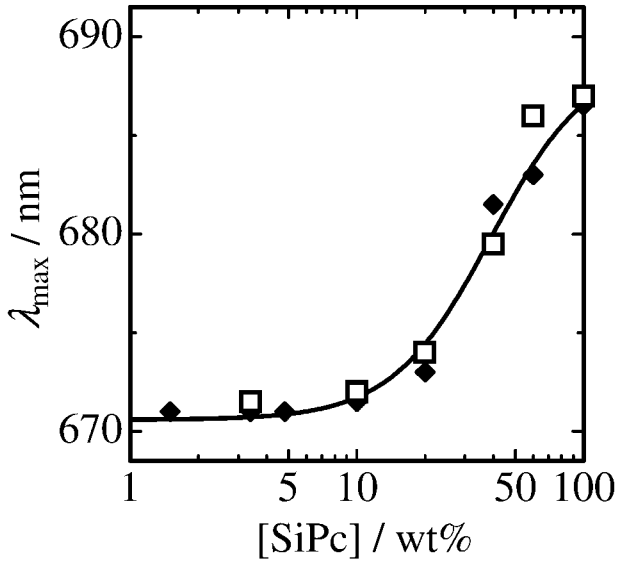


**Figure 5-A1.** Peak wavelengths of the SiPc absorption in RRa-P3HT (closed diamonds) and in PSt (open squares) plotted against the composition of SiPc. The solid lines are guided to the eye for SiPc doped in the RRa-P3HT film.

### *5.6.3. Effect of P3HT Crystallinity*

Figure 5-A2 shows the absorption spectra and the peak wavelengths of SiPc doped into RRa-P3HT (closed diamonds), RRa-P3HT:PCBM (open diamonds), RR-P3HT:PCBM (open triangles), and RR-P3HT:PCBM thermal-annealed (150 °C for 30 min) films (open circles). The SiPc composition was fixed to 3.4 wt% for all blends. The crystallinity of P3HT increased in the order of RRa-P3HT:PCBM, RR-P3HT:PCBM before thermal annealing, and after thermal annealing, because vibrational bands at around 500–600 nm were more distinguished in the same order (Figure 5-A2a). The absorption peak of SiPc was red-shifted in RRa-P3HT:PCBM blend films (674 nm) than in RRa-P3HT films (671 nm). Furthermore, the absorption peak of SiPc was red-shifted to 675 nm for RR-P3HT:PCBM blend films before thermal annealing and more red-shifted to 676 nm for RR-P3HT:PCBM blend films after thermal annealing according to the order of P3HT crystallinity.

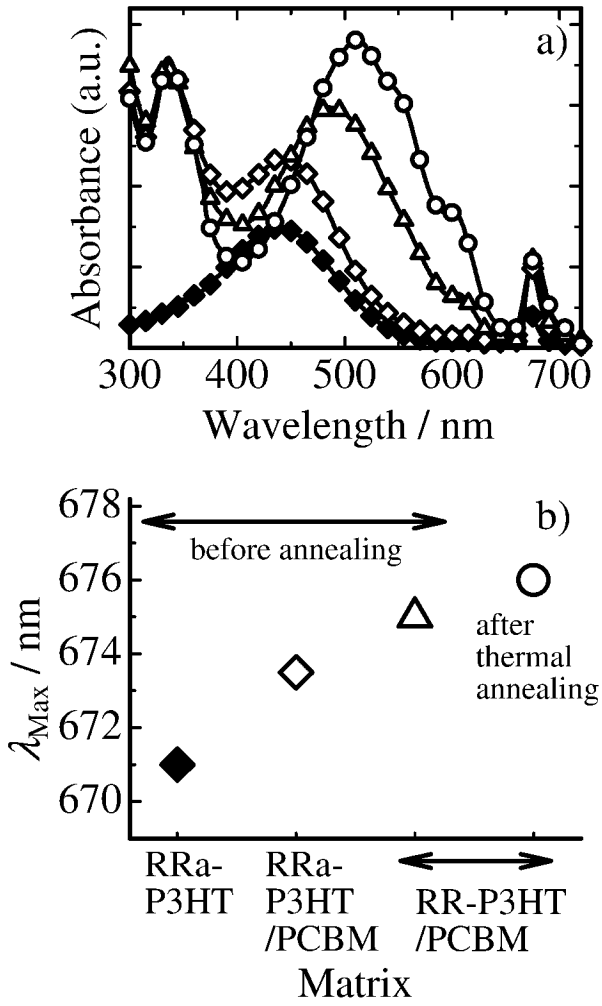


**Figure 5-A2.** a) Absorption spectra and b) SiPc peak wavelengths of SiPc doped into RRa-P3HT (closed diamonds), RRa-P3HT:PCBM (open diamonds), RR-P3HT:PCBM (open triangles), and RR-P3HT:PCBM thermal-annealed films (open circles).

## References

(1) Brabec, C. J.; Durrant, J. R. *MRS Bull.* **2008**, *33*, 670–675.

(2) Dennler, G.; Scharber, M. C.; Brabec, C. J. *Adv. Mater.* **2009**, *21*, 1323–1338.

(3) Helgesen, M.; Søndergaard, R.; Krebs, F. C. *J. Mater. Chem.* **2010**, *20*, 36–60.

(4) Brabec, C. J.; Gowrisanker, S.; Halls, J. J. M.; Laird, D.; Jia, S.; Williams, S. P. *Adv. Mater.* **2010**, *22*, 3839–3856.

(5) Ma, W.; Yang, C.; Gong, X.; Lee, K.; Heeger, A. J. *Adv. Funct. Mater.* **2005**, *15*, 1617–1622.

(6) Li, G.; Shrotriya, V.; Huang, J.; Yao, Y.; Moriarty, T.; Emery, K.; Yang, Y. *Nat. Mater.* **2005**, *4*, 864–868.

(7) Kim, Y.; Cook, S.; Tuladhar, S. M.; Choulis, S. A.; Nelson, J.; Durrant, J. R.; Bradley, D. D. C.; Giles, M.; McCulloch, I.; Ha, C.-S.; Ree, M. *Nat. Mater.* **2006**, *5*, 197–203.

(8) Irwin, M. D.; Buchholz, D. B.; Hains, A. W.; Chang, R. P. H.; Marks, T. J. *Proc. Natl. Acad. Sci. USA* **2008**, *105*, 2783–2787.

(9) Jo, J.; Kim, S.-S.; Na, S.-I.; Yu, B.-K., Kim, D.-Y. *Adv. Funct. Mater.* **2009**, *19*, 866–874.

(10) Bundgaard, E.; Krebs, F. C. *Sol. Energy Mater. Sol. Cells* **2007**, *91*, 954–985.

(11) Kroon, R.; Lenes, M.; Hummelen, J. C.; Blom, P. W. M.; de Boer, B. *Polym. Rev.* **2008**, *48*, 531–582.

(12) Peet, J.; Kim, J. Y.; Coates, N. E.; Ma, W. L.; Moses, D.; Heeger, A. J.; Bazan, G. C. *Nat. Mater.* **2007**, *6*, 497–500.

(13) Chen, H.-Y.; Hou, J.; Zhang, S.; Liang, Y.; Yang, G.; Yang, Y.; Yu, L.; Wu, Y.; Li, G.; *Nat. Photonics* **2009**, *3*, 649–653.

(14) Chen, Y.-C.; Yu, C.-Y.; Fan, Y.-L.; Hung, L.-I; Chen, C.-P.; Ting, C. *Chem. Commun.*

**2010**, *46*, 6503–6505.

(15) Peet, J.; Tamayo, A. B.; Dang, X.-D.; Seo, J. H.; Nguyen, T.-Q. *Appl. Phys. Lett.* **2008**, *93*, 163306.

(16) Honda, S.; Nogami, T.; Ohkita, H.; Benten, H.; Ito, S. *ACS Appl. Mater. Interfaces* **2009**, *1*, 804–810.

(17) Suresh, P.; Balraju, P.; Sharma, G. D.; Mikroyannidis, J. A.; Stylianakis, M. M. *ACS Appl. Mater. Interfaces* **2009**, *1*, 1370–1374.

(18) Honda, S.; Ohkita, H. Benten, H.; Ito, S. *Chem. Commun.* **2010**, *46*, 6596–6598.

(19) Campoy-Quiles, M.; Ferenczi, T.; Agostinelli, T.; Etchegoin, P. G.; Kim, Y.; Anthopoulos, T. D.; Stavrinou, P. N.; Bradley, D. D. C.; Nelson, J. *Nat. Mater.* **2008**, *7*, 158–164.

(20) Orimo, A.; Masuda, K.; Honda, S.; Benten, H.; Ito, S.; Ohkita, H.; Tsuji, H. *Appl. Phys. Lett.* **2010**, *96*, 043305.

(21) Germack, D. S.; Chan, C. K.; Kline, R. J.; Fischer, D. A.; Gundlach, D. J.; Toney, M. F.; Richter, L. J.; DeLongchamp, D. M. *Macromolecules* **2010**, *43*, 3828–3836.

(22) Arias, A. C.; Corcoran, N.; Banach, M.; Friend, R. H.; MacKenzie, J. D.; Huck, W. T. S. *Appl. Phys. Lett.* **2002**, 80, 1695–1697.

(23) Kim, J.-S.; Ho, P. K. H.; Murphy, C. E.; Friend, R. H. *Macromolecules* **2004**, *37*, 2861–2871.

(24) Wei, H. X.; Li, J.; Xu, Z. Q.; Cai, Y.; Tang, J. X.; Li, Y. Q. *Appl. Phys. Lett.* **2010**, *97*, 083302.

(25) Sumita, M.; Sakata, K.; Asai, S.; Miyasaka, K.; Nakagawa, H. *Polym. Bull.* **1991**, *25*, 265–271.

(26) Wu, M.; Shaw, L. *J. Appl. Polym. Sci.* **2006**, *99*, 477–488.

(27) Göldel, A.; Kasaliwal, G.; Pötschke, P. *Macromol. Rapid Commun.* **2009**, *30*, 423–

429.

(28) Baudouin, A.-C.; Devaux, J.; Bailly, C. *Polymer* **2010**, *51*, 1341–1354.

(29) Ma, C. G.; Zhang, M. Q.; Rong, M. Z. *J. Appl. Polym. Sci.* **2007**, *103*, 1578–1584.

(30) Cheng, T. W.; Keskkula, H.; Paul, D. R. *Polymer* **1992**, *33*, 1606–1619.

(31) Li, D.; Neumann, A. W. *J. Colloid Interface Sci.* **1990**, *137*, 304–307.

(32) Kudo, N.; Honda, S.; Shimazaki, Y.; Ohkita, H.; Ito, S.; Benten, H. *Appl. Phys. Lett.* **2007**, *90*, 183513.

(33) Liu, Y.; Summers, M. A.; Edder, C.; Fréchet, J. M. J.; McGehee, M. D. *Adv. Mater.*, **2005**, *17*, 2960–2964.

(34) Scully, S. R.; Armstrong, P. B.; Edder, C.; Fréchet, J. M. J.; McGehee, M. D. *Adv. Mater.*, **2007**, *19*, 2961–2966.

(35) Hardin, B. E.; Hoke, E. T.; Armstrong, P. B.; Yum, J.-H.; Comte, P.; Torres, T.; Fréchet, J. M. J.; Nazeeruddin, M. K.; Grätzel, M.;McGehee, M.D. *Nat. Photonics* **2009**, *3*, 406–411.

(36) Peumans, P.; Yakimov, A.; Forrest, S. R. *J. Appl. Phys.* **2003**, *93*, 3693–3723.

(37) Erb, T.; Zhokhavets, U.; Gobsch, G.; Raleva, S.; Stühn, B.; Schilinsky, P.; Waldauf, C.; Brabec, C. J. *Adv. Funct. Mater.* **2005**, *15*, 1193–1196.

(38) Wheeler, B. L.; Nagasubramanian, G.; Bard, A. J.; Schechtman, L. A.; Kenney, M. E. *J. Am. Chem. Soc.* **1984**, *106*, 7404–7410.

(39) Sasa, N.; Okada, K.; Nakamura, K.; Okada, S. *J. Mol. Struct.* **1998**, *446*, 163–178.

(40) Jaczewska, J.; Raptis, I.; Budkowski, A.; Goustouridis, D.; Raczkowska, J.; Sanopoulou, M.; Pamula, E.; Bernasik, A.; Rysz, J. *Synth. Met.* **2007**, *157*, 726–732.

(41) Björström, C. M.; Bernasik, A.; Rysz, J.; Budkowski, A.; Nilsson, S.; Svensson, M.; Andersson, M. R.; Magnusson, K. O.; Moons, E. *J. Phys.: Condens. Matter* **2005**, *17*, L529.

(42) Jaczewska, J.; Budkowski, A.; Bernasik, A.; Moons, E.; Rysz, J. *Macromolecules* **2008**, *41*, 4802–4810.

(43) Walheim, S.; Ramstein, M.; Steiner, U. *Langmuir* **1999**, *15*, 4828–4836.

(44) Tanaka, K.; Takahara, A.; Kajiyama, T. *Macromolecules* **1996**, *29*, 3232–3239.

(45) Swinnen, A.; Haeldermans, I.; van de Ven, M.; D'Haen, J.; Vanhoyland, G.; Aresu, S.; D'Olieslaeger, M.; Manca, J. *Adv. Funct. Mater.* **2006**, *16*, 760–765.

(46) Moon, J. S.; Lee, J. K.; Cho, S.; Byun, J.; Heeger, A. J. *Nano Lett.* **2009**, *9*, 230–234.

(47) Yang, X.; Loos, J.; Veenstra, S. C.; Verhees, W. J. H.; Wienk, M. M.; Kroon, J. M.; Michels, M. A. J.; Janssen, R. A. J. *Nano Lett.* **2005**, *5*, 579–583.

(48) van Bavel, S. S.; Sourty, E.; de With, G.; Loos, J. *Nano Lett.* **2009**, *9*, 507–513.

# *Chapter 6*

# Light-Harvesting Mechanism in Polymer/Fullerene/Dye Ternary Blends Studied by Transient Absorption Spectroscopy

## 6.1. Introduction

Polymer:fullerene bulk heterojunction solar cells have attracted much attention because of their potential advantages that include light weight, flexibility, low cost, large area and high-throughput productivity.[1–4] Among them, the blend of regioregular poly(3-hexylthiophene) (P3HT) and 1-(3-methoxycarbonyl)propyl-1-phenyl[6,6]methanofullerene (PCBM) has been most widely studied. The polymer solar cells based on P3HT:PCBM blends exhibit relatively high external quantum efficiency (EQE) more than 70% and high fill factor up to ~0.7, which are still the highest of the polymer solar cells.[5–9] The power conversion efficiency (PCE) of the P3HT:PCBM solar cell can be improved to 4–5% by the annealing of the active layer such as thermal annealing and solvent annealing,[5–9] although the photoluminescence (PL) from P3HT is still observed even for optimized P3HT:PCBM devices.[7] In other words, there still exists room to improve the photocurrent by more efficient exciton harvesting. In addition, the light harvesting in the near-IR region is required for further improvement because P3HT can absorb limited photons up to ~650 nm, which correspond to only a quarter of the total photons in the solar light.[10,11] Consequently, a variety of low band-gap polymers have been developed to absorb a broad range of the solar light.[10–14] On the other hand, dye sensitization has been recently reported as another approach to improving the light-harvesting efficiency in polymer

solar cells by several groups.[15–18]

In dye-sensitized polymer solar cells, dye molecules are simply blended as the third component to harvest solar photons at longer wavelengths that the original donor and acceptor materials cannot collect. This is a simple and versatile method and therefore various dye molecules can be employed. In Chapter 3, the author reported that an appropriate selection of dyes with bulky groups, silicon phthalocyanine bis(trihexylsilyl oxide) (SiPc), can improve the light-harvesting efficiency. Furthermore, in Chapter 4, the author demonstrated that this method is applicable even to multi-colored sensitization with different dye molecules.[18] The enhanced photocurrent due to dye molecules suggests that the majority of dye molecules are segregated to a donor/acceptor interface. In Chapter 5, the author studied such interfacial segregation of dyes in terms of the surface energy and the crystallinity of matrix. Interestingly, the addition of SiPc enhances both EQE peaks at the P3HT absorption and at the SiPc absorption. This is indicative of the efficient exciton harvesting due to the energy transfer from P3HT excitons to SiPc molecules followed by efficient charge generation at the interface of P3HT/PCBM. Recently, several spectroscopic studies have been reported on photophysical dynamics in polymer:fullerene blend films.[19–29] Only recently, the photophysics of P3HT:PCBM:dye ternary blends has been studied.[30] However, little is known about the details of the overall light-harvesting mechanism and the dye location in ternary blends.

Herein the author reports a comprehensive spectroscopic study on the photophysical dynamics in P3HT:PCBM:SiPc ternary blend films by femtosecond transient absorption in the wavelength region from 450 to 1500 nm upon excitation of SiPc or P3HT. On the basis of these detailed analyses, the author discusses the light-harvesting dynamics by dye molecules: dye sensitization and exciton-harvesting mechanism. Furthermore, the relevance of these mechanisms to the morphology of blend films depending on annealing conditions is also discussed.

## 6.2. Experimental Methods

### *6.2.1. Sample Preparation*

Ternary blend films of P3HT:PCBM:SiPc were fabricated as follows. Glass substrates were washed by ultrasonication in toluene, acetone, and ethanol for 15 min, dried with $N_2$, and then cleaned with a UV–$O_3$ cleaner for 30 min. For the films fabricated by thermal annealing, a blend layer of P3HT:PCBM:SiPc (ca. 100 nm) was spin-coated from a chlorobenzene solution on the cleaned glass substrates at 1200 rpm for 60 s and the film was annealed at 150 °C for 30 min in a $N_2$-filled glove box. For the films fabricated by solvent annealing, a blend layer of P3HT:PCBM:SiPc (ca. 200 nm) was spin-coated from an *o*-dichlorobenzene solution on the cleaned glass substrates at 600 rpm for 60 s. Then, the wet film was dried in a covered glass petri dish for 60 min. The blend solution was prepared as follows: P3HT (Plextronics, regioregularity > 98%, $M_n$ = ~45,000–65,000 g mol$^{-1}$) and PCBM (Frontier Carbon) were dissolved in chlorobenzene (10 and 10 mg mL$^{-1}$) or *o*-dichlorobenzene (17 and 17 mg mL$^{-1}$), the solution was stirred at 40 °C overnight, and then SiPc (Aldrich) was dissolved in the solution at room temperature. The dye concentration was fixed to be 3.4 wt%. For comparison, P3HT:PCBM binary blend films without dyes and P3HT neat films were also prepared separately under the same condition to give the same active layer thickness. Blend films of P3HT or PCBM and SiPc (P3HT:SiPc or PCBM:SiPc binary blend films) were prepared on the cleaned glass substrates by spin-coating from chlorobenzene (Aldrich) solutions of P3HT or PCBM at a concentration of ~10 mg mL$^{-1}$ or ~60 mg mL$^{-1}$ with 3.4 wt% of SiPc.

### *6.2.2. Measurements*

UV–visible absorption and photoliminescence spectra of blend films were measured with a UV–visible spectrophotometer (Hitachi, U-3500) and a fluorescence spectrophotometer (Hitachi, F-4500) equipped with a red-sensitive photomultiplier (Hamamatsu, R928F),

respectively.

Transient absorption data were collected with a pump and probe femtosecond transient absorption spectroscopy system (Ultrafast Systems, Helios)[22,25] and with a highly sensitive microsecond transient absorption system as described elsewhere.[22] The pump and probe femtosecond transient absorption spectroscopy system consists of a transient absorption spectrometer (Ultrafast Systems, Helios) and a regenerative amplified Ti:sapphire laser (Spectra-Physics, Hurricane). The amplified Ti:sappire laser provided 800-nm fundamental pulses at a repetition rate of 1 kHz with an energy of 0.8 mJ and a pulse width of 100 fs (FWHM), which were split into two optical beams with a beam splitter to generate pump and probe pulses. One fundamental beam was converted into pump pulses at 400 nm with a second harmonic generator (Spectra-Physics, TP-F) or pump pulses at other wavelengths with an ultrafast optical parametric amplifier (Spectra-Physics, TOPAS). The other fundamental beam was converted into white light continuum pulses employed as probe pulses in the wavelength region from 400 to 1700 nm. The pump pulses were modulated mechanically with a repetition rate of 100 Hz for visible and 500 Hz for near-IR measurements. The temporal evolution of the probe intensity was recorded with a Si CCD-array photodetector (Ocean Optics, S2000) for the visible measurement and with an InGaAs digital line scan camera (Sensors Unlimited, SU-LDV) for the near-IR measurement. Transient absorption spectra and decays were collected over the time range from −5 ps to 3 ns. Typically, 200–1000 laser shots were averaged on each delay time to obtain a detectable absorbance change as small as $10^{-4}$–$10^{-3}$ depending on the monitor wavelength range. In order to cancel out orientation effects on the dynamics, the polarization direction of the linearly polarized probe pulse was set at a magic angle of 54.7 ° with respect to that of the pump pulse. The sample films were sealed in a quartz cuvette purged with Ar for 30 min. Note that the transient absorption spectra and dynamics were highly reproducible even after the laser excitation. In

other words, the laser irradiation had negligible effects on the morphology change for the films.

## 6.3. Results

### *6.3.1. Steady-State Absorption Spectra*

Figure 6-1 shows the steady-state absorption spectra of P3HT:PCBM:SiPc(1:1:0.07) ternary and the P3HT:PCBM(1:1) binary blend films. The ternary blend films exhibited a sharp absorption band ascribable to SiPc at around 670 nm under both thermal and solvent annealing conditions. The solvent-annealed blend films exhibited more distinguished vibrational bands at around 500–600 nm, which are indicative of the crystallization of P3HT,[31] than the thermal-annealed blend films. Interestingly, these vibrational bands were clearly observed even in the presence of SiPc molecules under both annealing conditions. Thus, this result shows that the crystallization of P3HT is not disturbed by the addition of SiPc with a small composition of 3.4 wt%. In other words, the majority of SiPc molecules are unlikely to be located in the P3HT crystalline domains.

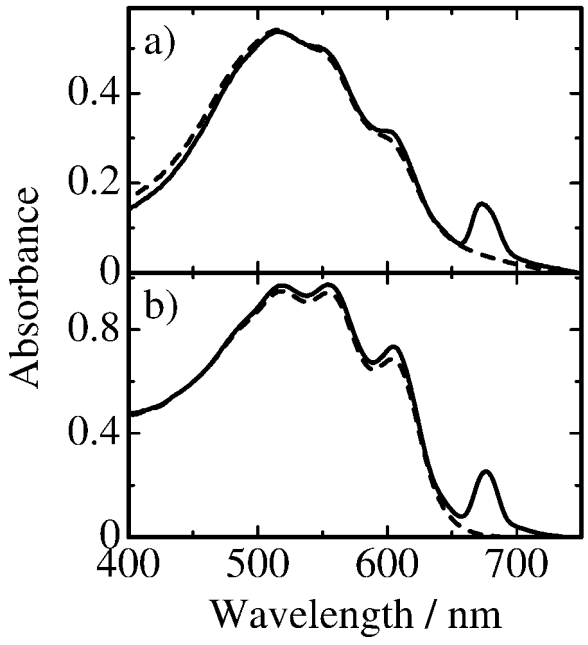


**Figure 6-1.** Absorption spectra of P3HT:PCBM:SiPc(1:1:0.07) (solid lines) and P3HT:PCBM(1:1) (broken lines) blend films after a) thermal and b) solvent annealing.

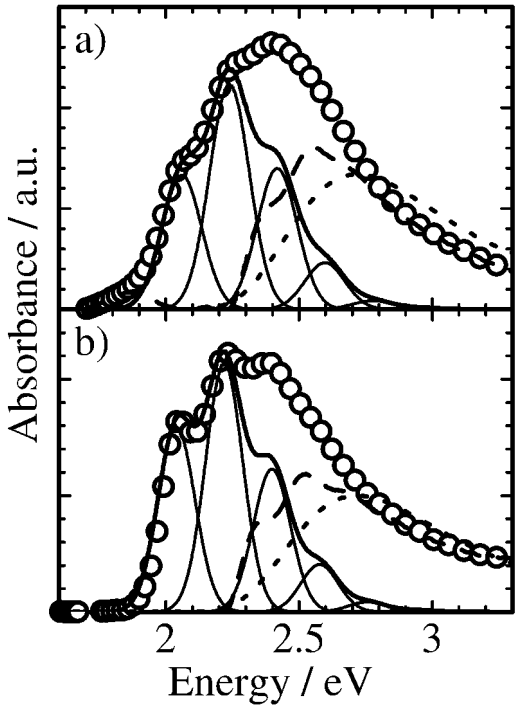


**Figure 6-2.** Absorption spectra measured for P3HT:PCBM blend films after a) thermal and b) solvent annealing. The open circle symbols represent the absorption spectra of P3HT in the blend, which is obtained by subtracting the absorption of PCBM from the absorption of P3HT:PCBM. The solid lines represent the simulated absorption spectra of P3HT due to the crystalline region, which is obtained by a sum of seven vibrational bands (thin solid lines) on the basis of a weakly coupled aggregate model.[32–37] Details are described in the Appendix. The broken lines are the differences between the whole spectra (circles) and the simulated spectra (solid lines), which correspond to the absorption spectra of P3HT due to more disordered region. The dotted lines are the absorption spectra of P3HT dissolved in toluene solution.

To evaluate the degree of P3HT crystallization quantitatively, the author analyzed the absorption spectra of P3HT in P3HT:PCBM blend films in detail. On the basis of a weakly coupled aggregate model,[32–35] the absorption spectra of P3HT in blends can be resolved into two parts: a lower energy absorption due to crystalline regions of P3HT where a weakly interacting H-aggregate state is formed, and a higher energy absorption due to more disordered regions of P3HT.[34] In accordance with this model, the lower energy absorption is simulated by a sum of seven vibrational bands due to 0–0 to 0–6 transitions. Thus, the higher

energy absorption can be obtained by subtracting the lower energy absorption spectra from the whole spectra observed. Details about the simulation method are described in the Appendix. As shown in Figure 6-2, the intensity ratio of the lower to higher energy absorption is larger for the solvent-annealed film than for the thermal-annealed film. As shown by the solid lines in the figure, the solvent-annealed P3HT:PCBM blends exhibited a larger 0–0 vibrational band of crystalline P3HT at around 2 eV than the thermal-annealed P3HT:PCBM blends. From the detailed analysis of the spectra, the degree of P3HT crystallization and the domain width are estimated as previously reported[35–37] to be 44% and 9.5 nm for the thermal-annealed films and 55% and 15.2 nm for the solvent-annealed films, respectively. The degree of crystallinity is consistent with a previous report: ~45% for the thermal-annealed blends and ~60% for the solvent-annealed blends.[38,39] These domain widths are also well consistent with those reported in transmission electron microscopy (TEM) studies: P3HT domains have a width of ~13 nm for the thermal-annealed P3HT:PCBM blends[40] and P3HT nanofibrils have a width of ~15 nm for the solvent-annealed P3HT:PCBM blends.[41] These results show that the solvent-annealed films have larger P3HT crystalline domains than the thermal-annealed films.

### *6.3.2. Photoluminescence Efficiencies*

To estimate how many excitons can reach the heterojunction, the author measured the PL efficiencies of P3HT in each blend film. For the thermal-annealed films, the PL intensity of P3HT:PCBM blends was 20% relative to that of P3HT pristine films, which is consistent with previous reports.[7,16] In other words, 80% of P3HT excitons can reach the interface of P3HT/PCBM and the remaining 20% cannot. On the other hand, the PL intensity of the P3HT:PCBM:SiPc blends was only 10% relative to that of P3HT pristine films, which is half that to the P3HT:PCBM blends. This indicates that the addition of only 3.4 wt% SiPc can further harvest 50% of unquenched P3HT excitons that cannot reach the interface in

P3HT:PCBM blends. For the solvent-annealed blend films, on the other hand, the relative PL intensity was 6% for the P3HT:PCBM binary and 2% for the P3HT:PCBM:SiPc ternary blends, both of which are lower than those of the thermal-annealed films. In this case, 94% of P3HT excitons generated in blend films can reach the interface of P3HT/PCBM even in the absence of SiPc and hence the addition of SiPc has a limited impact on the PL quenching in contrast to the thermal-annealed films. These results suggest that SiPc in P3HT:PCBM blends can act as an energy funnel for P3HT excitons particularly in the thermal-annealed films.

### *6.3.3. Transient Absorption upon Dye Excitation*

Here the author focuses on the dye sensitization mechanism in P3HT:PCBM:SiPc ternary blend films prepared under different annealing conditions upon dye excitation. The author measured the transient absorption spectra and decay dynamics of ternary blend films excited at around 670–680 nm where SiPc molecules can be selectively excited.

#### *6.3.3.1. Transient Absorption Spectra*

Before analyzing the transient absorption spectra of ternary blends, the author examined the transient spectra of binary blends of P3HT:SiPc or PCBM:SiPc as reference with a dye composition of 3.4 wt%. As shown in Figure 6-3a, P3HT:SiPc blends exhibited an almost flat absorption band from 850 to 1150 nm at 0 ps. This band is ascribed to singlet excitons of SiPc with a molar absorption coefficient of ~5 × $10^3$ $M^{-1}$ $cm^{-1}$ at 1000 nm because the same absorption band is observed for SiPc dissolved in toluene solution immediately after the laser excitation (see the Appendix). At 1 ps, the spectrum changed to a broad absorption band at around 850–1050 nm with a small and sharp band at 940 nm. These two absorption bands increased from 1 to 10 ps and then decayed similarly. The broad absorption band is ascribed to P3HT polarons as reported previously.[25,27] The sharp absorption band at 940 nm is ascribed to SiPc anions with a molar absorption coefficient of 4.3 × $10^3$ $M^{-1}$ $cm^{-1}$ (see the Appendix). On the other hand, as shown in Figure 6-3b, PCBM:SiPc blends exhibited two absorption

bands at around 855 and 1030 nm even at 0 ps. Both of them decayed monotonically. The sharp absorption band at 855 nm is ascribed to SiPc cations with a molar absorption coefficient of $1.1 \times 10^4$ $M^{-1}$ $cm^{-1}$ (see the Appendix). The small absorption band at 1030 nm is ascribed to PCBM anions with a molar absorption coefficient of $6 \times 10^3$ $M^{-1}$ $cm^{-1}$ as reported previously.[22] These results show that SiPc molecules can act as an electron donor in the PCBM domain and an electron acceptor in the P3HT domains.

Next the author moves onto P3HT:PCBM:SiPc ternary blend films. For thermal-annealed films, as shown in Figure 6-3c, an almost flat absorption band was observed from 850 to 1150

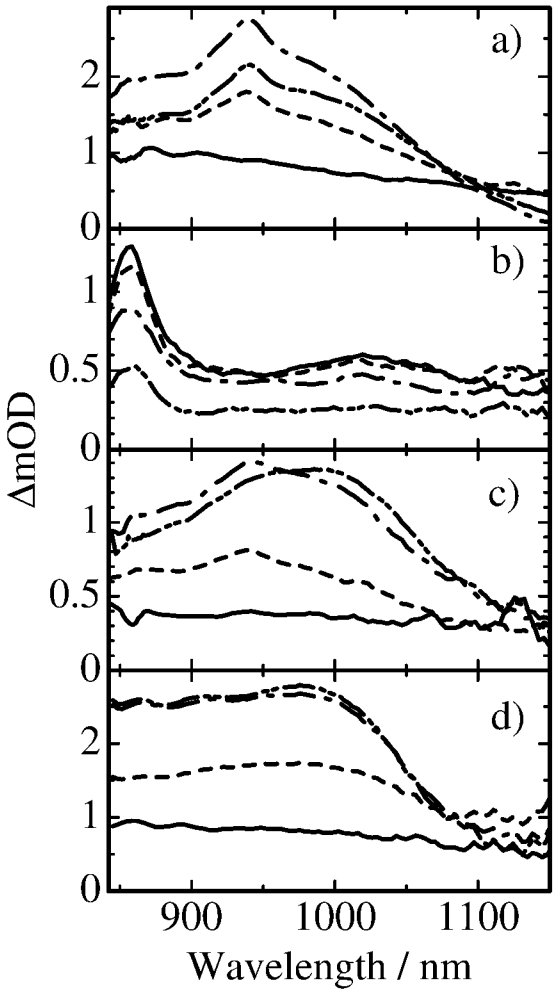


**Figure 6-3.** Transient absorption spectra of various blend films measured at a delay time of 0 (——), 1 (− − −), 10 (− • − • −), and 200 ps (− •• − •• −): a) P3HT:SiPc, b) PCBM:SiPc, c) thermal- and d) solvent-annealed P3HT:PCBM:SiPc blend films. The excitation wavelength and intensity were 680 nm and 7 μJ $cm^{-2}$, respectively. The composition of SiPc was fixed to 3.4 wt%.

nm at 0 ps and then a broad absorption band and a small and sharp band were observed at around 850–1050 nm and at 940 nm, respectively, at an earlier delay time of 1 to 10 ps. This spectral change is consistent with that observed for the P3HT:SiPc blend rather than that for the PCBM:SiPc blend. In other words, the charge separation from SiPc excitons generates P3HT polaron and SiPc anion pairs (not SiPc cation and PCBM anion pairs). This suggests that SiPc molecules are located in P3HT domains rather than in PCBM domains, which is consistent with the study in Chapter 5. At a later time stage (>10 ps), the sharp band at 940 nm disappeared and instead a broad absorption band at 1000 nm was observed with the increase in the absorption shoulder from 1000 to 1100 nm where PCBM anions have absorption. This spectral change suggests that SiPc anions decrease in this time domain and instead PCBM anions are generated. Note that the initial products (P3HT polaron and SiPc anion) at the charge generation are different from those previously reported.[30] The author will discuss this difference later. For solvent-annealed films, as shown in Figure 6-3d, an almost flat absorption band was again observed from 850 to 1150 nm at 0 ps as is the case for thermal-annealed films. On a time scale of >1 ps, a broad absorption band peaked at 1000 nm ranging from 800 to 1050 nm increased monotonically up to 10 ps after the laser excitation. Thereafter, no decay was observed even at 200 ps. Neither SiPc anions at 940 nm nor SiPc cations at 855 nm were observed over the whole time range measured. This result suggests that P3HT polarons and PCBM anions are almost simultaneously generated from SiPc excitons immediately after the laser excitation as discussed later.

#### *6.3.3.2. Charge Generation*

To study the charge generation dynamics, the author measured the time evolution of transient absorption signals of binary blends of P3HT:SiPc or PCBM:SiPc on a time scale of picoseconds. For the P3HT:SiPc blend, as mentioned above, three transient species are observed: SiPc excitons, P3HT polarons, and SiPc anions. As shown in Figure 6-3a, both

SiPc excitons and P3HT polarons have absorption at 900 nm. Thus, the decay of SiPc excitons and the rise of P3HT polarons should be observed with the same time constant $\tau_{CG}$ because P3HT polarons are generated from SiPc excitons. Indeed, the time evolution of transient signals at 900 nm was well fitted by Eq. 6-1 with a time constant of $\tau_{CG}$ = 2 ps.

$$\Delta OD(t) = A_{SiPc^*} \exp(-t/\tau_{CG}) + A_{P3HT^+} [1 - \exp(-t/\tau_{CG})] \quad (6\text{-}1)$$

At a later time stage of >10 ps, the transient signals at 900 nm are safely ascribed to P3HT polarons because SiPc excitons disappear completely. At this time domain, the signals of P3HT polarons decayed with a lifetime of ~2 ns. On the other hand, the time evolution of SiPc anions can be estimated from the projecting sharp absorption band at 940 nm (see the Appendix). As shown in Figure 6-4a, the rise and decay dynamics of SiPc anions were in good agreement with those of P3HT polarons, suggesting the charge generation and recombination of P3HT polarons and SiPc anions. For the PCBM:SiPc blend, as shown in Figure 6-3b, SiPc cations and PCBM anions are separately observed at 855 nm and at 1030 nm, respectively. As shown in Figure 6-4b, both signals were promptly generated within 100 fs and decayed exponentially with lifetimes of 35 ps (40%) and 2 ns (60%) at a later time stage. These findings show the charge generation from SiPc excitons is more rapid in PCBM than in P3HT.

Next, the author moves onto the charge generation dynamics in P3HT:PCBM:SiPc ternary blend films. For the thermal-annealed blends, as mentioned above, the charge generation dynamics from 1 to 10 ps is similar to that observed for P3HT:SiPc binary blend films. Thus, the time evolution of P3HT polarons and SiPc anions were analyzed in the same way as described above. As a result, as shown in Figure 6-4c, P3HT polarons and SiPc anions were generated with the same time constant of $\tau_{CG}$ = ~2 ps, which is in good agreement with that observed for the P3HT:SiPc blends. For the solvent-annealed films, as mentioned above, neither SiPc cations nor anions were observed, suggesting that P3HT polarons and PCBM

anions are rapidly generated almost simultaneously from SiPc excitons. As shown in Figure 6-4d, the time evolution of the P3HT polaron band at 900 nm was fitted with a time constant of ~2 ps. This is again in good agreement with that observed for the P3HT:SiPc blends. This indicates that the majority of SiPc molecules in the ternary blend films are embedded in P3HT

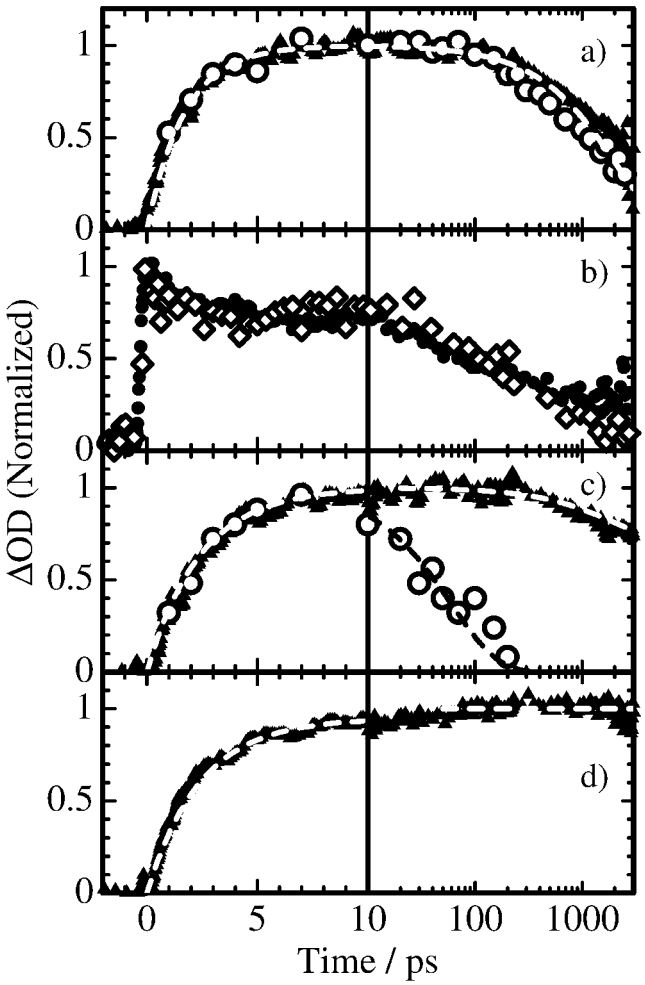


**Figure 6-4.** Normalized transient absorption signals of various blend films excited at 680 nm (7 μJ $cm^{-2}$): a) P3HT:SiPc, b) PCBM:SiPc, and c) thermal- and d) solvent-annealed P3HT:PCBM:SiPc blend films measured at 855 nm (SiPc cations; closed circles), 940 nm (SiPc anions; open circles), 1000 nm (P3HT polarons with (c, d) and without (a) PCBM anions; closed triangles), and 1030 nm (PCBM anions; open diamonds). The open circles show the rise fraction of SiPc anions at 940 nm that is evaluated by subtracting the transient absorption signals of SiPc excitons and P3HT polarons at 940 nm from the observed signals at 940 nm (see the Appendix). The broken lines are fitting curves base on the function described in the text.

domains rather than in PCBM domains under both annealing conditions. These findings suggest that the generation rates from SiPc excitons are independent on the annealing conditions. The detailed charge generation and shift mechanisms in the ternary blend films will be discussed later.

#### *6.3.3.3. Charge Shift*

Here, the author focuses on the charge shift from SiPc anions to PCBM. At a later time stage of 10 ps to 3 ns, as shown in the right of Figure 6-4c, SiPc anions decayed with a lifetime of 60 ps while P3HT polarons remain almost the same even at 3 ns. If SiPc anions recombined with P3HT polarons, P3HT polarons should decay with the same time constant. However, this is not the case. In other words, the recombination of SiPc anions with P3HT polarons is negligible but rather the charge shift from SiPc anions to PCBM is dominant at the interface with almost 100% efficiency. Furthermore, SiPc molecules embedded in P3HT domains are also negligible because SiPc anions generated from such isolated SiPc should recombine with P3HT polarons geminately.

To evaluate the rate constant of charge shift in more detail, the author analyzed the time evolution of the transient absorption spectra observed for P3HT:PCBM:SiPc ternary blend films by using the spectral template of a pair of P3HT polarons and SiPc anions ($P3HT^+/SiPc^-$) and a pair of P3HT polarons and PCBM anions ($P3HT^+/PCBM^-$). The transient absorption spectrum observed for P3HT:SiPc blends at 100 ps can be employed as the spectral template of $P3HT^+/SiPc^-$ because SiPc excitons completely disappear at this time domain. The transient absorption spectrum observed for P3HT:PCBM blends at 1 ns upon the P3HT excitation can be employed as the spectral template of $P3HT^+/PCBM^-$ because P3HT excitons completely disappear at this time domain as shown in the next section. As shown in Figure 6-5, the spectrum at 2 ps is almost reproduced with only a template of $P3HT^+/SiPc^-$.

The spectrum at 10 ps is not reproduced with only $P3HT^+/SiPc^-$ but is well reproduced with a sum of $P3HT^+/SiPc^-$ (75%) and $P3HT^+/PCBM^-$ (25%) and at 50 ps with a sum of $P3HT^+/SiPc^-$ (40%) and $P3HT^+/PCBM^-$ (60%). The spectrum at 1 ns is reproduced with only $P3HT^+/PCBM^-$. Figure 6-5e summarizes the time evolution of the fraction of each charge carrier in P3HT:PCBM:SiPc blends. The decay of SiPc anions and the rise of PCBM anions

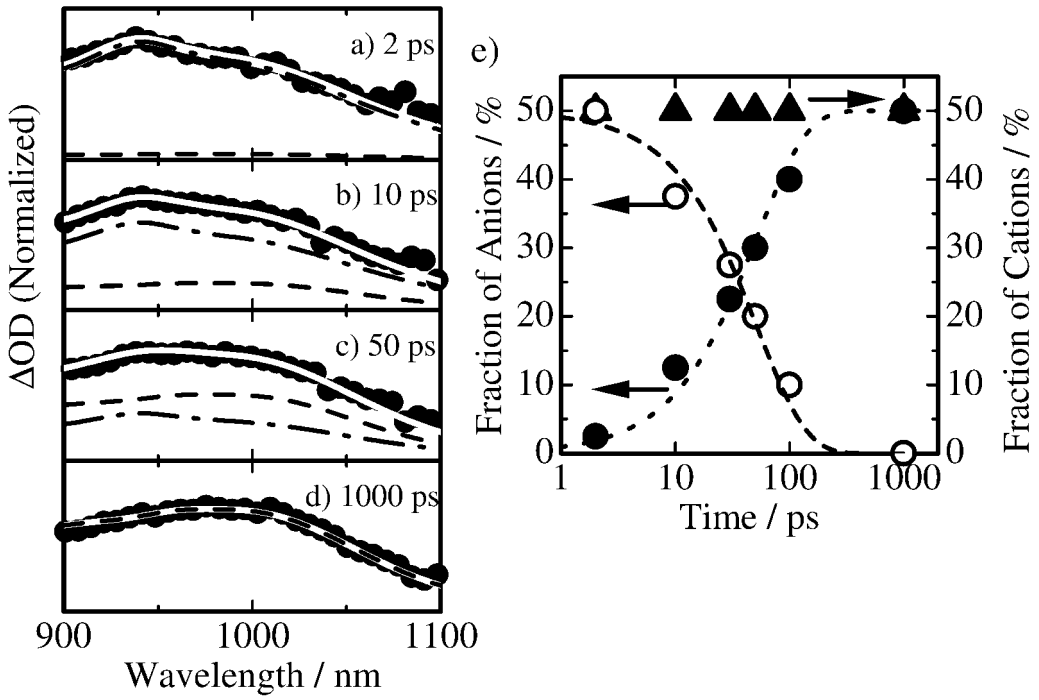


**Figure 6-5.** Transient absorption spectra of thermal-annealed P3HT:PCBM:SiPc blend films (closed circles) at a) 2, b) 10, c) 50, and d) 1000 ps after the excitation at 680 nm (7 μJ $cm^{-2}$). The white solid lines represent absorption spectra simulated by a sum of each absorption spectrum of charge carriers pairs: $P3HT^+/SiPc^-$ (the spectrum observed in P3HT:SiPc blends at 100 ps excited at 670 nm; dashed-dotted lines) and $P3HT^+/PCBM^-$ (the spectrum observed in P3HT:PCBM blends at 1000 ps excited at 400 nm; broken lines). The fraction ratio of each spectrum is $P3HT^+/SiPc^-$:$P3HT^+/PCBM^-$ = (a) 95:5, (b) 75:25, (c) 40:60, and (d) 0:100. e) The fractions of $P3HT^+$ (closed triangles), $SiPc^-$ (open circles) and $PCBM^-$ (closed circles) in thermal-annealed P3HT:PCBM:SiPc blend films against the time after the excitation at 680 nm (7 μJ $cm^{-2}$). The fraction is evaluated from the spectral simulation shown in a)–d). The fraction changes in $SiPc^-$ ($F_{SiPc-}$) and $PCBM^-$ ($F_{PCBM-}$) were fitted with monoexponential functions: $F_{SiPc-}(t) = 50 \exp(-t/\tau_{CSH})$ (broken line) and $F_{SiPc-}(t) = 50\,[1 - \exp(-t/\tau_{CSH})]$ (dotted line), respectively, with $\tau_{SCH}$ = ~50 ps.

are well fitted with a monoexponential function with the same time constant of ~50 ps, which is in agreement with the estimation mentioned above. Thus, the rate constant of the charge shift is evaluated to be ~2 × $10^{10}$ $s^{-1}$. On the other hand, as mentioned before, no distinct charge shift is observed for the solvent-annealed film. In other words, P3HT polarons and PCBM anions are rapidly generated simultaneously from SiPc excitons.

### *6.3.4. Transient Absorption upon P3HT Excitation*

Here the author focuses on the exciton harvesting mechanism in P3HT:PCBM:SiPc ternary blend films prepared under different annealing conditions upon P3HT excitation. The author measured the transient absorption spectra and decay dynamics of ternary blend films excited at 400 nm where P3HT can be selectively excited.

#### *6.3.4.1. Transient Absorption Spectra*

For thermal-annealed films, as shown in Figures 6-6a and 6-6b, both P3HT:PCBM binary and P3HT:PCBM:SiPc ternary blend films exhibited a large absorption band at around 1250 nm and negative signals at around 550–600 nm immediately after the laser excitation, which are attributable to singlet excitons of P3HT and photobleachings of the ground state of P3HT with molar absorption coefficients of 3 × $10^4$ and 3 × $10^4$ $M^{-1}$ $cm^{-1}$, respectively.[25,27] At 100 ps, the exciton band at 1250 nm disappeared and the P3HT photobleaching bands at around 550–600 nm decreased by almost half. Instead broad absorption bands were observed from 650 to 1050 nm, which are attributable to P3HT polarons.[25] These similar trends suggest that P3HT polarons are efficiently generated from P3HT excitons in both ternary and binary blends with and without SiPc. The author notes three differences in the spectra of ternary and binary blends with and without SiPc. First, the P3HT exciton band at 1250 nm decayed faster in the ternary blends than that in the binary blends. Second, a small and sharp depression was observed at around 680 nm only for P3HT:PCBM:SiPc ternary blends. This is ascribable to a

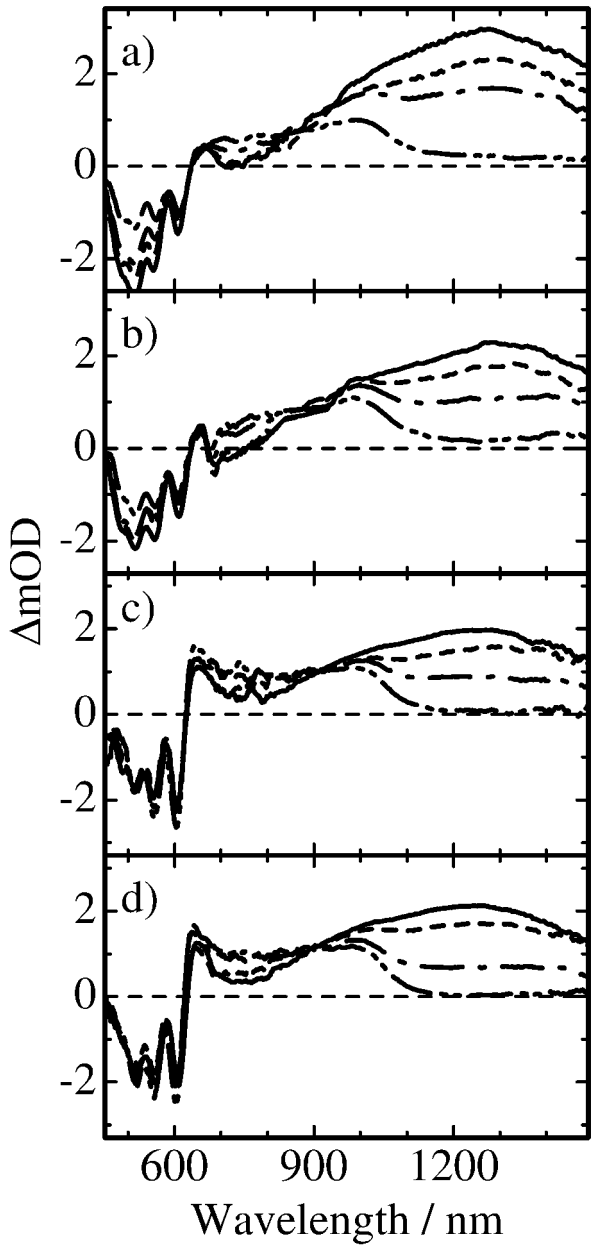


**Figure 6-6.** Transient absorption spectra of P3HT:PCBM (a and c) and P3HT:PCBM:SiPc blend films (b and d) after thermal (a and b) and solvent (c and d) annealing measured at a delay time of 0 (——), 1 (– – –), 10 (– • – • –), and 100 ps (– •• – •• –). The excitation wavelength and intensity were 400 nm and 6 μJ $cm^{-2}$, respectively.

photobleaching of the ground state of SiPc because SiPc has a sharp absorption peak in the ground state. Note that SiPc cannot be directly excited at 400 nm because of negligible absorption at 400 nm (see the Appendix). Third, the recovery in the P3HT photobleaching

bands at around 550–600 nm was smaller in the ternary blends than in the binary blends. These differences suggest that SiPc molecules play an important role in the charge generation in ternary blend films. For solvent-annealed films, as shown in Figures 6-6c and 6-6d, a similar spectral change was observed: the P3HT exciton and photobleaching bands were observed at 1250 nm and at around 550–600 nm immediately after the laser excitation and subsequently P3HT polaron bands were observed from 650 to 1050 nm with the decay of P3HT excitons. In contrast to the thermal-annealed films, there was no distinct difference in the transient spectra between P3HT:PCBM binary and P3HT:PCBM:SiPc ternary blend films although the P3HT exciton decayed slightly faster in ternary blends than in binary blends. This result suggests that the contribution of SiPc to the charge generation is limited in solvent-annealed films compared to thermal-annealed films. Nonetheless, the author notes four differences in the transient spectra between solvent-annealed and thermal annealed films. First, the photobleaching of SiPc was less distinguished in solvent-annealed films, which is consistent with rapid generation of P3HT polarons and PCBM anions as mentioned before. Second, the intensity ratio of the P3HT polaron band at 650 nm to the other polaron band at 1000 nm was much larger for solvent-annealed films than for thermal-annealed films, suggesting that delocalized polarons are more likely to be generated in the solvent-annealed films. Third, the intensity ratio of the P3HT photobleaching band at 600 nm to the other bands at around 550–580 nm was much larger for solvent-annealed films than for thermal-annealed films, which is consistent with the steady-state absorption as shown in Figure 6-1. Fourth, these P3HT photobleaching bands did not decay at all over the whole time range measured, suggesting that P3HT polarons do not deactivate to the ground state but rather can survive for longer time domains.

#### *6.3.4.2. Exciton Harvesting*

To study the exciton-harvesting dynamics in ternary blend films, the author examined the

time evolution of transient absorption signals upon the excitation of P3HT on a time scale of picoseconds. For the thermal-annealed binary blends, as shown in Figure 6-6a, P3HT excitons can be separately observed at 1200 nm while P3HT polarons are overlapped with P3HT excitons at 1000 nm. Thus, the time evolution of the P3HT polaron band is obtained by subtracting the P3HT exciton decay at 1200 nm from the signals at 1000 nm as reported previously.[26] Figure 6-7a shows the decay of P3HT excitons at 1200 nm and the formation of P3HT polarons in the thermal-annealed binary blends. For P3HT excitons, the transient decay at 1200 nm was fitted by Eq. 6-2 with two lifetimes of $\tau_{D0}$ = 25 ps (85%) and $\tau_{D1}$ = 330 ps (15%).

$$\Delta OD_{binary}(t) = A_{D0} \exp(-t/\tau_{D0}) + A_{D1} \exp(-t/\tau_{D1}) \quad (6\text{-}2)$$

The longer and minor lifetime is fixed to the monomolecular lifetime of P3HT excitons.[25] For P3HT polarons, the formation dynamics of polarons at 1000 nm was fitted with a sum of a monoexponential rise function with a lifetime of $\tau_{R1}$ = 25 ps (60%) and a constant fraction (40%). The good agreement in the rise and decay constants strongly suggests that P3HT polarons are generated from P3HT excitons via the exciton migration to the interface of P3HT/PCBM. The constant fraction (40%) is assigned to the prompt polaron generation from hot excitons generated near the interface of P3HT/PCBM (on a time scale of <100 fs). These assignments are consistent with recent transient absorption studies.[26,28,29]

Figure 6-7b shows the time evolution of P3HT excitons and P3HT polarons in the P3HT:PCBM:SiPc ternary blend films with thermal annealing. Compared to the binary blends, P3HT excitons decayed faster in the ternary blends, suggesting that there is another quenching pathway for P3HT excitons in the presence of SiPc. Therefore, the transient absorption decay at 1200 nm was fitted by Eq. 6-3 under the assumption that the additional quenching is independent of the other decay dynamics observed for the binary blends.

$$\Delta OD_{ternary}(t) = A_{D2} \exp(-t/\tau_{D2}) + B_{D2}\, \Delta OD_{binary}(t) \quad (6\text{-}3)$$

As a result, the lifetime $\tau_{D2}$ was evaluated to be 4 ps (50%), which is significantly shorter than the lifetime in the binary blends ($\tau_{D1}$ = 25 ps). In other words, half of the P3HT excitons

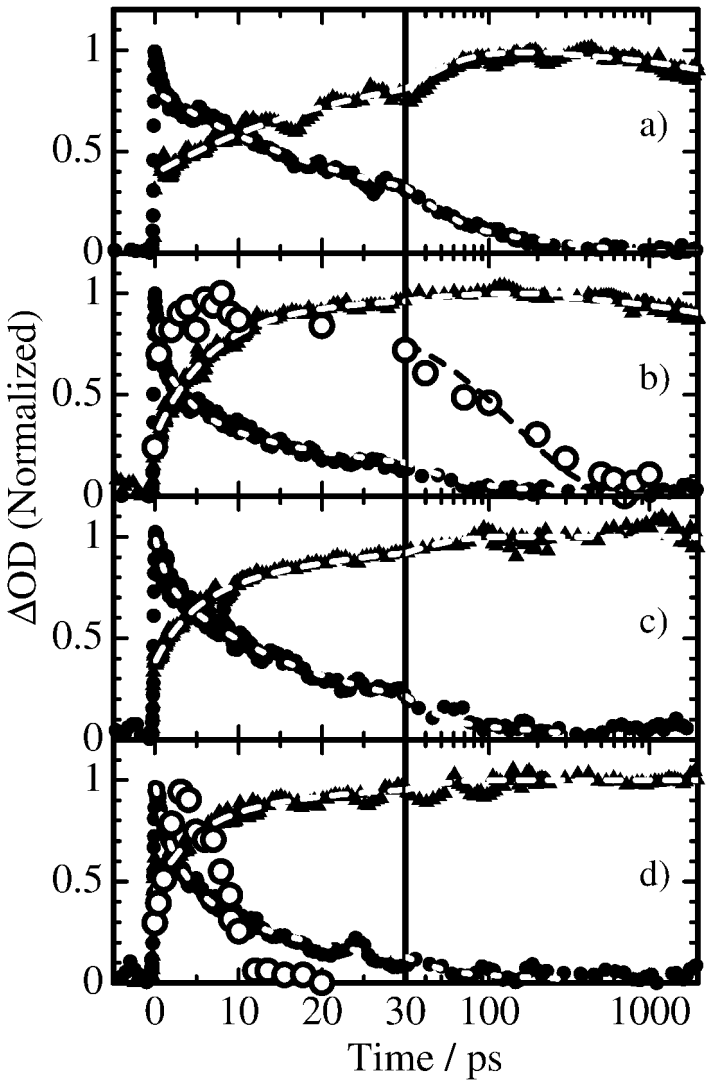


**Figure 6-7.** Normalized transient absorption signals of P3HT:PCBM (a and c) and P3HT:PCBM:SiPc blend films (b and d) for thermal (a and b) and solvent (c and d) annealing, at 1200 nm (P3HT excitons; closed circles) and 1000 nm (P3HT polarons; closed triangles) excited at 400 nm (6 μJ $cm^{-2}$). The rise signals at 1000 nm were evaluated by subtracting the transient absorption signals of P3HT excitons at 1200 nm from that at 1000 nm (see ref 26 for details). The open circles show the normalized rise fraction of the SiPc photobleaching evaluated by subtracting the transient absorption signals of P3HT polarons at 680 nm from the observed signals at 680 nm (see the Appendix). The broken lines are fitting curves based on the function described in the text.

observed at 0 ps are quenched with a lifetime of 4 ps by the addition of SiPc. The remaining half excitons decay as slowly as in binary blends without SiPc. As with the decay of P3HT excitons, the rise signals of P3HT polarons were fitted with a sum of two monoexponential rise functions with the rise time constant of $\tau_{R1}$ = 25 ps and $\tau_{R2}$ and a constant fraction. As a result, the shorter rise time constant $\tau_{R2}$ was evaluated to be 6 ps (55%), which is a little slower than $\tau_{D2}$ = 4 ps in ternary blends, and the constant fraction was 30%. The difference between $\tau_{D2}$ and $\tau_{R2}$ suggests that P3HT polarons are not directly generated from P3HT excitons. In other words, there exists an intermediate transient state between P3HT excitons and P3HT polarons. To address the origin of the intermediate species, the author focuses on the photobleaching band of SiPc at 680 nm (see the Appendix). As shown by the open circles in Figure 6-7b, the rise constant of the photobleaching band of SiPc was evaluated to be 4 ps. This is in good agreement with the decay constant of P3HT excitons ($\tau_{D2}$ = 4 ps). The author therefore assigns the fast quenching of P3HT excitons in ternary blends to an efficient energy transfer of P3HT excitons to SiPc molecules. Such efficient light harvesting based on energy transfer has also been reported for organic-inorganic hybrid solar cells and dye-sensitized $TiO_2$ solar cells.[42–46]

For the solvent-annealed films, similar dynamics were observed and hence analyzed by the same equations mentioned above, although each time constant was shortened compared to those observed in the thermal-annealed films. In binary blends, P3HT excitons decayed slightly faster with a lifetime of $\tau_{D0}^{S}$ = 13 ps (80%) and P3HT polarons was also generated slightly faster on a rise constant of $\tau_{R1}^{S}$ = 13 ps (55%) with a constant fraction (45%). This agreement in the rise and decay is again indicative of the direct generation of P3HT polarons from P3HT excitons. The faster time constant suggests the more rapid exciton migration in the solvent-annealed films. For ternary blends, P3HT excitons decayed slightly faster with a lifetime of $\tau_{D2}^{S}$ = 3 ps (38%) and P3HT polarons was also generated slightly faster with rise

constants of $\tau_{R1}^{S}$ = 13 ps (30%) and $\tau_{R2}^{S}$ = 4 ps (25%) with a constant fraction (45%) in the presence of SiPc. The smaller fraction of $\tau_{D2}^{S}$ and $\tau_{R2}^{S}$ compared to that observed for the thermal-annealed films suggests the smaller contribution of SiPc to exciton harvesting in the solvent-annealed films. Furthermore, the photobleaching of SiPc appeared with a rise constant of 3 ps. This is again in good agreement with the fast decay constant of P3HT excitons ($\tau_{D2}^{S}$ = 3 ps), suggesting the efficient energy transfer of P3HT to SiPc. These results show that the annealing conditions have little impact on the exciton-harvesting dynamics but significant impact on the fraction due to the energy transfer.

#### *6.3.4.3. Charge Shift*

The author moves onto a later time stage of 10 ps to 3 ns to examine the charge shift from SiPc to PCBM in ternary blends. For the thermal-annealed films, as shown by the open circles in Figure 6-7b, the SiPc photobleaching band decayed exponentially with a lifetime of 150 ps. On the other hand, P3HT polarons remain almost the same, suggesting the efficient charge shift without the charge recombination. Interestingly, the charge shift time is slower than that observed upon the dye excitation, which is indicative of different distribution of excited dye molecules at the interface depending on the excitation wavelength as will be discussed later. For the solvent-annealed films, as shown by the open circles in Figure 6-7d, the SiPc photobleaching band rapidly decayed monoexponentially with a lifetime of 5 ps, which is again slightly slower than that observed upon the dye excitation. On the other hand, no decay was observed for P3HT polarons up to 3 ns. In other words, most of SiPc anions can contribute to the charge shift to PCBM efficiently without the charge recombination to the ground state under either annealing condition. These results show that the charge shift at the interface is strongly dependent on the annealing conditions.

## 6.4. Discussion

### *6.4.1. Light-Harvesting Mechanism*

First the author discusses the light-harvesting dynamics in the ternary blend films. In the thermal-annealed films upon the P3HT excitation, P3HT polarons are promptly generated (<100 fs) at the interface and slowly generated via the exciton migration on a time scale of 25 ps in the absence of SiPc. Therefore, the overall exciton migration rate to the interface and the charge separation rate at the interface of P3HT/PCBM are estimated to be $k_{EM} = 4 \times 10^{10}$ $s^{-1}$ and $k_{CS}^{P/C60} > 10^{13}$ $s^{-1}$, respectively. In the presence of SiPc, SiPc excitons are generated on a time scale of 4 ps via the efficient energy transfer from P3HT excitons. Thus, the energy transfer rate is estimated to be $k_{EnT} = 3 \times 10^{11}$ $s^{-1}$. All these processes are more than one order of magnitude faster than the deactivation rate of P3HT singlet excitons ($k_f^P = 3 \times 10^9$ $s^{-1}$), suggesting the efficient exciton harvesting in ternary blends. Once SiPc excitons are generated by the energy transfer, the following photophysics is the same as the direct excitation of SiPc. Upon the SiPc excitation, P3HT polarons and SiPc anions are generated on a time scale of 2 ps. This is much more rapid than the deactivation rate of SiPc singlet excitons ($k_f^D = 2 \times 10^8$ $s^{-1}$), suggesting the efficient charge separation between SiPc singlet excitons and P3HT. Furthermore, most of the P3HT polarons and SiPc anions are followed by the efficient charge shift to PCBM with a time constant of 50 ps while the charge recombination of $P3HT^+/SiPc^-$ pairs is as slow as 2 ns. In summary, the charge separation rate at the interface of P3HT/SiPc, the charge recombination rate, and the charge shift rate from SiPc to PCBM are estimated to be $k_{CS}^{P/D} = 5 \times 10^{11}$ $s^{-1}$, $k_{CR}^{P/D} = 5 \times 10^8$ $s^{-1}$, and $k_{CSH} = 2 \times 10^{10}$ $s^{-1}$, respectively. The charge shift rate is 40 times faster than the backward recombination rate, suggesting the efficient charge shift from SiPc to PCBM. All the rate constants of the fundamental photophysical processes are summarized in Scheme 6-1a.

**Scheme 6-1. Energy Diagrams of Light-Harvesting and Charge Generation Mechanisms in P3HT:PCBM:SiPc Ternary Blend Films[a]**

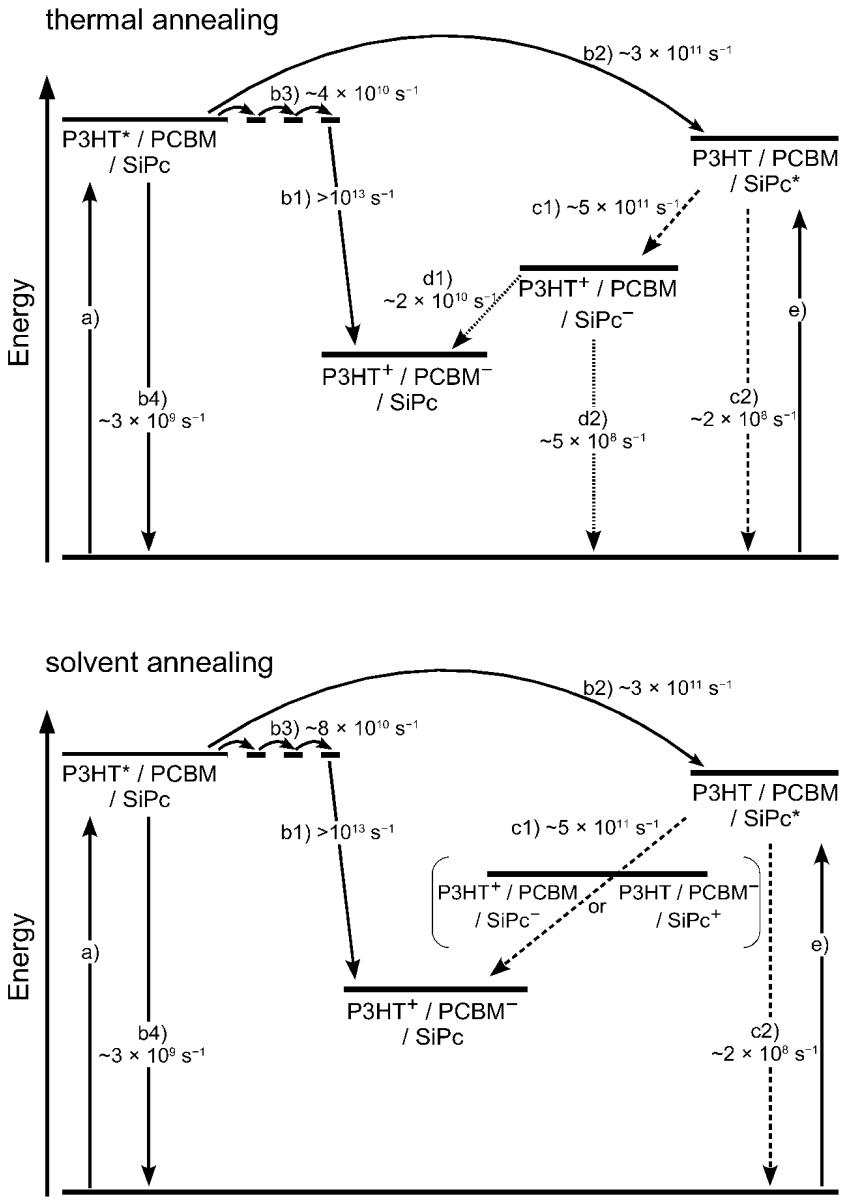


[a] The scheme of light-harvesting and charge generation mechanisms in thermal- (upper) and solvent-annealed P3HT:PCBM:SiPc blend films (lower): a) photon absorption of P3HT, b1) charge generation of $P3HT^+$ and $PCBM^-$ in the disordered P3HT phase, b2) energy transfer from P3HT* to SiPc, b3) exciton migration of P3HT* in P3HT crystal domains, b4) monomolecular deactivation of P3HT*, c1) charge generation of $P3HT^+$ and $SiPc^-$ for thermal annealing and of $P3HT^+$ and $PCBM^-$ through the intermediate charge state of SiPc (not observed) for solvent annealing, c2) monomolecular deactivation of SiPc*, d1) charge shift from SiPc to PCBM, d2) charge recombination between $P3HT^+$ and $SiPc^-$, and e) photon absorption of SiPc.

The author notes as mentioned before that the initial products at the charge generation are different from the previous report by Johansson et al.[30] In this study, P3HT polaron and SiPc anion are the first product at the charge generation. On the other hand, they reported that dye cation and PCBM anion are generated first in P3HT:PCBM:dye (metal-free phthalocyanine derivative) ternary blends. This is probably due to the different dye location in ternary blends. As studied in Chapter 5, the dye location in ternary blends is strongly dependent on the surface energy of blend component materials. The surface energy of SiPc (23 mJ $m^{-2}$) used in this study is closer to that of P3HT (20 mJ $m^{-2}$) rather than that of PCBM (29 mJ $m^{-2}$). In other words, SiPc molecules are likely to be located in P3HT rather than in PCBM domains. This is consistent with the observation of P3HT polaron and SiPc anion upon the dye excitation. On the other hand, the surface energy of the metal-free phthalocyanine derivative can be estimated to be 28 mJ $m^{-2}$ from the contact angle measurement reported in Chapter 5 (data are not shown), which is closer to that of PCBM rather than that of P3HT. In other words, the metal-free phthalocyanine derivative is likely to be located in PCBM rather than in P3HT domains. This is consistent with the previous report that dye cation and PCBM anion are generated first upon the dye excitation. The author therefore concludes that the difference in the initial products is due to the different dye location in ternary blends.

For the solvent-annealed films, all the rate constants are similarly estimated as summarized in Scheme 6-1b. The author notes that no distinct charge shift is observed upon the dye excitation although P3HT polarons and PCBM anions are generated almost simultaneously with a rise time constant of 2 ps. This finding shows charge generation of $P3HT^{+}/SiPc^{-}$ followed by rapid charge shift from SiPc to PCBM or charge generation of $SiPc^{+}/PCBM^{-}$ followed by rapid charge shift from SiPc to P3HT. Although it is not clear which process is dominant, in either case, SiPc molecules should be in proximity not only to P3HT but also to PCBM in solvent-annealed films. On the basis of these rate constants, all the efficiency of

each process is also estimated as summarized in Table 6-1. In either annealing condition, the overall charge dissociation to P3HT polarons and PCBM anions is kinetically almost 100% upon the dye excitation. These results show that SiPc molecules located at the interface of P3HT/PCBM can efficiently contribute to the photocurrent generation under either annealing condition even though the fundamental processes are slightly dependent on the annealing conditions. This is because all the forward processes are rapid compared to the backward processes as seen in the photosynthetic reaction center.[47,48]

**Table 6-1.** Efficiencies of Fundamental Processes in RR-P3HT:PCBM:SiPc Ternary Blend Films.[a]

| | $f_{EM}$ | $f_{EnT}$ | $\eta_{EM}$ | $\eta_{CS}^{P/C60}$ | $\eta_{EnT}$ | $\eta_{CS}^{P/Pc}$ | $\eta_{CSH}$ | $\eta_{CG}^{P/C60}$ | $\eta_{Total}$ |
|---|---|---|---|---|---|---|---|---|---|
| Thermal | | | | | | | | | |
| without SiPc | 1 | 0 | 0.80 | 1 | 1 | 1 | 0.98 | 0.98 | 0.80 |
| with SiPc | 0.6 | 0.4 | | | | | | | 0.87 |
| Solvent | | | | | | | | | |
| without SiPc | 1 | 0 | 0.94 | 1 | 1 | ··· | ··· | 1 | 0.94 |
| with SiPc | 0.6 | 0.4 | | | | | | | 0.96 |

[a] $f_{EM}$, fraction of P3HT* not effected by SiPc; $f_{EnT}$, fraction of P3HT* effected by SiPc; $\eta_{EM}$, efficiency for P3HT* diffusion to the P3HT/PCBM interface; $\eta_{CS}^{P/C60}$, charge-transfer efficiency from P3HT* to $P3HT^+/PCBM^-$ at the P3HT/PCBM interface; $\eta_{EnT}$, energy-transfer efficiency from P3HT* to SiPc; $\eta_{CS}^{P/Pc}$, charge-transfer efficiency from SiPc* to $P3HT^+/SiPc^-$; $\eta_{CSH}$, charge-shift efficiency from SiPc to PCBM; $\eta_{CG}^{P/C60}$, charge-generation efficiency of $P3HT^+/PCBM^-$ from SiPc* (proportion of $\eta_{CS}^{P/Pc}$ and $\eta_{CSH}$ for thermal annealing); $\eta_{Total}$, total efficiency of $P3HT^+/PCBM^-$ generation (evaluated by $\eta_{Total} = f_{EM} \times \eta_{EM} \times \eta_{CS}^{P/C60} + f_{EnT} \times \eta_{EnT} \times \eta_{CG}^{P/C60}$).

### *6.4.2. Exciton-Harvesting Mechanism*

To understand the contribution of the energy transfer in the presence of dye molecules, the author discusses how P3HT excitons are relaxed in ternary blends. As mentioned before, there are four relaxation pathways for P3HT excitons in ternary blends: 1) prompt quenching within 100 fs by the charge generation from hot excitons generated near the interface of P3HT/PCBM, 2) delayed quenching by the charge generation via the exciton migration to the P3HT/PCBM interface, 3) no quenching and just deactivation to the ground state with a lifetime of singlet excitons, 4) rapid quenching by the efficient energy transfer to SiPc. As shown in Figure 6-8, each fraction can be estimated from the PL and transient analyses (see the Appendix). In the thermal-annealed P3HT:PCBM binary blends, 31% of P3HT excitons are quenched by the prompt charge generation from hot excitons, 49% of excitons are quenched by the delayed charge generation via the exciton migration, and the remaining 20% of excitons are neither quenched nor contribute to the photocurrent generation. This is consistent with the previous report.[26] In P3HT:PCBM:SiPc ternary blends, the efficient energy transfer quenching accounts for 34% for thermal-annealed films and 21% for solvent-annealed films, suggesting that the energy transfer is more effective in thermal-annealed films than in solvent-annealed films. Interestingly, the ratio of the delayed quenching to the non-quenching is almost constant for both binary and ternary blends with thermal annealing (~25–29%) and for solvent annealing (~6–10%). This suggests that the energy transfer is independent of the delayed quenching and the non-quenching events. This is also consistent with the transient analysis by Eq. 6-3 assuming that the energy transfer quenching is independent of the other decay dynamics observed for binary blends. Indeed, the transient dynamics is well fitted by Eq. 6-3, as described before, suggesting that the assumption is valid. The author therefore concludes that the energy transfer to SiPc occurs separately from the other exciton decay dynamics such as prompt and delayed charge generation and emissive

pathway observed for binary blends. This is probably because SiPc molecules are inhomogeneously distributed at the interface of P3HT/PCBM. In other words, there are two interfaces: the interface with SiPc and the other interface without SiPc that is similar to the interface of P3HT:PCBM binary blends. Thus the author assumes that the ratio of the prompt and delayed quenching at the interface without SiPc is the same as that observed for binary blends. As shown by the white broken lines in Figure 6-8, the upper part of the black bar represents the fraction of the prompt quenching at the interface without SiPc and the bottom part represents the fraction of the prompt quenching at the interface with SiPc. Therefore, the interface with SiPc can be roughly estimated to be ~40% independently of the annealing

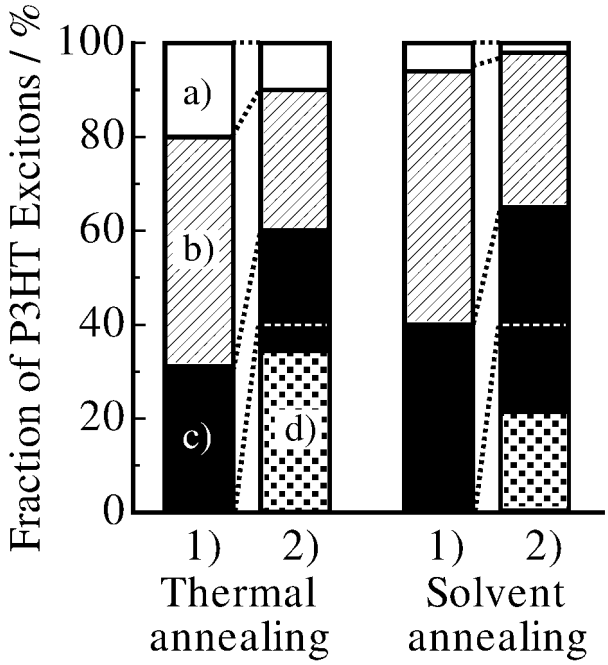


**Figure 6-8.** Bar chart for the fraction of each relaxation pathway of P3HT excitons in 1) P3HT:PCBM and 2) P3HT:PCBM:SiPc blend films after thermal and solvent annealing: a) prompt quenching within 100 fs by the charge generation via hot excitons near the P3HT/PCBM interface, b) delayed quenching by the charge generation via the exciton migration to the interface, c) no quenching and just deactivation to the ground state with a lifetime of P3HT excitons, d) rapid quenching by the efficient energy transfer to SiPc at the interface. The upper and bottom parts of (c) divided by the white broken lines represent the fraction of the prompt quenching at the interface without and with SiPc, respectively (see the text).

conditions. This suggests that the interfacial coverage of SiPc is about 40% in ternary blend films. The author will discuss this coverage again in terms of the interfacial morphology later.

Next the author discusses how efficient the energy transfer is at the interface in ternary blends. As reported in Chapter 3, the Förster radius for transfer from P3HT to SiPc is estimated to be 3.7 nm assuming point dipoles. This is valid if each SiPc molecule is isolated at the interface. However, as described above, SiPc molecules are localized at a part of the interface and hence likely to be concentrated. The author has reported that the local concentration of SiPc is as high as 25 wt%, which is 7 times as high as the original composition (3.4 wt%) in Chapter 5. These findings suggest that SiPc molecules are not homogeneously distributed but rather concentrated at a certain interface. Therefore, dipole–infinite-slab approximation is more appropriate to estimate the Förster radius $R_0$ rather than point dipoles: the energy transfer rate ($k_{EnT}$) is proportional to $1/r^3$ rather than $1/r^6$ where $r$ is the distance between donor and acceptor. Such approximation has been reported to be valid for the energy transfer in P3HT/interlayer/$C_{60}$ devices.[49] In accordance with the method of Scully *et al.*,[44] the Förster radius $R_0$ is estimated to be as long as ~7 nm for transfer from P3HT to a slab of SiPc, which is embedded in disordered P3HT interface with a local concentration of 25 wt%. On the other hand, as estimated from the steady-state P3HT absorption (Figure 6-2), the domain size of crystalline P3HT is estimated to be ~10 nm for the thermal-annealed blends. In other words, the distance from the domain center to the interface is smaller compared to the Förster radius ~7 nm. Therefore, almost all excitons of P3HT would be quenched by the energy transfer to SiPc molecules if SiPc molecules were dispersed in the disordered P3HT domains homogeneously (see the Appendix). However, this is not the case as shown in Figure 6-3: 10% of P3HT excitons are still not quenched even in the ternary blend films after thermal annealing. These results suggest that some P3HT excitons cannot reach the interface without SiPc but almost all the excitons are efficiently collected to the

interface with SiPc molecules. This is consistent with the assumption in the kinetic analysis described before.

In the solvent-annealed films, on the other hand, P3HT excitons are more efficiently quenched even though the domain size of P3HT crystalline is ~15 nm larger than in the thermal-annealed films (~10 nm). Indeed, the apparent exciton migration time $t_{EM}$ is shorter (~13 ps) compared to the thermal-annealed films (~25 ps). Considering the PL efficiency of P3HT:PCBM binary blends, the apparent exciton diffusion length $L_{Da}$ is estimated to be as long as 6.8 nm even in the absence of SiPc, which is more than one and a half times that for the thermal-annealed films (4 nm). Thus, the apparent diffusion constant of P3HT excitons is roughly estimated by $D_a = L_{Da}^2/(2t_{EM})$ to be $1.8 \times 10^{-2}$ cm$^2$ s$^{-1}$ for the solvent-annealed and $3.2 \times 10^{-3}$ cm$^2$ s$^{-1}$ for the thermal-annealed films. Although this is a rough estimation, it is noteworthy that the apparent diffusion constant is more than 5 times larger in the solvent-annealed than in the thermal-annealed films. This is partly because of the higher crystallization of P3HT after solvent annealing. Possibly, this would be also dependent on the interfacial structure as discuss later. The author concludes that the efficient exciton diffusion results in the relatively small contribution of dye molecules to the P3HT exciton harvesting in the solvent-annealed ternary blends. In other words, there is still room to improve the exciton-harvesting efficiency in solvent-annealed ternary blends if the crystalline P3HT domains could be grown up furthermore.

### *6.4.3. Interfacial Structures in Ternary Blend Films*

First, the author considers the distribution of SiPc molecules in ternary blends. From the absorption spectra in Figure 6-1, the author concludes that SiPc molecules are not likely to be located in P3HT crystalline domains. From the transient study, the author also obtains several important findings as follows. Note that all the SiPc anions disappear completely within 1 ns while most of P3HT polarons are still observed up to 3 ns for all the ternary blends. This

finding suggests, as mentioned before, that SiPc molecules embedded in P3HT domains are negligible, because they would generate isolated $P3HT^{+}/SiPc^{-}$ pairs in P3HT domains and hence should recombine geminately. Furthermore, SiPc molecules embedded in PCBM domains are also negligible, because the charge separation from SiPc excitons generates not PCBM anions but P3HT polarons first. In other words, most of the SiPc molecules should be surrounded by not PCBM but P3HT. From these findings, the author concludes that the majority of SiPc molecules should be embedded in P3HT matrix with PCBM at the interface of P3HT/PCBM. This is consistent with the kinetic analysis described above and the efficient photocurrent generation in the device. This is also in good agreement with the study of the ternary blends in terms of the surface energy of component materials and the crystallization of P3HT in Chapter 5. Furthermore, as mentioned before, the charge shift time is dependent on the excitation wavelength: upon P3HT excitation, the efficient energy transfer from P3HT to SiPc at the interface followed by the charge shift (150 ps) and upon dye excitation, the charge shift from SiPc to PCBM (50 ps). Such difference is probably due to the special distribution of SiPc excitons in the interface depending on the excitation wavelength. In the case of dye excitation, SiPc molecules are homogeneously excited in the interface with dye. In the case of P3HT excitation, on the other hand, SiPc molecules close to P3HT crystal domains are dominantly excited by the energy transfer from P3HT excitons. If the interfacial width were as thin as ~1 nm (molecular size of SiPc), the charge shift time should be the same in either case. Indeed, the width of the P3HT disordered domain is estimated to be ~6 nm, which is enough larger than dye molecules, for both thermal- and solvent-annealed films from the width of the crystalline P3HT domains and the degree of the crystallization.

The author further discusses on the distribution of SiPc molecules at the interface. From the transient analysis, as described before, the interfacial coverage of SiPc is estimated to be ~40% in thermal- and solvent-annealed ternary blend films. Such partial coverage suggests

that SiPc molecules are inhomogeneously distributed at the interface and therefore concentrated relative to the original composition. This is consistent with the local concentration of SiPc in the ternary blend films estimated from the spectral shift of the SiPc absorption band. The local concentration is as high as 25 wt% under both annealing conditions, which is 7 times higher than the original dye composition of 3.4 wt%. If SiPc molecules were homogeneously distributed at the disordered P3HT domains (40% for thermal annealing and 30% for solvent annealing) in P3HT:PCBM(1:1) blends, the local concentration would be concentrated to 8.5–11.2 wt%. This is still less than half the estimated local concentration of 25 wt%. In other words, SiPc molecules should be further concentrated at the disordered interface, indicating inhomogeneous distribution of dyes. To account for the local concentration as high as 25 wt%, SiPc should be about two to three times concentrated furthermore. In other words, SiPc should be located in 36–48% of the disordered domain. This is in good agreement with the 40% of the interfacial coverage of SiPc estimated from the transient analysis. The author concludes that SiPc molecules are located at the interfacial disordered domains inhomogeneously with the coverage of ~40% as shown in Scheme 6-2a.

Finally, the author focuses on the distribution of PCBM molecules at the interface. The charge shift from SiPc to PCBM upon the dye excitation is slower in thermal-annealed than in solvent-annealed ternary blends. As mentioned above, the interfacial width of the P3HT disordered domain is estimated to be ~6 nm under either annealing condition. Thus, the difference in the charge shift time suggests that the concentration of PCBM at the interface is lower in thermal-annealed than in solvent-annealed ternary blends as illustrated in Scheme 6-2b. This is consistent with the difference in the fraction of the prompt polaron generation upon the P3HT excitation depending on the annealing conditions. As mentioned before, the prompt fraction is ascribed to the charge generation at the disordered interface of P3HT mixed with PCBM molecules. As shown in Figure 6-8, the prompt fraction is ~40% for solvent-

**Scheme 6-2. Schematic Illustration of Phase-Separated Structures in P3HT:PCBM:SiPc Ternary Blends**[a]

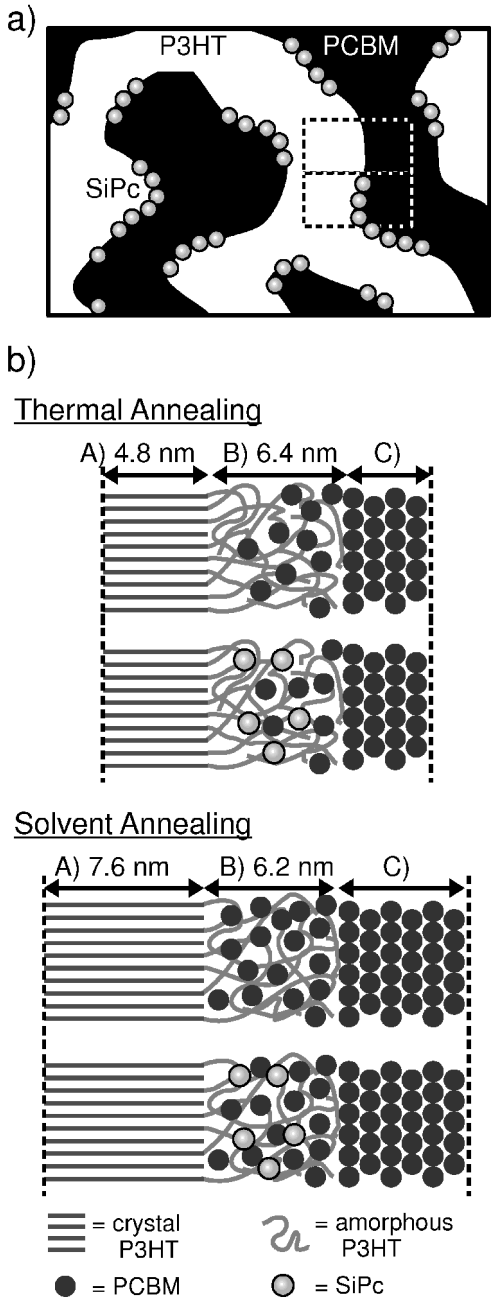


[a] The upper figure (a) shows the phase-separated structures of P3HT:PCBM:SiPc ternary blend films. The lower figures (b) show an enlarged local area of the top figures. The regions A, B, and C represent three characteristic phases of P3HT:PCBM blend films: fibrillar network of P3HT crystals, relatively disordered P3HT matrices with PCBM nanocrystals, and aggregates of PCBM nanocrystals, respectively. The widths of crystal and disordered P3HT phases are estimated from the simulated absorption spectra as shown in Figure 6-2.

annealed binary blends. This is in good agreement with the disordered fraction (45%) estimated from the absorption analysis. Thus, as shown in the lower figure of Scheme 6-2b, PCBM molecules are embedded at the disordered interface with a concentration enough to generate P3HT polarons promptly. On the other hand, the prompt fraction is ~30% for the thermal-annealed binary blends, which is smaller than the disordered fraction (56%). In other words, the lower prompt fraction is ascribed to the lower concentration of PCBM molecules at the disordered interface for thermal-annealed blends as shown in the upper figure of Scheme 6-2b. Such lower concentration of PCBM can be rationally explained in terms of thermal diffusion of PCBM molecules at high temperatures. The author concludes that the annealing condition has critical impact on the PCBM distribution at the interface. In particular, the solvent annealing can localize SiPc molecules with high PCBM concentration at the interface, resulting in the surprisingly highly efficient ternary blend solar cells.

## 6.5. Conclusions

The author has comprehensively studied the light-harvesting mechanism in polymer:fullerene:dye ternary blend films by transient absorption spectroscopy. On the basis of detailed analyses of the transient absorption spectra and decays, the author found the efficient light harvesting by the dye sensitization and the polymer exciton harvesting. Upon dye excitation of thermal-annealed P3HT:PCBM:SiPc blend films, SiPc excitons are rapidly quenched by surrounding P3HT to generate the charge pair of $P3HT^{+}/SiPc^{-}$ with a time constant of 2 ps, followed by efficient charge shift from SiPc anions to PCBM with a time constant of 50 ps. The charge separation and shift reactions are much faster than the backward recombination reactions. Consequently, both efficiencies are as high as almost 100%: the charge generation $\eta_{CG}^{P/Pc}$ = 100% and the charge shift $\eta_{CSH}$ = 98%. From these observations, the author concludes that the majority of SiPc molecules are selectively localized in disordered P3HT domains with PCBM molecules at the P3HT/PCBM interface.

In solvent-annealed ternary blends, on the other hand, the charge pairs of $P3HT^{+}/PCBM^{-}$ are rapidly generated from SiPc excitons with a time constant of 2 ps with no intermediate state such as SiPc anions observed for the thermal annealed film. In other words, the charge generation efficiency of $\eta_{CG}^{P/C60}$ is as high as 100% (= $\eta_{CG}^{P/Pc}\ \eta_{CSH}^{Pc/C60}$ or $\eta_{CG}^{Pc/C60}\ \eta_{CSH}^{P/Pc}$). The rapid charge generation of $P3HT^{+}/PCBM^{-}$ from SiPc excitons indicates that SiPc molecules are embedded at the interface in proximity to both P3HT and PCBM. The difference in the charge generation can be explained in terms of the PCBM concentration at the disordered interface. The author concludes that the PCBM concentration is lower in the thermal annealed films than in the solvent annealed films. This is because of thermal diffusion of PCBM at the interface to the PCBM domain. In particular, the thermal diffusion is enhanced in the presence of SiPc because of the plasticizer effect at the interface. On the other hand, upon polymer excitation of the thermal-annealed P3HT:PCBM:SiPc blends, half of the unquenched P3HT excitons are efficiently collected by energy transfer to SiPc molecules at theP3HT/PCBM interface. Such efficient energy transfer quenching accounts for 34% for thermal annealing and 21% for solvent annealing, suggesting that the energy transfer is more effective in the thermal annealed films. The relatively small contribution of dye molecules to the P3HT exciton harvesting in the solvent-annealed blends is due to the higher exciton diffusion of P3HT and the higher PCBM concentration at the interface. From the detailed analyses of the relaxation pathways of P3HT excitons, the author concludes that SiPc molecules are inhomogeneouly distributed at the P3HT/PCBM interface. The interfacial coverage of SiPc is estimated to be about 40% for both thermal and solvent annealed ternary blends. In summary, the light harvesting based on the dye sensitization and the polymer exciton harvesting is highly efficient under either annealing condition because SiPc molecules are selectively localized at the polymer/fullerene interface. In particular, SiPc molecules are closely in contact with both P3HT and PCBM at the interface in solvent annealed ternary

blends, which is an ideal interfacial structure for the efficient cascaded photoconversion. These findings provide experimental evidence that ideal interfacial structures can be fabricated even by a simple spin-coating from blend solutions, which will help in designing efficient polymer solar cells with the ternary blend bulk heterojunction active layer.

## 6.6. Appendix

### Absorption spectrum of SiPc

Figure 6-A1 shows the absorption spectrum of SiPc in toluene. SiPc exhibited a strong absorption at around 670–680 nm and almost no absorption band at 400 nm. Therefore, it can be said that no SiPc excitons are directly generated by the laser excitation at 400 nm.

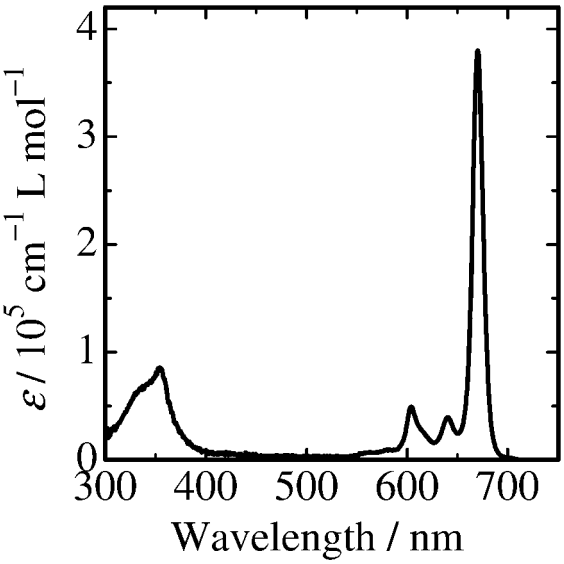


**Figure 6-A1.** Molar absorption coefficient of SiPc in toluene solution.

### Spectral Analysis of Crystalline P3HT Films

Before simulating the absorption spectra of P3HT in blends, the author first extracts the absorption spectra of P3HT from the absorption spectra of P3HT:PCBM blend films by subtracting the absorption of PCBM to eliminate the peak at around 3.7 eV (330 nm) ascribed to PCBM absorption, as shown in Figure 6-A2a. Then, the P3HT absorption spectra are simulated by the two parts of P3HT absorption: a lower energy part from crystalline regions of P3HT, which form a weakly interacting H-aggregate state, and a higher energy part from more disordered regions of P3HT. In accordance with a weakly coupled aggregate model,[32–35] the absorption spectrum of the crystalline P3HT is simulated by the following Equation (6-

A1) at around 2.0–2.3 eV, where disordered P3HT has no absorption bands.

$$A \propto \sum_{m=0}\left(\frac{S^m}{m!}\right)\cdot\left(1-\frac{We^{-S}}{2E_p}\sum_{n\neq m}\frac{S^n}{n!(n-m)}\right)^2\cdot\exp\left(\frac{(E-E_0-mE_p-WS^me^{-S}/2)^2}{2\sigma^2}\right) \quad (6\text{-A1})$$

Here, $W$ is the exciton bandwidth, $E_0$ is the 0–0 transition energy of the crystalline species, $E_p$ is the frequency of the vibronic transition, $\sigma$ is the width of the line shape that is assumed to be Gaussian, $S$ is the Huang–Rhys factor, and $m$ counts the vibrational excitation (calculated up to the 0–6 transition). The fitting procedure is followed by Ref 36. As reported previously,[32–35] $S$ and $E_p$ were fixed to 1.0 and 0.179 eV, respectively, while $E_0$, $\sigma$, $W$ were treated as free parameters. The best-fits to Equation (6-A1) is shown in Figure 6-A2b as the black solid line. The absorption spectrum of disordered P3HT was calculated by subtracting that of crystal P3HT (black solid line) from the absorption spectra of P3HT (open circles). The spectrum of disordered P3HT was similar to the spectrum of P3HT dissolved in solution (gray solid line), suggesting that such a spectral resolution is valid.

Next, the author evaluated the widths and the percentages of crystal P3HT in P3HT:PCBM blends according to the previous reports.[35–37] The author used the simulation data from Gierschner et al. to estimate the widths of crystal P3HT from the parameter $W$, obtained by above analysis.[35,36] The percentages of crystal P3HT was evaluated by the relative oscillator strength of the crystal species compared to the disordered species and the relation of molar absorption coefficient for these species: $\varepsilon_{2.05\ eV} = 1.39 \times \varepsilon_{2.7\ eV}$, where $\varepsilon_{2.05\ eV}$ and $\varepsilon_{2.7\ eV}$ represent the molar absorption coefficient at 2.05 eV (for crystal P3HT) and 2.7 eV (for disordered P3HT), respectively.[35] By using these procedures, the author estimated that the widths and the percentages of crystal P3HT in P3HT:PCBM blends are 9.5 nm and 44% for thermal-annealed films and 15.2 nm and 55% for solvent-annealed films, respectively.

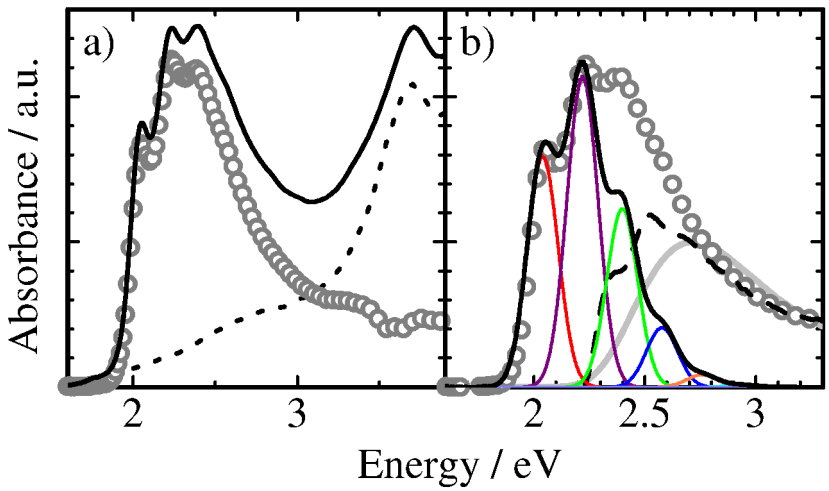


**Figure 6-A2.** a) Absorption spectra of P3HT:PCBM blends fabricated by solvent annealing (solid line), PCBM neat films (broken line), and P3HT in P3HT:PCBM blends (open circles) subtracted the absorption of PCBM from solid line. b) Absorption spectra of P3HT in P3HT:PCBM blends (obtained in a); open circles), crystal P3HT simulated by the best-fits to Equation (6-A1) to the region of crystalline absorption at 2.0–2.3 eV (black solid line, consisting of seven bands of 0–0 to 0–6 transition shown as colored thin lines), and disordered P3HT calculated by subtracting black solid line from open circles (broken line). The gray line in b) represents a spectrum of P3HT dissolved in toluene solution for comparison.

**Assignment of SiPc Exciton**

Figure 6-A3 shows the transient absorption spectrum of SiPc dissolved in toluene after the laser excitation at 670 nm (60 μJ $cm^{-2}$) measured at 0 ps. The spectrum shows two absorption peaks at around 460 nm and 650 nm with a broad skirt trailing to around 1000 nm. The sharp valleys at around 600 nm, 670 nm, and 750 nm are attributable to the photobleaching and the stimulated emission of SiPc because the wavelength corresponded to the absorption and fluorescence band of SiPc. The inset figure shows that the decay of the transient absorption signal at 1000 nm is well fitted with a monoexponential decay function with a lifetime of 4.2 ns, which is similar with the reported lifetime of siglet excitons of SiPc (5.8 ns).[A1] Therefore the broad absorption band at around 1000 nm is attributable to SiPc excitons. Similar spectrum is also observed in previous reports.[A1,A2] The molar absorption coefficient of SiPc

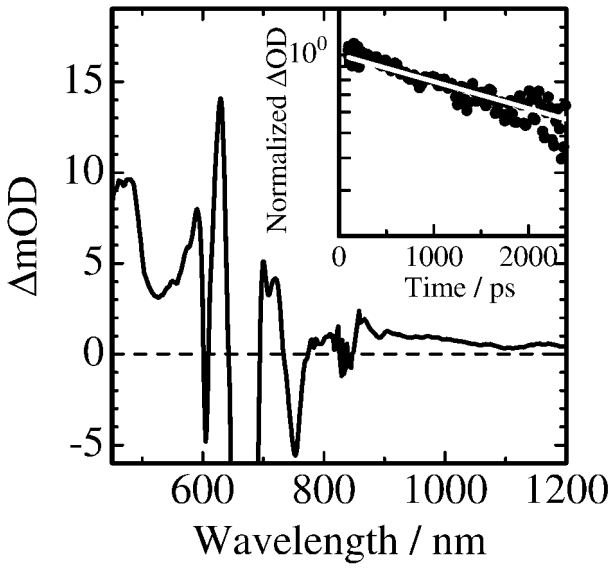


**Figure 6-A3.** Transient absorption spectrum of SiPc dissolved in toluene excited at 670 nm (60 μJ $cm^{-2}$) measured at 0 ps. The inset shows transient absorption decays at 1000 nm as closed circles, fitted with monoexponential function with a lifetime of 4.2 ns (the gray line).

excitons was estimated to be ~5 × $10^3$ $M^{-1}$ $cm^{-1}$ at 1000 nm by the comparison with the photobleaching of SiPc shown at 600 nm ($\varepsilon_{600}$ = 6.5 × $10^4$ $M^{-1}$ $cm^{-1}$; separately evaluated in advance).

**Assignment of SiPc Anion**

The spectrum and the molar absorption coefficient of SiPc anions were measured by using *N,N,N′,N′*-tetramethyl-*p*-phenylenediamine (TMPD) as an electron donor. Figure 6-A4 shows microsecond transient absorption spectra of TMPD:SiPc in *N,N*-dimethylformamide (DMF). The absorption band from 500 to 650 nm is ascribed to the characteristic absorption of TMPD cations.[A3,A4] As shown in the insert of this figure, the 940 nm band decayed at the same rate as the TMPD cations and therefore was assigned to the SiPc anions. Similar spectrum is also observed in previous reports.[A5,A6] Consequently, the molar absorption coefficient of SiPc anions can be evaluated be $\varepsilon$ = 4.3 × $10^3$ $M^{-1}$ $cm^{-1}$ at 940 nm in comparison with that of TMPD cations ($\varepsilon$ = 1.2 × $10^4$ $M^{-1}$ $cm^{-1}$ at 570 nm).[A3,A4]

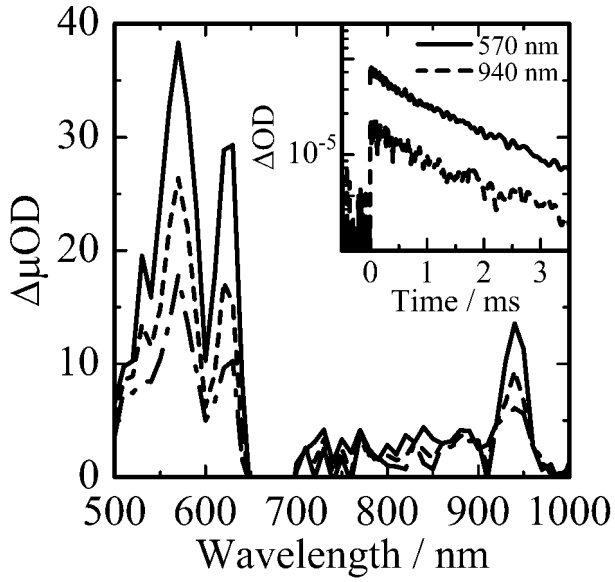


**Figure 6-A4.** Microsecond transient absorption spectra of TMPD/SiPc in DMF excited at 630 nm (20 μJ $cm^{-2}$) measured at 0.1 (solid line), 1 (broken line), and 2 (dashed-dotted line) ms. The inset shows transient absorption decays at 570 and 940 nm.

**Assignment of SiPc Cation**

The spectrum and the molar absorption coefficient of SiPc cations were measured by using nitric acid ($HNO_3$) or PCBM as an electron acceptor. Figure 6-A5a shows absorption spectra of SiPc with and without $HNO_3$ in dichloromethane solution. By adding $HNO_3$, two absorption bands at around 550 nm and 850 nm were observed with the decrease in the ground-state absorption band at around 600–700 nm. The author assigned the absorption bands at around 550 nm and 850 nm to SiPc cations. These bands are also observed in previous reports.[A2,A7–A9] The molar absorption coefficient of SiPc cations was estimated by the transient absorption spectra of PCBM:SiPc blend films under the assumption that the spectra can be reproduced by the spectra of PCBM anions and SiPc cations. Figure 6-A5b shows transient absorption spectrum of PCBM:SiPc blends at 3 ps after the excitation of SiPc (open circles), PCBM anions (broken line; from ref 22), and SiPc cations (solid line; estimated by the subtracting the broken line from the observed spectrum). From this estimation, the molar

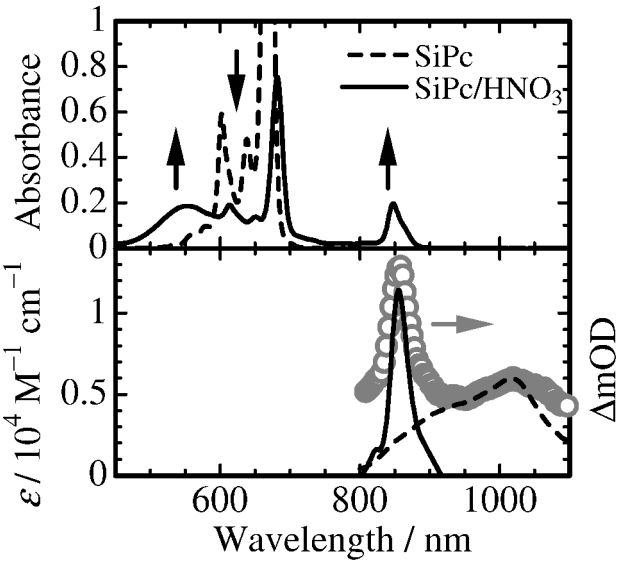


**Figure 6-A5.** (a) Absorption spectra of SiPc in dichloromethane with and without $HNO_3$. (b) Femtosecond transient absorption spectra of PCBM:SiPc blend films excited at 680 nm (5 μJ $cm^{-2}$) measured at 3 ps (open circles). The broken and solid lines are PCBM anions[22] and SiPc cations, respectively.

absorption coefficient of SiPc cations can be evaluated to be $\varepsilon = 1.1 \times 10^4$ $M^{-1}$ $cm^{-1}$ at 855 nm in comparison with that of PCBM anions ($\varepsilon = 6.0 \times 10^3$ $M^{-1}$ $cm^{-1}$ at 1030 nm).[22]

**Spectral Analysis to Extract SiPc Anions**

The optical density of SiPc anions generated in P3HT:PCBM:SiPc blend films after the excitation of SiPc was roughly estimated as follows. SiPc anions have a band at around 910–960 nm with a peak at 940 nm and have a negligible absorption at 900 and 970 nm. First, the base line (black line)is drawn as shown in Figure 6-A6 to cross the point ΔOD at 900 nm and ΔOD at 970 nm of the observed spectra, and then, the difference at 940 nm shown as the bar in Figure 6-A6 between the observed data and the black line is measured as the optical density of SiPc anions ($\Delta OD_{SiPc-}$).

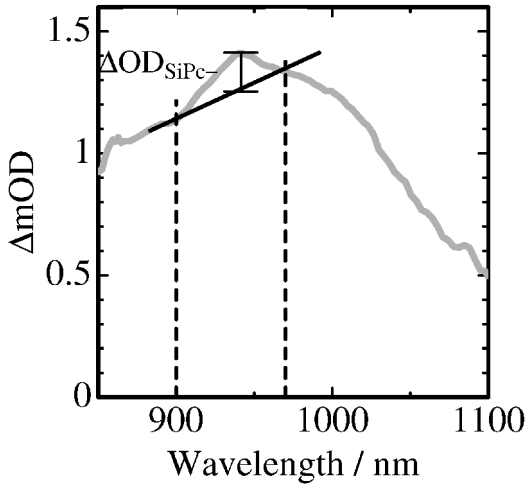


**Figure 6-A6.** Transient absorption spectrum of P3HT:PCBM:SiPc blend films after the excitation of SiPc (as an example here shows spectrum at 10 ps as the gray line) for the estimation of the optical density of SiPc anions ($\Delta OD_{SiPc-}$).

**Spectral Analysis to Extract SiPc Photobleaching**

The optical density of SiPc photobleaching observed in P3HT:PCBM:SiPc blend films after the excitation of P3HT was estimated as follows. SiPc photobleaching have a band at around 660–700 nm with a peak at 680 nm and have a negligible absorption at 660 and 710

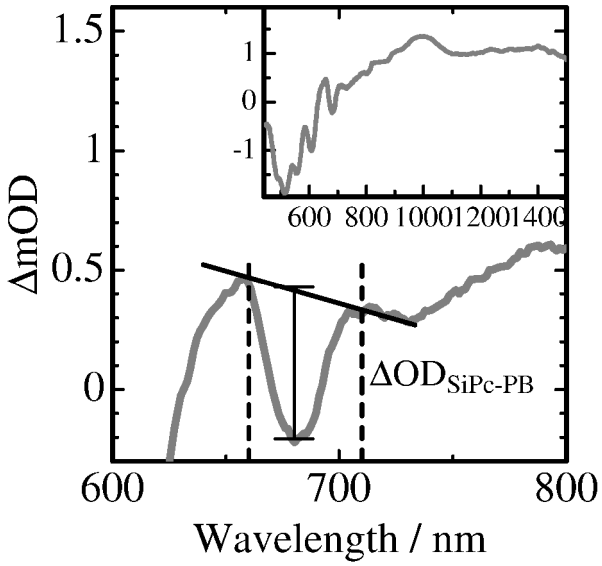


**Figure 6-A7.** Transient absorption spectrum of P3HT:PCBM:SiPc blend films after the excitation of P3HT (as an example here shows spectrum at 10 ps as the gray line) for the estimation of the optical density of SiPc photobleaching ($\Delta OD_{SiPc-PB}$). The inset shows the same spectrum in wide wavelengths range scale.

nm. First, the base line (black line) is drawn as shown in Figure 6-A7 to cross the point ΔOD at 660 nm and ΔOD at 710 nm of the observed spectra, and then, the difference at 680 nm shown as the bar in Figure 6-A7 between the observed data and the black line is measured as the optical density of SiPc photobleaching ($\Delta OD_{SiPc\text{-}PB}$).

**Estimation of the Fractions of P3HT Exciton Relaxation upon P3HT Excitation**

The fractions of P3HT excitons are estimated as follows. Here the author explains for the thermal-annealed ternary blends for example. First, the exciton fraction neither quenched nor contributed to the photocurrent generation is estimated from the PL efficiency of P3HT excitons (10%). Next, the prompt quenching fraction is estimated from the proportion of the remaining fraction (90%) and the ratio of the amount of P3HT polarons generated promptly to the amount of the total P3HT polarons (29%). Thus, the prompt quenching fraction is estimated to be 26%. Finally, the remaining fraction is divided into two fractions for the delayed quenching after exciton migration and for the faster quenching by the energy transfer to SiPc, on the basis of the ratio between the fraction of $A_{D2}$ and $B_{D2}$ in Eq. 6-3 described in the main text (48:52). Therefore, the quenching fractions after the energy migration and the energy transfer fraction are estimated to be 31% and 33%, respectively. For the other samples, the same procedures were performed. The results are summarized in Figure 6-8.

**Förster Radius Based on Dipole–Infinite-Slab Approximation**

Figure 6-A9 shows the distance dependent quenching efficiency, $\eta_Q(R)$, of P3HT exciton in the crystal P3HT domain calculated by the Förster radius based on dipole–infinite-slab approximation using Eq. 6-A2 and 6-A3. The $\tau_F$, $R_0$, and $r$ represent the photoluminescence lifetime of P3HT exciton, the Förster radius, and the distance between a donor and an acceptor (in this case $r$ equals to the distance between P3HT exciton and the interface). The

$C_A$ in Eq. 6-A2 is the acceptor chromophore density. From the crystal volume of SiPc ~1.4 $nm^3$, the $C_A$ is estimated to be 0.71 $nm^{-3}$ if only SiPc is located at the interface. The author has previously estimated the local concentration of SiPc = 25 wt% fr the original dye composition of 3.4 wt%. Thus, the author considered that the $C_A$ in this system was 0.18 $nm^{-3}$. As shown in Figure 6-A8, 92% of P3HT excitons in crystal domain can be collected by the energy transfer even without considering energy migration of excitons.

$$k_{EnT}(R) = \frac{C_A}{\tau_F}\frac{\pi}{6}\left(\frac{R_0}{r}\right)^3 \qquad (6-A2)$$

$$\eta_Q(R) = \frac{k_{EnT}}{k_{EnT}+k_F} \qquad (6-A3)$$

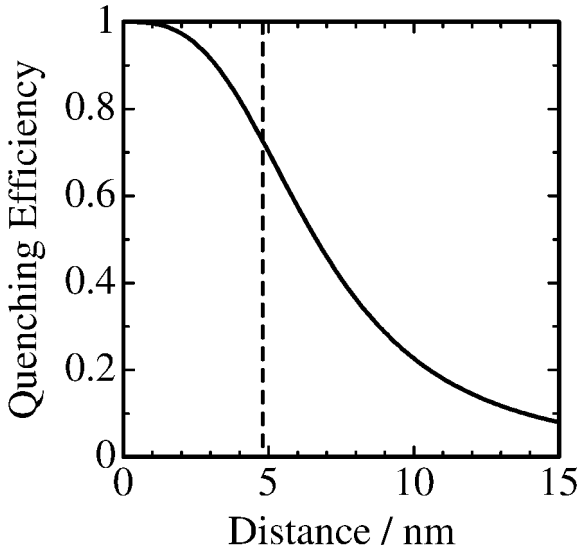


**Figure 6-A8.** Distance dependence quenching efficiency of P3HT exciton generated in crystal P3HT domain. The thick solid line represents the quenching efficiency calculated by the equation 6-A2 and 6-A3. Thin broken line represents the domain center of crystal P3HT for thermal annealing (the distance between the domain center and the interface is evaluated to be 4.8 nm in Figure 6-A2).

## References


(1) Brabec, C. J.; Durrant, J. R. *MRS Bull.* **2008**, *33*, 670–675.

(2) Dennler, G.; Scharber, M. C.; Brabec, C. J. *Adv. Mater.* **2009**, *21*, 1323–1338.

(3) Helgesen, M.; Søndergaard, R.; Krebs, F. C. *J. Mater. Chem.* **2010**, *20*, 36–60.

(4) Brabec, C. J.; Gowrisanker, S.; Halls, J. J. M.; Laird, D.; Jia, S.; Williams, S. P. *Adv. Mater.* **2010**, *22*, 3839–3856.

(5) Ma, W.; Yang, C.; Gong, X.; Lee, K.; Heeger, A. J. *Adv. Funct. Mater.* **2005**, *15*, 1617–1622.

(6) Li, G.; Shrotriya, V.; Huang, J.; Yao, Y.; Moriarty, T.; Emery, K.; Yang, Y. *Nat. Mater.* **2005**, *4*, 864–868.

(7) Kim, Y.; Cook, S.; Tuladhar, S. M.; Choulis, S. A.; Nelson, J.; Durrant, J. R.; Bradley, D. D. C.; Giles, M.; McCulloch, I.; Ha, C.-S.; Ree, M. *Nat. Mater.* **2006**, *5*, 197–203.

(8) Irwin, M. D.; Buchholz, D. B.; Hains, A. W.; Chang, R. P. H.; Marks, T. J. *Proc. Natl. Acad. Sci. USA* **2008**, *105*, 2783–2787.

(9) Jo, J.; Kim, S.-S.; Na, S.-I.; Yu, B.-K., Kim, D.-Y. *Adv. Funct. Mater.* **2009**, *19*, 866–874.

(10) Bundgaard, E.; Krebs, F. C. *Sol. Energy Mater. Sol. Cells* **2007**, *91*, 954–985.

(11) Kroon, R.; Lenes, M.; Hummelen, J. C.; Blom, P. W. M.; de Boer, B. *Polym. Rev.* **2008**, *48*, 531–582.

(12) Peet, J.; Kim, J. Y.; Coates, N. E.; Ma, W. L.; Moses, D.; Heeger, A. J.; Bazan, G. C. *Nat. Mater.* **2007**, *6*, 497–500.

(13) Chen, H.-Y.; Hou, J.; Zhang, S.; Liang, Y.; Yang, G.; Yang, Y.; Yu, L.; Wu, Y.; Li, G.; *Nat. Photonics* **2009**, *3*, 649–653.

(14) Chen, Y.-C.; Yu, C.-Y.; Fan, Y.-L.; Hung, L.-I; Chen, C.-P.; Ting, C. *Chem. Commun.* **2010**, *46*, 6503–6505.

(15) Peet, J.; Tamayo, A. B.; Dang, X.-D.; Seo, J. H.; Nguyen, T.-Q. *Appl. Phys. Lett.* **2008**, *93*, 163306.

(16) Honda, S.; Nogami, T.; Ohkita, H.; Benten, H.; Ito, S. *ACS Appl. Mater. Interfaces* **2009**, *1*, 804–810.

(17) Suresh, P.; Balraju, P.; Sharma, G. D.; Mikroyannidis, J. A.; Stylianakis, M. M. *ACS Appl. Mater. Interfaces* **2009**, *1*, 1370–1374.

(18) Honda, S.; Ohkita, H. Benten, H.; Ito, S. *Chem. Commun.* **2010**, *46*, 6596–6598.

(19) Barbour, L. W.; Hegadorn, M.; Asbury, J. B. *J. Am. Chem. Soc.* **2007**, *129*, 15884–15894.

(20) Parkinson, P.; Lloyd-Hughes, J.; Johnston, M. B.; Herz, L. M. *Phys. Rev. B* **2008**, *78*, 115321.

(21) Hwang, I.-W.; Moses, D.; Heeger, A. J. *J. Phys. Chem. C* **2008**, *112*, 4350–4354.

(22) Yamamoto, S.; Guo, J.; Ohkita, H.; Ito, S. *Adv. Funct. Mater.* **2008**, *18*, 2555–2562.

(23) Piris, J.; Dykstra, T. E.; Bakulin, A. A.; van Loosdrecht, P. H. M.; Knulst, W.; Trinh, M. T.; Schins, J. M.; Siebbeles, L. D. A. *J. Phys. Chem. C* **2009**, *113*, 14500–14506.

(24) Cook, S.; Katoh, R.; Furube, A. *J. Phys. Chem. C* **2009**, *113*, 2547–2552.

(25) Guo, J.; Ohkita, H.; Benten, H.; Ito, S. *J. Am. Chem. Soc.* **2009**, *131*, 16869–16880.

(26) Guo, J.; Ohkita, H.; Benten, H.; Ito, S. *J. Am. Chem. Soc.* **2010**, *132*, 6154–6164.

(27) Guo, J.; Ohkita, H.; Yokoya, S.; Benten, H.; Ito, S. *J. Am. Chem. Soc.* **2010**, *132*, 9631– 9637.

(28) Marsh, R. A.; Hodgkiss, J. M.; Albert-Seifried, S.; Friend, R. H. *Nano Lett.* **2010**, *10*, 923–930.

(29) Howard, I. A.; Mauer, R.; Meister, M.; Laquai, F. *J. Am. Chem. Soc.* **2010**, *132*, 14866–14876.

(30) Johansson, E. M. J.; Yartsev, A.; Rensmo, H.; Sundström, V. *J. Phys. Chem. C* **2009**,

*113*, 3014–3020.

(31) Erb, T.; Zhokhavets, U.; Gobsch, G.; Raleva, S.; Stühn, B.; Schilinsky, P.; Waldauf, C.; Brabec, C. J. *Adv. Funct. Mater.* **2005**, *15*, 1193–1196.

(32) Spano, F. C. *J. Chem. Phys.* **2005**, *122*, 234701.

(33) Spano, F. C. *Chem. Phys.* **2006**, *325*, 22–35.

(34) Clark, J.; Silva, C.; Friend, R. H.; Spano, F. C. *Phys. Rev. Lett.* **2007**, *98*, 206406.

(35) Clark, J.; Chang, J.-F.; Spano, F. C.; Friend, R. H.; Silva, C. *Appl. Phys. Lett.* **2009**, *94*, 163306.

(36) Pingel, P.; Zen, A.; Abellón, R. D.; Grozema, F. C.; Siebbeles, L. D. A.; Neher, D. *Adv. Funct. Mater.* **2010**, *20*, 2286–2295.

(37) Gierschner, J.; Huang, Y. S.; van Averbeke, B.; Cornil, J.; Friend, R. H.; Beljonne, D. *J. Chem. Phys.* **2009**, *130*, 044105.

(38) van Bavel, S. S.; Sourty, E.; de With, G.; Loos, J. *Nano Lett.* **2009**, *9*, 507–513.

(39) van Bavel, S.S.; Bärenklau, M.; de With, G.; Hoppe, H.; Loos, J. *Adv. Funct. Mater.* **2010**, *20*, 1458–1463.

(40) Moon, J. S.; Lee, J. K.; Cho, S.; Byun, J.; Heeger, A. J. *Nano Lett.* **2009**, *9*, 230–234.

(41) van Bavel, S. S.; Sourty, E.; de With, G.; Loos, J. *Nano Lett.* **2009**, *9*, 507–513.

(42) Kudo, N.; Honda, S.; Shimazaki, Y.; Ohkita, H.; Ito, S.; Benten, H. *Appl. Phys. Lett.* **2007**, *90*, 183513.

(43) Liu, Y.; Summers, M. A.; Edder, C.; Fréchet, J. M. J.; McGehee, M. D. *Adv. Mater.* **2005**, *17*, 2960–2964.

(44) Scully, S. R.; Armstrong, P. B.; Edder, C.; Fréchet, J. M. J.; McGehee, M. D. *Adv. Mater.* **2007**, *19*, 2961–2966.

(45) Hardin, B. E.; Hoke, E. T.; Armstrong, P. B.; Yum, J.-H.; Comte, P.; Torres, T.; Fréchet, J. M. J.; Nazeeruddin, M. K.; Grätzel, M.; McGehee, M. D. *Nat. Photonics*

**2009**, *3*, 406–411.

(46) Hardin, B. E.; Yum, J.-H.; Hoke, E. T.; Jun, Y. C.; Péchy, P.; Torres, T.; Brongersma, M. L.; Nazeeruddin, M. K.; Grätzel, M.; McGehee, M. D. *Nano Lett.* **2010**, *10*, 3077–3083.

(47) Deisenhofer, J.; Epp, O.; Miki, K.; Huber, R.; Michel, H. *Nature* **1985**, *318*, 618−624.

(48) Bixon, M.; Jortner, J.; Michel-Beyerle, M. E. *Biochim. Biophys. Acta* **1991**, *1056*, 301–315.

(49) Coffey, D. C.; Ferguson, A. J.; Kopidakis, N.; Rumbles, G. *ACS Nano* **2010**, *4*, 5437–5445.

(A1) Fujitsuka, M.; Ito, O.; Konami, H. *Bull. Chem. Soc. Jpn.* **2001**, *74*, 1823–1829.

(A2) Martín-Gomis, L.; Ohkubo, K.; Fernández-Lázaro, F.; Fukuzumi, S.; Sastre-Santos, Á. *Chem. Commun.* **2010**, *46*, 3944–3946.

(A3) Guo, J.; Togami, T.; Benten, H.; Ohkita, H.; Ito, S. *Chem. Phys. Lett.* **2009**, *475*, 240–244.

(A4) Steigman, J.; Cronkright, W. *J. Am. Chem. Soc.* **1970**, *92*, 6736–6743.

(A5) Kawaguchi, T.; Seki, S.; Okamoto, K.; Saeki, A.; Yoshida, Y.; Tagawa, S. *Chem. Phys.Lett.* **2003**, *374*, 353–357.

(A6) Mack, J.; Kirkby, S.; Ough, E. A.; Stillman, M. J. *Inorg. Chem.* **1992**, *31*, 1717–1719.

(A7) Kodis, G.; Herrero, C.; Palacios, R.; Mariño-Ochoa, E.; Gould, S.; de la Garza, L.; van Grondelle, R.; Gust, D.; Moore, T. A.; Moore, A. L.; Kennis, J. T. M. *J. Phys. Chem. B* **2004**, *108*, 414–425.

(A8) Nyokong, T.; Gasyna, Z.; Stillman, M. J. *Inorg. Chem.* **1987**, *26*, 548–553.

(A9) Martín-Gomis, L.; Ohkubo, K.; Fernández-Lázaro, F.; Fukuzumi, S.; Sastre-Santos, Á. *J. Phys. Chem. C* **2008**, *112*, 17694–17701.

# *Summary*

In this thesis, the author has demonstrated the dye sensitization at the donor/acceptor interface in polymer solar cells and elucidated the influence of dye molecules on device performance, film morphology, and photophysical dynamics. The author found that the dye at the interface can serve not only as a photosensitizer but also as an energy funnel for dye-sensitized polymer/metal oxide hybrid solar cells and, interestingly, this is also true for devices based on the ternary or quaternary blends of a polymer, a fullerene, and one or two dye(s) though the dye molecules are simply loaded into polymer fullerene blends.

Chapter 1 describes the historical background and motivation of this thesis in terms of polymer solar cells, dye sensitization, energy transfer, and ternary blend films were described to clarify the significance of this thesis.

In Part I, the dye-sensitized polymer/metal oxide hybrid solar cells were studied as a model system of the interfacial dye sensitization.

In Chapter 2, the dye modification at the interface of donor/acceptor with Black Dye molecules in organic-inorganic hybrid solid solar cells was studied using double layered cells consisting of RR-P3HT and a flat layer of dense $TiO_2$. The EQE of the chemically modified cell was nearly double that expected from the photosensitizing effect of the dye molecules. The additional increase shows that the chemical modification with dye molecules can serve not only as a photosensitizer but mainly as an energy funnel and/or an electronic mediator to significantly improve the electron injection efficiency from RR-P3HT to $TiO_2$.

On the basis of these results, the dye-sensitized polymer:fullerene:dye ternary blend solar cells were developed in Part II.

In Chapter 3, the enhancement of the light-harvesting efficiency in RR-P3HT:PCBM BHJ solar cells was demonstrated by the introduction of phthalocyanine molecules as the third

component at the P3HT/PCBM interface. The author employed two kinds of phthalocyanine dyes with different chemical structures ZnPc, which is easy to stack and aggregate together, and SiPc, which is difficult to stack. ZnPc showed little absorption in ternary blend films due to dye aggregations. On the other hand, SiPc exhibited intense absorption in ternary blend films even after annealing. The introduction of SiPc increased the short-circuit current density and hence improved the overall power conversion efficiency by 20%, compared to the RR-P3HT:PCBM control device. For RR-P3HT:PCBM:SiPc devices, two distinct EQE peaks were observed at wavelengths for the absorption bands of SiPc as well as RR-P3HT before and after thermal annealing, suggesting that SiPc molecules are located at the RR-P3HT/PCBM interface because of crystallization of the P3HT and PCBM domains. Furthermore, the EQE for the device increased even at wavelengths for the absorption band of RR-P3HT by the introduction of SiPc molecules. This indicates that P3HT excitons can be dissociated into charge carriers more efficiently in the presence of SiPc molecules at the RR-P3HT/PCBM interface by energy transfer from RR-P3HT to SiPc molecules. The author therefore concludes that there are two origins for the increase in the photocurrent by the introduction of SiPc; SiPc molecules serve not only as a light-harvesting photosensitizer but also as an energy funnel for RR-P3HT excitons at the RR-P3HT/PCBM interface.

In Chapter 4, multi-colored dye-sensitized blend solar cells based on quaternary blends of RR-P3HT and PCBM with two different dyes, SiPc and SiNc, having complementary spectral absorption in the near-IR region was studied. The photocurrent was increased ~10% in the individual ternary blend solar cells and was simply doubled to ~20% in the quaternary blend solar cells. This is probably because both dye molecules are located at the interface without unfavorable aggregation. In other words, the device performance of polymer solar cells can be easily improved by multi-colored dye-sensitization with suitable selection of near-IR dyes and concentration of dyes. An appropriate combination of more than two dyes with different

absorption bands or dyes with wider absorption bands compared to phthalocyanines and naphthalocyanines employed in this study could increase PCE to more than 5%. Moreover, this method is simple and versatile and therefore can be easily applied not only to various material combinations but also directly in the existing industrial processes. Thus, this approach could boost the photocurrent generation even for highly efficient polymer solar cells based on low-bandgap polymer and fullerene with PCE > 7%.

In Part III, furthermore, the detailed mechanism of dye localization and light harvesting in such dye-sensitized ternary blend solar cells were clarified.

Chapter 5 describes the selective localization of dye molecules at the interface of polymer and fullerene domains in RR-P3HT:PCBM:SiPc ternary blend solar cells. The absorption and surface energy measurements showed that SiPc is likely to be located in disordered P3HT domains at the RR-P3HT/PCBM interface rather than in PCBM and crystal P3HT domains. From the peak wavelength of SiPc absorption, the local concentration of SiPc ($[SiPc]_{Local}$) was estimated for the RR-P3HT:PCBM:SiPc ternary blends. Even for amorphous films of RRa-P3HT:PCBM:SiPc blends, $[SiPc]_{Local}$ was 14 wt%, which is higher than the original composition (3.4 wt%), suggesting dye segregation into the RR-P3HT/PCBM interface. For RR-P3HT:PCBM:SiPc blends, $[SiPc]_{Local}$ increased furthermore to 20 wt% even before thermal annealing and furthermore to 25 wt% after thermal annealing with the increase in the P3HT crystallization. Such interfacial segregation of dye molecules in ternary blend films can be rationally explained in terms of the surface energy of each component and the crystallization of P3HT enhanced by annealing. In particular, the solvent annealing can effectively segregate dye molecules into the interface without the formation of PCBM crystals.

In Chapter 6, the light-harvesting mechanism by dye molecules loaded into polymer:fullerene blends was comprehensively studied by transient absorption spectroscopy

for ternary blend films, consisting of RR-P3HT, PCBM, and SiPc as a light-harvesting dye. Upon dye excitation of thermal annealed RR-P3HT:PCBM:SiPc blends, RR-P3HT polarons and SiPc anions were first generated from SiPc excitons on a time scale of ~2 ps and then electrons were shifted from SiPc to PCBM on a time scale of ~50 ps, suggesting that SiPc molecules are selectively located in the disordered P3HT matrix mixed with PCBM molecules at the RR-P3HT/PCBM interface. Upon polymer excitation, RR-P3HT excitons decayed more rapidly in ternary blends than in binary blends with an identically rapid formation of SiPc photobleaching, suggesting efficient energy transfer from RR-P3HT to SiPc on a time scale of ~4 ps, followed by slightly delayed generation of P3HT polarons. Subsequently, the photobleaching disappeared while the RR-P3HT polaron band still remained the same, suggesting a charge shift from SiPc anion to PCBM. All these photovoltaic conversion processes are much more rapid than backward reactions, and therefore highly efficient light harvesting is achieved in ternary blend solar cells.

# *List of Publications*

***Chapter 2.***

"Improvement of Charge Injection Efficiency in Organic-Inorganic Hybrid Solar Cells by Chemical Modification of Metal Oxides with Organic Molucules"

Naomi, K.; Honda, S.; Shimazaki, Y.; Ohkita, H.; Ito, S.; Benten, H.

*Appl. Phys. Lett.* **2007**, *90*, 183513.

***Chapter 3.***

"Improvement of the Light-Harvesting Efficiency in Polymer/Fullerene Bulk Heterojunction Solar Cells by Interfacial Dye Modification"

Honda, S.; Nogami, T.; Ohkita, H.; Benten, H.; Ito, S.

*ACS Appl. Mater. Interfaces* **2009**, *1*, 804–810.

***Chapter 4.***

"Multi-Colored Dye Sensitization of Polymer/Fullerene Bulk Heterojunction Solar Cells"

Honda, S.; Ohkita, H.; Benten, H.; Ito, S.

*Chem. Commun.* **2010**, *46*, 6596–6598.

***Chapter 5.***

"Selective Dye Modification at the Interface in Polymer/Fullerene Solar Cells Designed by Surface Energy and Annealing Condition"

Honda, S.; Ohkita, H.; Benten, H.; Ito, S.

*J. Am. Chem. Soc.* submitted.

***Chapter 6.***

"Light Harvesting by Dye Molecules Selectively Located at Polymer/Fullerene Interface Studied by Transient Absorption Spectroscopy"

Honda, S.; Yokoya, S.; Ohkita, H.; Benten, H.; Ito, S.

*J. Am. Chem. Soc.* submitted.

***Other Publication.***

"Surface Segregation at the Aluminum Interface of Poly(3-hexylthiophene)/Fullerene Solar Cells"

Orimo A.; Masuda, K.; Honda, S.; Benten, H.; Ito, S.; Ohkita, H.; Tsuji, H.

*Appl. Phys. Lett.* **2010**, *96*, 043305.

# *Acknowledgments*

The present thesis is based on the studies that the author and his co-workers have carried out at Department of Polymer Chemistry, Graduate School of Engineering, Kyoto University, Japan, from 2006 to 2011, under the guidance of Professor Shinzaburo Ito. The author sincerely expresses his gratitude to Professor Shinzaburo Ito for his kind guidance, valuable advices and heartful encouragement throughout this work, and for giving this opportunity to do a PhD's work in his Lab.

The author is deeply and heartily grateful to Associate Professor Hideo Ohkita for his kind supports, advices, and continuous discussions throughout this work. So many ideas in this thesis were born from these fruitful discussions. The author is also indebted to Associate Professor Hiroyuki Aoki and Assistant Professor Hiroaki Benten for their valuable suggestions and discussions. The author thanks to his co-workers, Ms. Naomi Kudo, Mr. Yuta Shimazaki, Mr. Takahiro Nogami, and Mr. Seiichirou Yokoya, for helping the studies in this thesis and to Mr. Junichi Kakuta, who introduced the powerful material; “silicon phthalocyanine bis(trihexylsilyl oxide)”, into Ito Lab. This provides two third parts of the author's publications and is absolutely necessary for this thesis.

The author is in acknowledgment of the Japan Student Services Organization, the Grobal COE program (International Center for Integrated Research and Advanced Education in Materials Science), the Integrative Industry–Academia Partnership (IIAP) project including Kyoto University and Mitsubishi Chemical Corporation, and the JST PRESTO program.

The author wishes to express his thanks to all members of Ito Lab., in particular, Dr. Li-Ting Lee, Dr. Ryojun Sekine, Dr. Kohji Masuda, Dr. Jiamo Guo, Dr. Michihiro Ogawa, Ms. Naomi Kudo, Dr. Toru Ube, Mr. Yoshifumi Ikeda, Mr. Syunsuke Yamamoto, Ms. Akiko Orimo, Mr. Seiichirou Yokoya, Mr. Junya Kosaka, Mr. Kazuki Mori, Mr. Daisuke Mori, Mr.

Toshiaki Hirata, and Mr. Yuta Izumiya for their attentive advices, helpful discussions, and for having a good time in Lab. They sensitized the author's monochrome life with vivid colors. The author is much obliged to Mrs. Aki Yamasaki and Ms. Yuki Munemoto for their assistance during the author's school life. The author specially thanks to Dr. Hiroaki Benten, Dr. Ryojun Sekine and Mr. Yoshifumi Ikeda for taking care of the author's physical conditions.

The author greatly thanks to Dr. Tetsuo Matsuda for healing the author's depression and giving the chance to live again.

Finally, the author express his heartful thanks to his parents, Mr. Masami Honda and Mrs. Keiko Honda, his brother, Mr. Yoshinori Honda and Dr. Shinya Honda, and his grandparents, Mr. Yoshio Honda and Mrs. Tsutako Honda, for their constant financial support, hearty assistance and encouragement.

March 2011

*Satoshi HONDA*